Available online at www.sciencedirect.com
ScienceDirect
Prog. Polym. Sci. 33 (2008) 683–731
PROGRESS IN POLYMER SCIENCE
www.elsevier.com/locate/ppolysci

Theories and simulations of polymer-based nanocomposites: From chain statistics to reinforcement

Giuseppe Allegra[a], Guido Raos[a,*], Michele Vacatello[b]

[a]*Dipartimento di Chimica, Materiali e Ingegneria Chimica "G. Natta", Politecnico di Milano, Via L. Mancinelli 7, Milano 20131, Italy*
[b]*Dipartimento di Chimica "P. Corradini", Università di Napoli Federico II, Via Cintia, Napoli 80126, Italy*

Received 1 August 2007; received in revised form 7 January 2008; accepted 20 February 2008
Available online 4 March 2008

Abstract

A survey of the present understanding of particle-filled polymers is presented, as obtained from either theoretical or computational approaches. We concentrate on composites in which the nanoparticles are either spherical or statistically isotropic aggregates, and the matrix is a homopolymer melt or a cross-linked elastomer. Recent progress has been prompted by the preparation and careful characterization of well-defined model systems, as well as by theoretical developments and the application of computer simulation to increasingly realistic models. After an introduction providing the main motivations (Section 1), an overview of the basic phenomenology and recent experimental results is presented (Section 2), with special emphasis on the Payne effect and related aspects. In Section 3, we discuss results of equilibrium molecular dynamics and Monte Carlo simulations of polymer chains in the presence of nanoparticles. After a concise theoretical description, these are compared with those obtained from integral equation and density functional approaches (Section 4). The molecular origins of the inter-particle-depletion interaction are discussed, as well as the phase-separation diagram of the nanoparticle/polymer system. The related issue of polymer chains and networks compressed between planar surfaces is also dealt with. In Section 5 simulations and theories of polymer dynamics at the interface are discussed, with special emphasis on the effects of surface roughness and on the vicinity of the glass transition. In Section 6 the overall viscoelastic response of polymer nanocomposites is considered, both from the point of view of molecular-level simulations and of continuum mechanics approaches. The concluding remarks (Section 7) discuss some of the open challenges in the field.

Keywords: Rubber reinforcement; Molecular dynamics; Monte Carlo; Polymer theory; Interfacial phenomena; Viscoelasticity

Contents

*Corresponding author.
E-mail addresses: giuseppe.allegra@polimi.it (G. Allegra), guido.raos@polimi.it (G. Raos), michele.vacatello@unina.it (M. Vacatello).

0079-6700/$ - see front matter © 2008 Elsevier Ltd. All rights reserved.
doi:10.1016/j.progpolymsci.2008.02.003

1. Introduction and scope

The aim of this review is to provide a survey of the state of our understanding of the behaviour of particle-filled polymer—especially melts or cross-linked networks—with a special emphasis on recent results and insights from either theoretical or computational approaches. In order to provide some background information, recent and not-so-recent experimental results will be briefly discussed as well, but in this case we do not aim at completeness and generality.

"With the exception of vulcanization, no process in the rubber industry is more important or as widely practiced as the reinforcement of elastomers by particulate fillers, especially carbon black… The incorporation of a colloidal material into a high polymer with subsequent conversion to a filled network by vulcanization leads to a system of great complexity… It is not surprising, therefore, that the very mechanism of reinforcement is still not completely understood and that certain aspects of it are subject to various interpretations which are not entirely consistent with one another…" Thus wrote 40 years ago Gerard Kraus, in his preface to the book "Reinforcement of Elastomers" [1]. Many of these statements could have been written today. It is certainly true that the field of rubber reinforcement—or, more generally, polymer modification by dispersion of solid particles—has retained all its importance. The observation that, other things being equal, the effectiveness of the filler increases with the increase in their surface/volume ratio has provided impetus to the shift from micron- to nanosized particles. In fact, the study of polymer-based nanocomposites has experienced explosive growth over the last decade and may be rightfully considered as an important branch of the emerging field of nanotechnology. Progress has been pushed forward by the development of new materials such as precipitated silica, which has been increasingly used alongside carbon black as the filler of choice in "conventional" applications such as automotive tyres. The introduction of even more unconventional fillers, such as carbon nanotubes, metallic, semi-conducting or magnetic nanoparticles and clay platelets promises to open a vast array of completely new applications for polymer-based nanocomposites [2–5]. Some of these building blocks can be produced with precisely controlled sizes, shapes and effective interaction potentials (including polyhedra, stars, patterned spheres, etc.), and as a consequence they have the potential to assemble into a wealth of complex patterns [5]. Their use in conjunction with self-assembling block copolymers can result in ordered hierarchical structures with significantly

enhanced properties, compared to those with "randomly" dispersed particles [5–7]. Sometimes, the nanoparticles actually drive the microphase separation of the block copolymers towards new or unexpected morphologies. See Refs. [8–14] for representative theoretical studies of these systems. Here we shall concentrate on the description of more conventional composites, in which the nanoparticles are either spherical or statistically isotropic aggregates of spherical particles (carbon back), and the matrix is a homopolymer melt or a cross-linked elastomer. Nanocomposites with semi-crystalline polymers (possibly also semi-conducting: to date, the most efficient organic photovoltaic cells are based on blends of polythiophenes and fullerene nanoparticles [15]) or hydrogels [16] will also be excluded. So far they have received little attention from the theoretical and computational points of view, but due to their importance and their challenging level of complexity we expect that they will soon start to be the subject of intensive study. Similarly, we shall concentrate mostly on the mechanical properties of the nanocomposites. Thermal, electrical and gas-transport properties, which are also important and even simpler from some points of view, will be left out to keep the review within reasonable limits.

Going back to Kraus' words [1], it is certainly true that the elastomeric materials obtained by incorporation of fillers (together with several other minority components) and subsequent cross-linking still represents a complex system by many standards. Still, in the latest years we have witnessed the emergence of a certain consensus about the basic mechanisms of elastomer reinforcement by fillers, including the way it is affected by particle size, degree of dispersion, surface modification, etc. The credit for this progress goes to important advances in the preparation and careful characterization of *well-defined* model systems, but also to theoretical developments and the application of computer simulation to increasingly realistic models. We emphasize that, even though the experiments have been given precedence within the outline of this review, these developments have occurred simultaneously and there has been a two-way exchange of ideas among theorists and experimentalists. Thus, it is quite appropriate to say that progress has relied on an fruitful interplay of experiment and theory/simulation, following a pattern which has characterized the whole history of polymer science [17]. The aim of this review is to present these recent developments, highlighting not only the successes but also the "failures" which, to the optimistic mind, represent the open challenges in the field.

Several related reviews have been produced in recent years by Heinrich, Vilgis and coworkers [18–21]. These concerned mostly theoretical developments (i.e., analytical calculations, scaling analyses [22], etc.), while the present review gives greater emphasis to recent computer simulation work, thus providing a complementary view of the field. We stress that, while computer simulation of nanocomposites has become a relatively "hot" topic over the last 6–7 years, theory still plays an important role as a support to both experimental and computational work. Furthermore, theory can address time- and length-scales, which are still not accessible to conventional computational approaches. For example, all the simulations to be discussed here consider spherical or near-spherical nanoparticle geometries. At present, all the important issues related to the fractal structure of carbon black or silica aggregates can only be addressed by the not-so-old-fashioned theoretical tools.

The general outline of this review is as follows:

- *Section 2*: Illustration of "classic" results on the linear and non-linear viscoelastic properties of filled elastomers, together with a brief overview of recent experimental results obtained by applying innovative characterization techniques (solid-state NMR, high-resolution microscopies or scattering methods, for example) on well-defined model systems.
- *Section 3*: Monte Carlo and molecular dynamics simulations of the equilibrium behaviour of the polymer chains within the matrix (chain conformation and packing at the interface with the filler, for example).
- *Section 4*: Molecular-scale theories of the equilibrium behaviour of polymers in nanocomposites and narrow slits, including also the equilibrium distribution of the nanoparticles.
- *Section 5*: Molecular-scale computer simulations and theories, describing the dynamical aspects of polymer chain behaviour in nanocomposites (reduced or enhanced chain mobility and alteration of the glass transition temperature next to a particle surface).
- *Section 6*: Molecular, mesoscopic or continuum-level approaches towards the calculation of the

overall viscoelastic response of the polymer–nanoparticle composite.

- *Section 7*: Conclusions and perspectives.

2. Overview of the basic phenomenology and recent experimental results

The dispersion of micro- or nano-scale rigid particles within a polymer matrix often—but by no means always—produces an enhancement in the properties of these materials [1–3,23–27]. As mentioned in the Introduction, the most important application of this sort involves rigid colloidal particles (originally carbon black, later also silica) in a cross-linked elastomer matrix, where an improvement of mechanical properties is sought. This so-called "rubber reinforcement" is a complex phenomenon, which may involve an enhanced grip of tyres on wet roads, an improved resistance to wear and abrasion, and an increase of its ultimate mechanical strength (toughness, tearing resistance). The latter problem has recently started to be addressed also by computer simulations [28]. For the purpose of the present review, however, we shall be mostly concerned with gaining an understanding of two basic facts:

(a) under very small cyclic deformations, there is a linear viscoelastic regime characterized a very significant increase—by one, sometimes almost two orders of magnitude compared to the reference unfilled network—of the in-phase storage modulus, both under elongation (E') and under shear (μ', alternatively indicated also by G');
(b) at medium-to-large strains, the system has a markedly non-linear response which is absent in unfilled elastomers ("Payne effect"). The degree of non-linearity increases strongly with particle loading. An order-of-magnitude drop in the modulus is often observed on going to 5–10% deformation (under shear), bringing the asymptotic modulus of the filled systems much closer to those of the reference unfilled network.

These phenomena are illustrated in Figs. 1 and 2 for two completely different systems, thus demonstrating their ubiquity. Very similar phenomena are actually observed in cross-linked elastomers and in particle-filled polymer melts, which are of interest in the context of rubber processing [27]. As will be

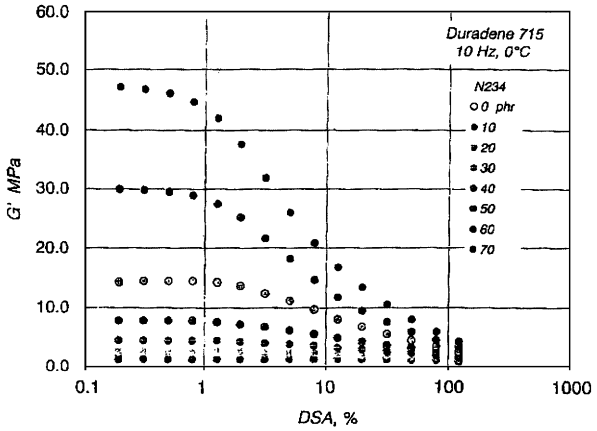

Fig. 1. Strain-dependence of the shear storage moduli of a cross-linked styrene–butadiene rubber filled with N234 carbon black at different loading levels (in phr: grams of filler per 100 g of polymer). On the abscissa, DSA stands for "double strain amplidude". Reproduced with permission from Wang [26], copyright (1998) of the Rubber Division, American Chemical Society.

clear shortly, this near-universality does not necessarily imply a universal explanation, or that this explanation is universally accepted. In fact, this is precisely the main point for arguments. Many research efforts have been devoted to devising ways of reducing the Payne effect (b), without compromising (a) or other important material properties.

Other related effects are commonly observed in filled elastomers. One is deformation hysteresis ("Mullins effect"): under cyclic deformation, the elastic modulus in first cycle is higher than that in the following ones. This points to some kind of "damage" of the material, which, however, is often reversible. The original properties are recovered within a few hours, by high-temperature annealing of the sample. Secondly, fillers affect also the dissipative, out-of-phase components of the modulus (E'' and μ''). This is expected, since (for example) friction of the polymer chains against the filler surfaces or of two particles against each other produces new energy dissipation mechanisms, which are absent in unfilled elastomers. Elastic and dissipative effects likely share a common origin, as demonstrated by the fact that the height and position of the maximum in μ'' (as a function of strain) is related to the magnitude and position of the drop in μ'. Finally, reinforcement effects have a remarkable temperature dependence. The small-strain (linear) modulus μ' of filled rubbers *decreases* with temperature. This points to important enthalpic effects, such as "bonds" or "interactions" which

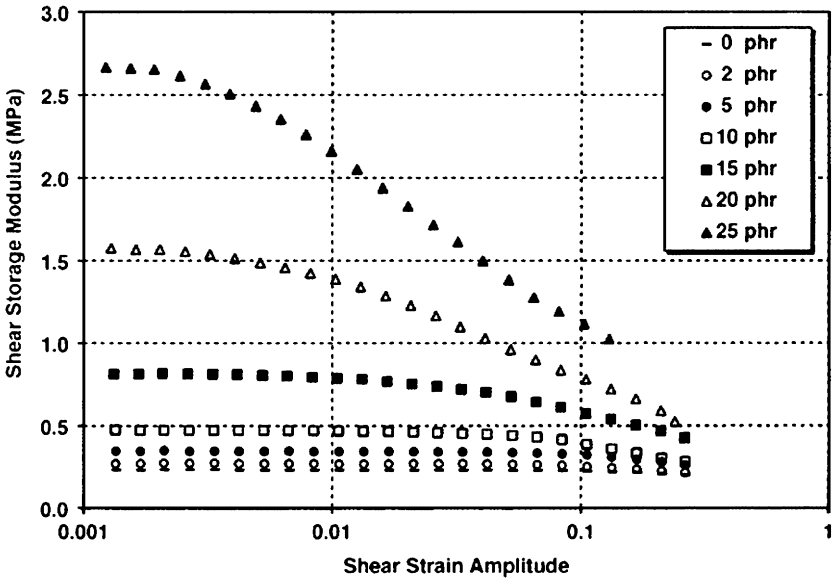

Fig. 2. Strain-dependence of the shear storage moduli of a poly(vinyl acetate) melt filled with fumed silica particles at different loadings, measured at 90 °C and 5 Hz. Reproduced with permission from Sternstein and Zhu [33], copyright (2002) of the American Chemical Society.

are broken or loosened on going to progressively higher temperatures. The situation is completely reversed compared to unfilled elastomers, where the modulus *increases* linearly with absolute temperature due to the entropic nature of rubber elasticity. Enthalpic interactions must also be summoned to stabilize nanoparticle dispersions in polymer melts against re-aggregation. The reason is that entropy actually works against dispersion, mainly because of the polymer-mediated "depletion attraction" among the particles (to be discussed in the Section 4).

One way or the other, most of the arguments about the origin of rubber reinforcement and its non-linear behaviour have been about the precise nature of these enthalpic interactions. The "textbook interpretation" was first proposed long ago by Payne himself (see e.g., Chapter 3 in Refs. [1,23]). According to this model, *particle–particle interactions* (van der Waals, hydrogen bonding, or other [29]) produce the main part of the reinforcement at small strains. The breakup of the "secondary network" formed by the filler particles is also responsible for the softening of the material at moderate-to-large strains. Eventually, at large strains all these interactions are disrupted, thus bringing the modulus close to that of the unfilled network. This interpretation was first formalized within a theoretical framework by Kraus [20,30] (see Section 6). Recently, this particle–particle picture has been increasingly challenged, first by Maier and Göritz [31] and later by others. Because of these disagreements, it is important to distinguish between the "Payne effect" and the "Payne interpretation" of this effect. These Authors [31] suggested that strain softening (including its frequency and temperature-dependence) could be explained by a dynamic adsorption/desorption process of the polymer chains at the interface with the filler. Even though this picture may not be necessarily correct or apply to all situations, it makes a strong point by putting much greater emphasis on *polymer–particle interactions*. Their importance has been increasingly appreciated, especially since the introduction of surface modifications of silica particles to enhance their compatibility with hydrocarbon polymers (no modification is usually necessary in the case of carbon blacks). Unfortunately, it has proved difficult to reach a consensus because it is very difficult to discriminate clearly between polymer–polymer and polymer–particle interactions, since surface modification of the particles inevitably affects both of them [29]. Instead, compared to experimental studies, computer simulation has the appealing feature of allowing "virtual experiments" in which these components are varied independently in well-defined way.

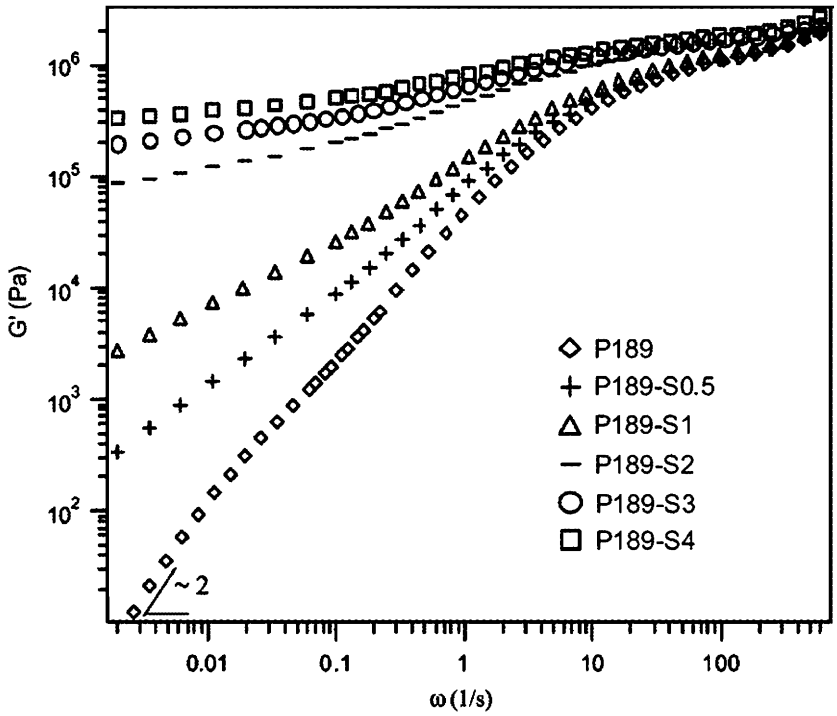

Fig. 3. Liquid-to-solid-like transition in silica-filled melts of poly(ethylene oxide), as evidenced by plots of $G'(\omega)$ in the linear regime (small strains). The figure shows the effect of particle volume fraction (S0.5 to S4 indicate filler contents from $\phi = 0.5\%$ to 4%), for a fixed polymer molecular weight (P189 indicates a polymer sample with $M_n = 189{,}000$ g/mol). Reproduced with permission from Zhang and Archer [34], copyright (2002) of the American Chemical Society.

A related thread of arguments concerns the appropriate level of description for these systems. Can reinforcement be understood under the continuum hypothesis, or is the molecular nature of the matrix important? The Payne interpretation, being based on particle–particle interactions, is insensitive to molecular-level details. Indeed, Payne himself had observed shear thinning also in carbon black dispersions in short-chain hydrocarbons. For obvious cultural reasons, the continuum picture has been popular also with mechanical engineers, approaching the field of polymer nanocomposites "from the top" (i.e., with a background in conventional composites with larger particles). Instead, other authors have emphasized the importance of (macro)molecular-level phenomena. Again for obvious reasons, this approach has been taken mostly by scientists with a polymer background, approaching the problem "from the bottom". Can we reconcile or find a compromise between these seemingly opposite views?

As mentioned in the Introduction, over the last decade some of these long-standing problems have started to be addressed by careful experimentation on well-defined model systems [32–38]. Significantly, all these studies concentrated on polymer melts rather than networks—often with a narrow molecular weight distribution—and, with the exception of Ref. [32], silica nanoparticles. Compared to carbon black, silica has two important advantages for fundamental studies: it has a simpler geometry (it can be produced in spherical particles, sometimes also nearly monodisperse) and it can be functionalized in different ways [24,38] to control its degree of interaction with the polymer (i.e., compatibility to enhance dispersion and/or mechanical coupling by covalent or non-bonded interactions). Very low particle loadings (less than 5% in volume, say) have also been investigated, to study the particle–filler interface without the interference of particle–particle interactions. An example of the insights which can be obtained in this way is given in Fig. 3, [34] showing a transition from liquid-like ($G' \cong \omega^2$) to solid-like behaviour ($G' \cong$ const.) on increasing the particle volume fraction. Increasing the polymer molecular weight lowers the particle volume

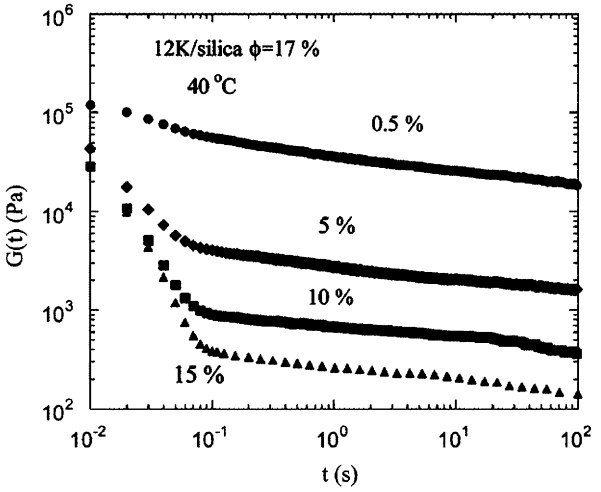

Fig. 4. Relaxation modulus of a filled elastomer (PB with $M_W = 11.6$ kg/mol, filled with silica at $\phi = 17\%$), following an instantaneous shear deformation (from 0.5% to 15%). Reproduced with permission from Zhu et al. [37], copyright (2005) of the American Chemical Society.

fraction at the transition. This can be as low as 2%, for a high-molecular-weight polymer. A likely explanation put forward by these [34] and other Authors [32,37], is that the systems turns solid-like when the polymer chains are long enough to form long-lived bridges between the particles, which effectively behave as highly functional cross-links. Another example is given in Fig. 4, showing the time-dependent response of a silica-filled butadiene (PB) melt obtained in a stress-relaxation experiment [37]. This system also exhibits a liquid-to-solid-like transition with particle content, as probed by linear viscoelasticity. When subjected to an instantaneous shear deformation of at least 5% (i.e., in the non-linear regime), the system responds by a well-defined two-step process. The first process has been identified with particle displacements roughly following the macroscopic deformation, and the second one with the ordinary linear relaxation as seen in small-strain experiments. This may involve both small adjustments in the particle positions, and the relaxation of the polymer chains to the new equilibrium configuration.

Going back to particle–particle and polymer–particle interactions, a lot of direct experimental evidence has accumulated recently, demonstrating their presence and its consequences in particle-filled polymers. Friedlander and coworkers have used atomic force microscopy (AFM) and high-resolution electron microscopies (SEM, TEM) to study individual filler aggregates, their deformation and breakup [39–41]. They argue that the measured forces are of the correct order of magnitude to explain the observed mechanical behaviour of nanocomposites. Most of their measurements were performed *in vacuo* (but see Ref. [40]). However, in a polymer nanocomposite—especially one in which the polymer and the particles are sufficiently compatible—there should be few direct particle–particle contacts. Most of these are likely to be mediated by a (possibly very thin) intervening layer of adsorbed polymer chains.

In the early days, the strength of polymer–filler interactions was gauged by the phenomenon of ''bound rubber'', namely the fraction of polymer in an uncured compound which cannot be extracted by a good solvent due to adsorption of the macromolecules onto the filler surface [27,42–44]. Unfortunately, this is a very indirect measure, which does not discriminate clearly between physical and chemical interaction mechanisms, nor provide an estimate of the interaction between the filler and a single-polymer segment (a long polymer chain may have multiple adsorption sites). A more direct measure of polymer–filler interactions is provided by inverse gas chromatography (IGC) [24,45,46], in which the filler is used as the stationary phase in a chromatographic column. The retention times of a whole series of small-molecule gas probes (e.g., saturated or unsaturated hydrocarbons containing 1–10 C atoms) are correlated with their adsorption energies on the filler. A recent application of this technique has demonstrated the existence of at least four types of interaction sites on the surface of carbon black, with energies between 16 and 30 kJ/mol [46].

Another manifestation of polymer–filler interactions is the so-called ''rubber shell'' [26]. This is a layer of polymer at the interface with the filler, in which the mobility of the chains is restricted in comparison to those in the bulk at the same temperature. It may be due to strong chain adsorption, but also to an increased density of entanglements due to polymer–filler attachments. In a polymer melt, its thickness should be roughly comparable to the average radius of gyration of the chains. This interfacial layer is certainly present also in conventional polymer composites, but it becomes increasingly important in nanocomposites, where the average chain radius becomes comparable to average particle size and interparticle spacing.

Experimental evidence of the existence of a broad distribution or even two distinct glass transition temperatures (T_g's)—one for the bulk polymer and the other (usually higher) for the chains belonging to this rubber shell—has increasingly accumulated thanks to a range of methods, such as dynamic mechanical thermal analysis (DMTA) [47], quasi-elastic neutron scattering (QENS) [48], solid-state NMR techniques [49–52] and spectroscopy of fluorescent molecular probes [53]. Comparable T_g shifts have been observed also in simple as well as polymeric liquids confined between closely spaced surfaces or within nano-sized pores [54].

The rubber shell has implications for the Maier-Göritz model [31] as well as other, non-conventional interpretations of reinforcement, which localize the Payne effect at the rubber–filler interface. Sternstein and Zhu [33] suggested that the Payne effect is produced by the release of trapped entanglements at the rubber–filler interface, under large strains. Lequeux, Montes et al. [35,36] proposed an even simpler picture, in which the polymer is divided into a rubbery bulk region (above its T_g) and a glassy shell of thickness δ close to the particles (below its T_g). The boundary between them is represented by the material whose glass transition coincides with the actual measurement temperature. Within this framework, strain softening arises from the plasticization of the rubber shell bridging neighbouring particles. Note that this is a generic continuum picture [35,36], which, unlike those of Maier and Göritz [31] and Sternstein and Zhu [33], does not invoke polymer-specific phenomena at the rubber/filler interface. Wang and coworkers [37] challenged the universality of this interpretation, mainly because of their observation of a significant Payne effect even at temperatures 100 °C above the T_g of the unfilled polymer (1,4-polybutadiene) and the dependence of reinforcement on polymer molecular weight. They stressed once more the importance of polymer bridges directly connecting neighbouring particles, following earlier suggestions by others [32,34].

Sample morphology—size, shape and above all the degree of dispersion of the particles—is clearly an important parameter for elastomer reinforcement. Nowadays, several methods have become available which provide a direct measure of this morphology. The simplest and most widely used one is probably AFM. Transmission electron microscopy (TEM) [45,55] can in principle provide higher resolution, but requires more elaborate sample preparation and careful data analysis to avoid artefacts. Small-angle X-ray and neutron scattering (SAXS, SANS) have also reached a high level of sophistication. With modern instrumentation, it is now possible to probe extremely small q-vectors, corresponding to structures above the 100 nm range [56–58]. Also in this case, interpretation of the scattering data to obtain the real-space morphology is not straightforward. The analysis is generally performed by fitting the scattering data with some pre-defined functional form (structure factors for spheres or fractal aggregates, for example). Thus, data modelling is not automatic and it requires the *a priori* definition of a structural model. Reverse Monte Carlo techniques may provide a more flexible, robust and model-independent tool for the analysis of scattering data [59].

AFM and SANS/SAXS measurements have also been performed on stretched samples [56,57,60]. Deformation at the scale of the filler particles is expected to be non-affine (i.e., different from the macroscopic deformation), to avoid particle "collisions" perpendicular to the direction of stretching. This is indeed the case, as demonstrated by careful AFM measurements tracking the motion of individual silica nanoparticles [60]. At large deformations, the particles actually tend to form layers or bands, oriented perpendicularly to the direction of stretching. In this respect, there is consistency between the AFM [60] and SANS [56] or SAXS [57] measurements on silica- and carbon-black-filled elastomers, which at relatively large loadings exhibit a characteristic "butterfly pattern" seen also in gels and other heterogeneous soft materials. SANS measurements on partially deuterated polymer samples have also been used to investigate the average conformation of the chains, both in the underfomed state (are the chains unperturbed, as in unfilled polymer melts?) [61] and stretched samples (do the chains deform affinely?) [62].

An interesting model study of nanoparticle dispersion in macromolecular melts was recently published by Mackay et al. [63]. In their experiments the polymer is linear polystyrene whereas the nanoparticles consist of either branched, dendritic polyethylene or branched polystyrene. The Authors show that, in the homogeneous nanoparticle dispersions: (i) the system is thermodynamically favoured if the radius of gyration of the linear polymer is larger than that of the nanoparticle, and (ii) under these conditions the polymer radius of gyration increases, growing with the nanoparticle

volume fraction. In the Author's view, with long chains the homogeneous system is favoured by the enthalpy gain from polymer–particle interactions and the particles act as swelling solvent molecules. If the chains are short, the classic phase-separating blends may form; in the particle-rich phase polymer–particle interactions still exist due to accommodation of the chains in the inter-particle voids.

In this brief summary of experimental results, we have highlighted a number of general problems and open questions, and also hinted at some possible explanations. It is now time to turn to the main subject of this review, namely the way in which these problems have been addressed by theoretical and computational tools.

3. Molecular-level simulations: equilibrium aspects

3.1. Introduction

Computer simulations of chemical systems consisting of conformationally rigid molecules in disordered or partially disordered states (liquids, solutions, sometimes even liquid crystals) are limited today only by the availability of detailed information on the forces acting between the atomic centres. Given a suitable force field, the molecular dynamics (MD) and the Monte Carlo (MC) methods [64,65] are normally quite efficient for equilibrating and sampling the system under study at a given temperature and for evaluating the properties of interest. When the system contains large and conformationally flexible species—as in amorphous or semi-crystalline polymers—the simulation procedure becomes much less straightforward [66]. On one side, the applicability of the MD method depends on the intrinsic time scale of the conformational transitions, so that the total time that can be covered in a simulation may be insufficient to sample adequately all possible chain conformations. On the other side, the efficiency of the MC method is lowered by sample attrition (i.e., the larger the change of molecular shape when going from one conformation to the other, the lower the probability that the transition is accepted due to unfavourable interactions with adjacent molecules). Simulations performed at the atomistic level are then usually confined to relatively short oligomers, while continuum or lattice coarse-grained models are used when the properties under study require the simulation of longer chains [66].

When attempting to simulate polymer-based nanocomposites, one has to deal with two further problems. Although current research efforts are focusing on increasingly small nanoparticles, the average filler diameter in most materials of theoretical and practical interest is much larger than the transverse diameter of the chains. Even using a coarse-grained model, a simulated cell with nanoparticles of this size would contain an excessive number of polymer beads for any practical volume fraction of filler. Therefore, simulations of polymer-based nanocomposites can be performed only with relatively small particles. Furthermore, these simulations are scarcely useful if they do not provide information on fundamental points such as the nature of the polymer/particle interface, the conformational changes induced by the presence of the particles, the average number of different particles in contact with a given chain, the average length of the polymer segments connecting two different particles, and so on. Except for the polymer/particle interface, that can be also studied by simulating the polymer in contact with the surface of a single nanoparticle or an infinite flat wall (equivalent to a particle of very large radius), it is then necessary to have a base cell with several (and consequently smaller) nanoparticles. In practice, simulations of this kind can be only performed for coarse-grained models and for particles of diameter less than 20 times the diameter of the beads.

The second problem originates from the relatively short length of the chains that can be simulated (the simulation of cross-linked polymer *networks* incorporating nanoparticles is of course even more problematic than the simulation of filled polymer *melts* and has hardly been attempted so far). While the properties of polymer systems can often be extrapolated from those of systems with chains of various length, this is not viable for the most relevant properties characterizing the molecular arrangement in nanocomposites. In fact, systems with the short chains that can be simulated contain a more or less large proportion of free chains (i.e., chains with all units far from the surface of any particle) and/or of chains that are in contact with only one particle and have thus long dangling terminal segments. Since free chains and dangling terminal segments are substantially converted to bridge segments connecting different particles when the chain length is increased, these simulations are unable to provide reliable information on the molecular arrangements in systems with chain

length in the polymer range. Therefore, methods based on phantom (i.e., non-interacting) chains have been recently developed to study this important aspect of polymer-based nanocomposites.

The present part of the review is focused on simulations of melts of chain molecules containing discrete nanoparticles. The first simulations of systems of this kind have been independently performed a few years ago by Starr et al. [67,68] using MD and by Vacatello [69] using MC coarse-grained methods. Essentially similar models and methods have been subsequently used in various MD [70–75] and MC [76–80] calculations to explore the effects of changing the size of the nanoparticles, the filling density and the strength of the nanoparticle–polymer interactions. Atomistic simulations of a silica nanoparticle embedded in a polymethylene matrix have been performed using MD methods [81]. Other MC simulations have been carried out for coarse-grained chains on the cubic [82,83] and on the tetrahedral lattices [84–87]. The MC method has been also used for phantom chain simulations with atomistic [76,88–92] and coarse-grained [76,93,94] chains.

The simulation of polymers near infinitely extended two-dimensional surfaces or confined within slits comprises a large body of work in itself, and for this reason these are largely excluded from the present review. However, they will be mentioned later in connection with theoretical description of chain packing close to a solid surface. The polymer reference interaction site model (PRISM) [95–99] and classical density functional theories (DFT) [99–101] represent two important theoretical tools for this type of problem. The former also provides the basis for the theoretical calculation of the polymer-mediated interaction energy between two particles as a function of their relative distance (the so-called potential of mean force or PMF). In turn, knowledge of this PMF allows a exploration of different scenarios and eventually calculation of a full polymer–particle phase diagram (e.g., addressing the question of the miscibility of the two components under equilibrium conditions). This problem cannot be easily studied by neither MC nor MD with present-day approaches and computational resources, mainly due to the fact that the particles are necessarily limited in number and they are virtually immobile over the time span of such simulations. Unless they are very small, the particles tend to retain the positions assigned to them at the beginning of the simulations, independently of whether this is an equilibrium or out-of-equilibrium one.

3.2. Strategy of MD simulations

The systems simulated in Refs. [67,68] consist of three-dimensional periodic arrays of cubic cells containing a single-filler nanoparticle in a melt of chains of 20 monomers each. Here, as well as in most other coarse-grained MD simulations, the chains are modelled as sequences of Lennard–Jones (LJ) centres. This is specified by a well depth ε and a bead diameter σ. The LJ minimum is found at $r_{min} \cong 1.122\sigma$. The beads are connected via finitely extensible non-linear elastic (FENE) anharmonic springs, characterized by a stiffness k and a maximum extension $R_0 = 1.5\sigma$ [102]. Similar, but stiffer FENE springs are used to tether 356 LJ centres to fixed positions, chosen to model the icosahedral nanoparticle of diameter approximately 10 times the diameter of the chain units. Calculations are performed at various reduced temperatures for the reference pure melt (100 chains at melt density), for filled systems with full monomer–nanoparticle LJ interactions (100, 200 or 400 chains, in order to model different volume fractions of filler) and for filled systems including only the repulsive part of the LJ potential (400 chains in all cases). The size of the base cell is chosen in the various calculations such that the polymer density far from the nanoparticle deviates in each case less than 0.2% from the density of the pure melt. The relative size of the various components in a 400 chains system is shown in Fig. 1.

An overall set-up similar to that of Refs. [67,68] is used in the MD calculations of Smith et al. [70], in which the chains are modelled as bead-necklace chains of 20 LJ units with constrained bond lengths, while the single nanoparticle placed in the base cell is modelled as a nearly spherical array of the same units, maintained rigid through the use of bond constraints. Systems with repulsive, neutral and attractive polymer–nanoparticle interactions are simulated. Only the repulsive part of the LJ potential is used in the first case, while the strength of the LJ nanoparticle–polymer interactions is doubled in the latter case with respect to the strength of the polymer–polymer interactions in neutral systems.

An essentially similar model with a slightly different set-up is used in the simulations of Hooper et al. [71], aimed at checking the PRISM predictions

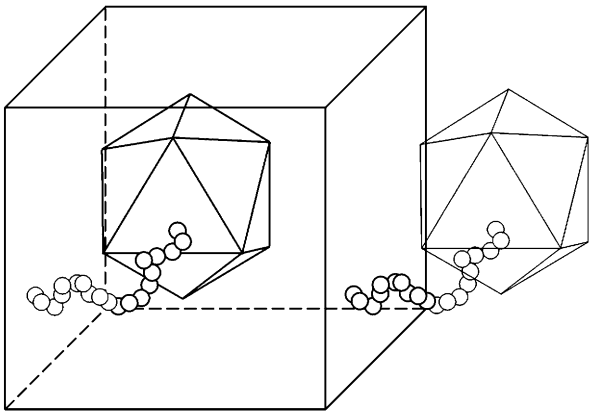

Fig. 5. Schematic representation of the base cell of Refs. [67,68], showing approximately the relative size of the various components in a system of 400 chains.

[95–97] for systems with various concentrations of polymer chains in the presence of nanoparticles. The base cell, of size $14*14*24\sigma^3$, contains in this case a variable number of chains of 80 units and two small nanoparticles of diameter 5σ placed along the longest side at various distances. The two nanoparticles are modelled as spherical centres interacting with the polymer units through an appropriate potential. The polymer density is varied from 0.13 to $0.85\,\sigma^{-3}$, i.e., from a semi-dilute solution up to a polymer melt. The same overall set-up (chains of 80 units and particles of diameter 5σ) has been later adopted by Desai et al. [72] to study the effect of the nanoparticles on chain diffusion. Calculations are performed in this case with one single nanoparticle in the centre, with two nanoparticles placed at the body centred cubic sites or with four nanoparticles placed at the face centred cubic sites of the base cell, giving a filling density equal to 2.5%, 5% or 10%, respectively.

The model of Refs. [67,68] (see Fig. 5), with a single relatively large nanoparticle in the base cell, corresponds to a spatial distribution in which the nanoparticles are placed at the nodes of a cubic array. Systems containing in the base cell many nanoparticles of this size are prohibitively large for the MD method. Therefore, particle clustering in polymer-based nanocomposites has been more recently studied by Starr et al. [73] by simulating smaller icosahedral nanoparticles and shorter chains of 10 units, in such a way that the diameter of the particles is approximately equal to the chain radius of gyration. Simulations are performed for filler volume fractions between 0.05 and 0.3 and for various nanoparticle–polymer interaction strengths. The systems are prepared by introducing the nanoparticles into cavities grown in the equilibrated melt; they are then relaxed at quite high temperatures, and finally at the desired temperature under constant pressure. The final production simulations are performed in the NVT ensemble. Similar systems with several small nanoparticles of diameter nearly half the root mean square (rms) radius of gyration of the chains have been simulated by Kairn et al. [74] with the purpose of comparing the steady-state shear behaviour of such systems with experiments. In close analogy with the actual experimental conditions, the viscosity of these model systems was measured by applying a shear field through appropriate boundary conditions and measuring the resulting stress (non-equilibrium molecular dynamics method or NEMD). An alternative approach to the evaluation of the shear viscosity of a nanocomposite was followed by Smith et al. [70] and Keblinski et al. [75], who obtained it from the analysis of standard equilibrium MD simulations. These two approaches will be discussed in Section 6.

The MD method has been also used by Brown et al. [81] to perform atomistic simulations of a silica nanoparticle embedded in a polymethylene matrix. The silica nanoparticle is obtained by first creating and equilibrating an α-quartz structure, and then discarding all atoms outside a sphere of 2 nm radius in such a way to have an electrically neutral cluster of 914 silicon atoms and 1828 oxygen atoms. The polymer matrix consists of a single long chain of 30,000 CH_2 groups (represented at the united atom level) with fixed bond lengths and appropriate valence angle and torsion angle potentials. After relaxing the polymer alone (without the nanoparticle) to a near-equilibrium condition using first MC and then MD methods, a cavity is grown in the centre of the base cell while also expanding the cell, slowly enough to avoid disruption of the polymer matrix. The nanoparticle is then inserted into the cavity and the composite system of 32,742 atoms relaxed under NPT conditions to reach the appropriate melt density.

3.3. Strategy of MC simulations

MD simulations are well suited to study local arrangements and dynamics of the polymer units at the polymer/nanoparticle interface. However, due to the set up of the models (very small nanoparticles and quite short chains), they do not provide insight

on the overall arrangement of chains and particles in practical polymer-based nanocomposites. This requires systems with longer chains and several larger nanoparticles in the base cell, which are more accessible to MC methods. Simulations of this kind have been performed in Ref. [69] for a reference polymer melt and for two filled systems containing 409 chains and 34 randomly distributed nanoparticles of diameter 10σ in one case, and with 9 nanoparticles of diameter 16σ in the other case. The polymer chains are modelled as strings of 100 LJ centres connected by links of fixed length, equal to the minimum-energy distance of the LJ potential. The chain stiffness is regulated by a bending potential $E(\theta) = k_\theta\theta^2$ (θ being the angle between consecutive links; $\theta = 0$ for collinear links). All parameters are chosen such that, when the chain beads are identified with poly(methylene) isodiametric units (i.e., $\sigma = 0.45$ nm, 3.5 CH_2 groups per unit [103]) the unfilled system models quite well packing and conformations in a poly(methylene) melt. The nanoparticles are simulated as spherical entities, where the same LJ parameters used for the interactions among polymer units is used also for particle–particle and polymer–particle interactions (but, in these cases, distances entering the LJ potential are measured from the particles *surfaces* rather than the particle centres).

The nanoparticles are first randomly placed in the base cell, in such a way that the minimum distance between their surfaces is not less than 0.7σ. The chains are then grown at random in the environment of the nanoparticles with an appropriate mechanism, such that all bead–bead and bead–particle distances are also greater than 0.7σ. The systems are then equilibrated using reptation for the chains and local displacements for the nanoparticles. Fig. 6 shows a partial snapshot of an equilibrium configuration of the system with nanoparticles of diameter 16σ. Systems with base cells containing several randomly distributed nanoparticles of various size (from 4 to 28σ) and various filling densities (from 0.1 to 0.5 volume fraction of filler) have been subsequently studied using the same methods [76–78].

Essentially similar models have been later used by Zhang and Archer [79] to simulate systems with longer chains of 550 units in the presence of nanoparticles of diameter 12σ, and by Papakonstantopoulos et al. [80] to study the local mechanical properties in systems of shorter chains of 32 units and smaller nanoparticles of diameter 5σ. One

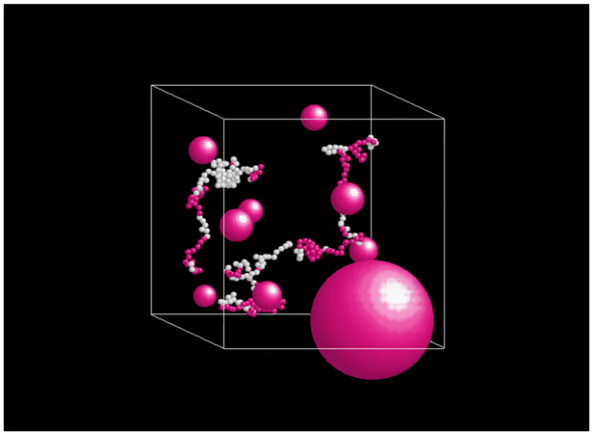

Fig. 6. Partial snapshot of an equilibrium configuration of a system with nanoparticles of diameter 16σ. The size of the nanoparticles (except one) has been reduced to show the spatial arrangements of some chains. Chain units in white are at less than 2σ from the surface of a nanoparticle. Redrawn with permission from Vacatello [69], copyright (2001) of the American Chemical Society.

distinctive feature of Ref. [79] is that the authors evaluated by a preliminary set of simulations the polymer-mediated PMF between the nanoparticles. Pure nanoparticle systems without polymer were then equilibrated with this potential and used as starting points for generating filled systems with the equilibrium distribution of nanoparticles. Several different MC jump mechanisms were used in Ref. [80] to accelerate equilibration of the polymer chains near the surface of the nanoparticle, including random local moves, configurational-bias reptation moves, internal rebridging and double rebridging.

MC simulations with chains of 100, 200 or 400 units have been performed by Ozmusul et al. [82] on a simple cubic lattice with bond lengths between 1 and $\sqrt{3}$ lattice spacings (i.e., the coordination number is 26). All cells contain 27 fixed nearly spherical nanoparticles, placed in a cubic arrangement or at random, of radius similar in each case to the radius of gyration R_g of the chains. The size of the base cell is chosen such that the closest distance between the surfaces of neighbouring nanoparticles (when in the cubic arrangement) equals $0.5R_g$, R_g or $2R_g$. Except for the excluded volume condition, there are no interactions between polymer units, while weak, moderate or strong interactions between polymer units and filler are imposed through a potential well of depth 0.2, 2 or 10 kT, respectively, extending up to $\sqrt{3}$ lattice spacings from the surface of the filler.

A different model set-up has been later used by Lin et al. [84] and by Erguney et al. [85] to simulate poly(methylene) (PM) and poly(oxyethylene) (POE) melts in the presence of nanoparticles. The systems are modelled in this case according to the second nearest neighbour diamond lattice method (SNND), originally developed by Rapold and Mattice [104,105]. The conformational statistics of the chains is regulated by first and second interactions in the frame of the rotational isomeric state (RIS) approximation, while the interactions between polymer beads are modelled using a lattice approximation of the LJ potential. This model represents the conformation of real chains better than other coarse-grained methods, and it allows a simple reverse mapping of the simulated systems to continuous space atomistic models [106]. Well-equilibrated SNND melts of PM and POE have been used in Refs. [84,85] as starting points for simulating these two polymers in the presence of nanoparticles. The latter are generated by arbitrarily increasing the strength of the attractive intramolecular interactions for a number of chains selected at random. The filler nanoparticles are thus modelled by polymer chains that are forced to collapse to a variable extent, depending on the strength of the additional attractions (i.e., the selected chains can be more or less partially collapsed, and the filler particles are thus more or less partially permeable to the matrix chains). Various systems are simulated with different lengths of the polymer chains and of the collapsed chains and with different sizes and number densities of nanoparticles. The SNND method has been used also by Dionne et al. [86,87] for simulating a PM melt containing spherical nanoparticles. Simulations are performed for chains of 80 beads (220 in one case) at various partial volumes of filler (from 1% to 10%) with one single nanoparticle of diameter from 0.7 to $1.3R_g$ in the base cell. The latter is a distorted cube with 60° angles, such that the nanoparticles are arranged in a close-packed array.

The conformational distribution of chain molecules in the presence of nanoparticles has been studied by Mark and coworkers in a series of MC simulations [88–92] of phantom (i.e., non-interacting) PM and poly(dimethylsiloxane) (PDMS) chains with nanoparticles in various arrangements. The phantom chains are generated according to the conditional probabilities dictated by a RIS model appropriate for the polymer under study, and all situations leading to overlaps of any part of the chains with the filler are discarded. The nanoparticles, modelled as spherical entities (oriented ellipsoids in Ref. [91]), are placed either in a simple cubic arrangement [89,91] or at random [90,92]. Chain lengths of 50–300 skeletal bonds are considered in most simulations with relatively small particles, while much longer PM chains of 1000 or 2500 bonds are considered in Ref. [92] with nanoparticles of diameter from 2 to 40 nm at various filling densities. Similar calculations for PM and PDMS chains of 300 bonds with randomly distributed nanoparticles have been performed by Vacatello [76]. This paper shows that the distribution of matter and the chain conformation obtained from phantom chain simulations of this kind approximate those in dilute polymer solutions with suspended nanoparticles, but are quite different from those in filled polymer melts. Therefore, in subsequent phantom chain simulations [93,94], Vacatello applied an enhanced LJ attraction between the polymer and filler in order to compensate the entropic repulsion of the polymers from the surfaces. This re-establishes a homogeneous polymer density within the sample, restoring at the same time the conformational distribution and all other equilibrium properties. The same method can thus be applied to systems with very long chains and large particles. For instance, recent calculations [94] have been performed for large systems with chains of realistic length (2000 units, corresponding to PM chains of molecular mass on the order of 10^5 amu) and nanoparticles of diameter 50 times the diameter of the chain units at filling densities between 5% and 20%.

3.4. Structure of the polymer/nanoparticle interface

Figs. 7 and 8 show the density of polymer as a function of the distance from the centre of a nanoparticle for the two coarse-grained MC systems with nanoparticles of diameter 10σ (system M_{10}) and 16σ (system M_{16}) [69] (Fig. 7), and for the atomistic PM system containing a single silica nanoparticle simulated by MD in Ref. [81] (Fig. 8). Although the calculations have been carried out with totally different methods and for quite different models, the organization of the polymer at the interface with the nanoparticles in the equilibrated systems turns out to be very similar. In all cases, the curves are characterized by a series of maxima and minima of decreasing intensity from

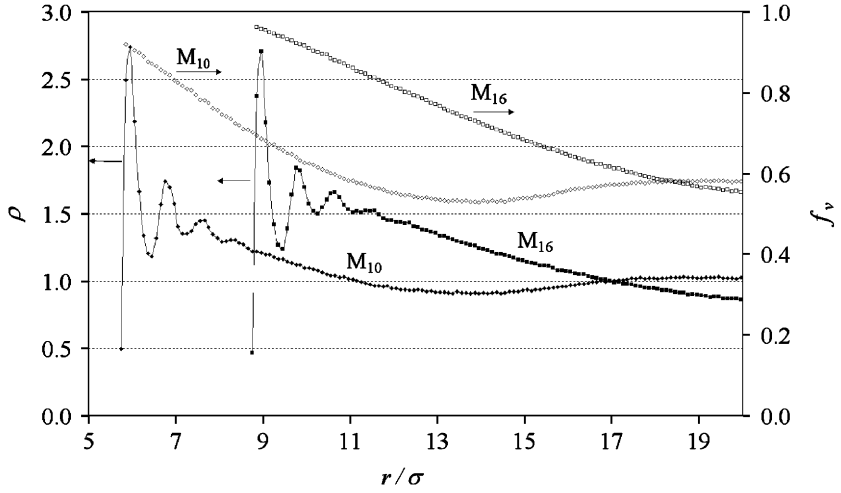

Fig. 7. Normalized density of polymer units (ρ, full symbols, left scale) and volume fraction not occupied by filler particles (f_v, open symbols, right scale) as a function of the distance r from the centre of a nanoparticle. Redrawn with permission from Vacatello [69], copyright (2001) of American Chemical Society.

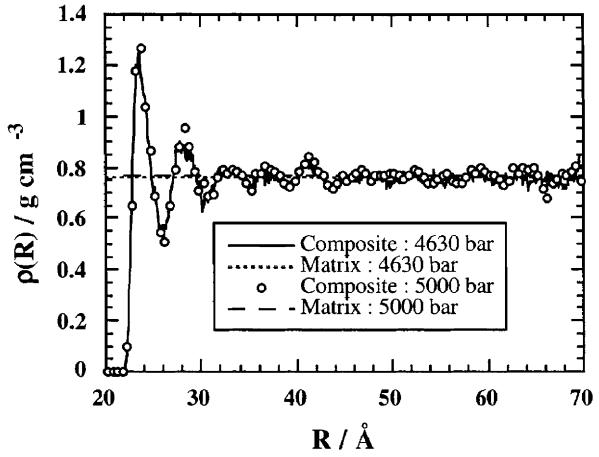

Fig. 8. Mass density of polymer as a function of the distance from the centre of the silica particle. Reprinted with permission from Brown et al. [81], copyright (2003) of the American Chemical Society.

the surface of the nanoparticles, with a characteristic spacing of approximately 0.8σ in Fig. 7 and 0.4 nm in Fig. 8. Since σ is nearly 0.45 nm for PM [103], the results of considerably different simulations are in good agreement in this respect. The same sequence of maxima and minima with spacing close to the transverse diameter of the chains has been observed in all other calculations performed for polymers in the presence of nanoparticles, the location and relative intensity of the maxima depending on the strength of the polymer/nanoparticle interaction forces. Not unexpectedly, this behaviour is closely similar to that found near planar surfaces (see for instance [107,108] and references therein).

On the other hand, the plots in Fig. 7 show a number of peculiar features not observed in Fig. 8, i.e., a broad maximum near the surface of the nanoparticles followed by a broad minimum centred around 14σ for system M_{10} or by a monotonous decrease for system M_{16}. Similar features are present in the corresponding plots for all other systems simulated in Refs. [77,78]. This behaviour is related to the fact that the base cells of Refs. [69,77,78] contain several nanoparticles placed at random, rather than one single nanoparticle. Therefore, the various spherical shells surrounding a given particle are partly occupied by other particles (upper curves, right scale in Fig. 7), such that the volume fraction of each shell available to the polymer depends on the mutual arrangement of the nanoparticles. When this is properly taken into account, the distribution of the polymer units in the available volume of the various shells turns out to be practically coincident with the distribution of Fig. 8 and with that near planar solid surfaces.

The high densities observed in the first polymer shells surrounding the nanoparticles are expected to be associated with a correspondingly high degree of orientational and conformational order. The former has been studied in Refs. [69,81] by plotting the second Legendre function $P_2(\cos\theta) =$

$(3\langle\cos^2\theta\rangle-1)/2$ as a function of the distance from the particle surface, where θ is the angle between the local direction of the polymer chain and the outward normal to particle. P_2 tends to -0.5 for polymer segments arranged parallel to the surface, while it is 0 for totally random orientation. Although the local direction of the chains is defined differently in the two cases [69,81], the two calculations confirm the natural intuition that polymer segments in close contact with the nanoparticles are preferentially oriented parallel to their surface. In fact, the value of P_2 for segments within the first density peak is largely negative in both cases. Following this region, the atomistic system of Ref. [81] shows a series of maxima and minima of P_2 analogous to those seen for the density in Fig. 8, the maxima of P_2 corresponding to the density minima and vice versa. Short-range features of this kind are not observed in the system of Ref. [69], due to the more coarse-grained representation of the chain and its envelope. However, the curves of P_2 show in this case broad maxima and minima in correspondence to the broad maxima and minima seen in Fig. 7, with the broad maxima of P_2 corresponding to the broad minima of the density and vice versa. Like for the density, these features are related to the presence of many independent nanoparticles in the base cell of Ref. [69]. The atomistic calculations of Ref. [81] also suggest that the chain segments in contact with the nanoparticle tend to be more in *trans* conformation than bulk segments. Although not unreasonable, the conclusion cannot be considered fully supported by the data of Ref. [81], since the average fraction of *trans* bonds in the composite and in the pure polymer are too high compared to that expected for PM at the same temperature (more than 80% in the simulations, compared to nearly 65% expected on the basis of the RIS model of Ref. [109]). Unfortunately, the distribution of *trans* bonds has not been analysed in the various SNND lattice simulations performed up to now.

In summary, the polymer/nanoparticle interface is characterized by a series of decreasingly dense and partly ordered shells of thickness slightly less than the transverse diameter of the chains. The perturbation of density and order due to the presence of a nanoparticle extends into the polymer several times this diameter (5–6 nm in Ref. [81]). However, the effects are mainly concentrated within approximately 2σ (slightly less than 1 nm in the case of PM) from the surface of the nanoparticles.

3.5. Conformations of the polymer chains

It is widely accepted that the polymer chains in a melt are unperturbed Gaussian coils and that their conformations can be described by RIS models appropriate for each polymer [109]. The nature and entity of the conformational perturbation induced in PM chains by the presence of nanoparticles have been first studied by the RIS phantom chain simulations described previously [88]. The calculations have been subsequently extended to PDMS chains of various lengths generated within a cubic [89] or random [90] arrangement of spherical nanoparticles of various sizes, the chains being started in the centre of the cube in the first case and in the centre of a hollow sphere in the second case. A relevant aspect of the calculations performed in Ref. [90] for randomly distributed nanoparticles is that they show a decrease of chain dimensions for large particles and short chains, and a strong increase of chain dimensions for small particles and long chains. For instance, the characteristic ratio of PDMS chains of 200 bonds at 400 K is found to be as large as 9.65 in a system with nanoparticles of 2 nm radius at a 7.5% filling density, to be compared with 6.41 in the unfilled system. In agreement with this prediction, subsequent small-angle neutron scattering (SANS) experiments on PDMS filled with polysilicate nanoparticles [61] show a decrease of the root-mean-square radius of gyration when the polymer chains are approximately the same size as the filler particles, and a substantial increase when the polymer chains are much larger. The experimental behaviour has thus been attributed in Ref. [61] to the same excluded volume effects responsible for the analogous behaviour of the RIS chains in Ref. [90] and seems to be related to the results by Mackay et al. [63].

However, similar MC simulations performed in Ref. [76] for PDMS and PM RIS chains of 300 bonds in the presence of randomly distributed nanoparticles fail to reproduce this behaviour, giving characteristic ratios of the chains smaller than the unperturbed value in all filled systems, irrespective of the relative size of chains and nanoparticles. In particular, the characteristic ratios of PDMS with nanoparticles of 2 nm radius at filling densities 5% and 10% are found to be at 400 K only 6.2 and 5.9, respectively (to be compared with 9.65 for 7.5% filling density in Ref. [90]; see before). It has been then suggested in Ref. [76] that the

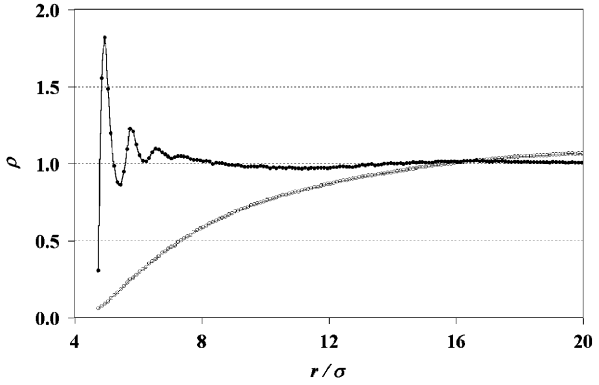

Fig. 9. The normalized density of chain units as a function of the distance from the centre of a nanoparticle for a system with 10% volume fraction of nanoparticles of diameter 8σ (upper curve) and for the same system with phantom chains (lower curve). Reprinted with permission from Vacatello [76], copyright (2002) of the American Chemical Society.

behaviour observed in the SANS experiments for the PDMS/polysilicate system cannot be simply attributed to excluded volume effects. Remarkably, further calculations on long PM chains carried out by the two groups predict an exceptionally large chain expansion (characteristic ratio nearly doubled for 1% partial volume of nanoparticles of diameter as small as 2 nm) in one case [92], and chain dimensions always smaller than in the unfilled melt in the other [111]. It would be clearly desirable that analogous simulations be independently performed by others in order to resolve this controversy.

On the other hand, the chain expansion found for some compositions in the PDMS/polysilicate systems studied in Ref. [61] and more recently in the PS systems studied in Ref. [63] cannot be explained on the basis of phantom chain simulations of this kind. In fact, despite of their theoretical interest, these simulations do not model accurately the behaviour of polymer nanocomposites. This has been clearly shown in Ref. [76], where well-equilibrated systems of coarse-grained chains have been used as starting points for new simulations in which the chains are converted to phantom chains by turning off the LJ interactions between chain units. Fig. 9 compares the normalized density of units as a function of the distance from the centre of a nanoparticle in a system simulated at full density (10% volume fraction of nanoparticles of diameter 8σ; upper curve) with the corresponding data obtained for the same system after converting the chains to phantom chains (lower curve).

Fig. 9 shows that the distribution of matter in the two systems is substantially different and that the density of units near the surface of the nanoparticles becomes negligible when the polymer chains are converted to phantom chains. By inspecting various simulations snapshots, it is seen that the phantom polymer units tend to concentrate in the largest cavities of the base cell. This behaviour is due to the loss of orientational and conformational freedom of the segments when the chain is brought in contact with a solid surface, and is consistent with the observation that polymer chains in dilute solutions tend to avoid non-adsorbing solid surfaces [112]. Increasing the attractive interactions between the nanoparticles and the phantom chain units within the interface shells progressively modifies the density curves until they become practically coincident with those for the corresponding systems simulated at full density (except for the oscillatory features close to the particle surfaces) [93,94]. With this correction, the chain conformation in the presence of nanoparticles has been found to be very similar to that in the unfilled melt, irrespective of the relative size of chains and nanoparticles.

Fig. 10 shows plots of $R_n^2/n\sigma^2$, with R_n^2 the mean-square distance of units belonging to the same chain and separated by n links, for various coarse-grained systems simulated in Ref. [71] with chains of 100 units and randomly distributed spherical nanoparticles. The subscripts indicate the diameter of the nanoparticles, and the filling density is 20%. The curve for the unfilled melt (system M_0) coincides with the theoretical prediction [109] for freely rotating chains with the bending potential $E(\theta)$ used in the simulations, showing that the model chains are actually bulk-like and unperturbed in this system. Considering that the radius of gyration of the chains is about 6.5σ, the systems studied in Fig. 10 cover the whole range from nanoparticles much larger than the chains to nanoparticles much smaller than the chains. The chain size in the filled systems is always decreased with respect to the pure melt, the decrease being anyway quite small.

Similar results are found in simulations performed for other models and with different methods. For instance, the radius of gyration and the mean-square end-to-end distance of the short chains simulated by MD in Refs. [68,71] show no changes with respect to the unfilled melt, irrespective of the attractive or repulsive nature of the interactions. As expected, however, chains close to the surface of the nanoparticles are found to be partly flattened and

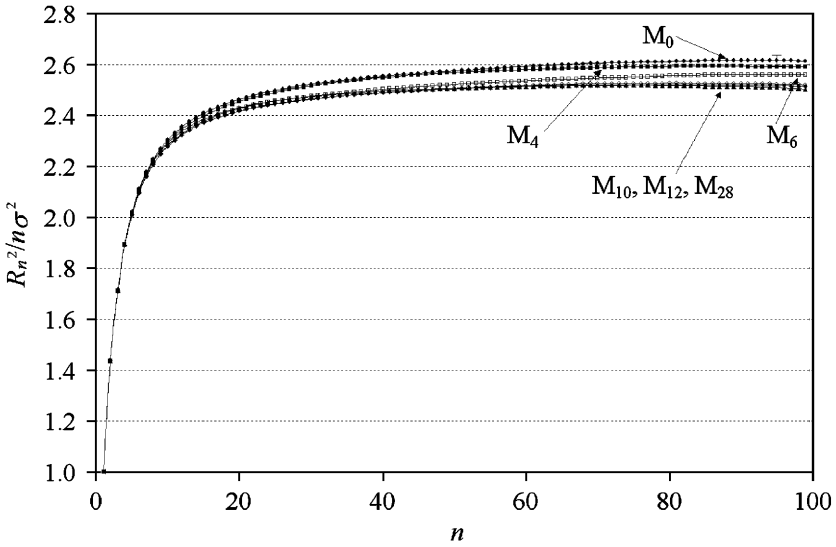

Fig. 10. $R_n^2/n\sigma^2$, with R_n^2 the mean-square distance of units belonging to the same chain and separated by n links, for various coarse-grained systems with chains of 100 units and randomly distributed spherical nanoparticles. Reprinted with permission from Vacatello [78], copyright (2003) of Wiley-VCH Verlag GmbH & Co. KGaA.

elongated, suggesting a corresponding behaviour for segments of longer chains in contact with the nanoparticles [68]. More recent simulations of PM chains on the SNND lattice [86] also show that the end-to-end distance distribution, the radius of gyration and the ratios of the eigenvalues of the gyration tensor coincide with the corresponding quantities in the pure melt, irrespective of the distance between neighbouring nanoparticles and of the strength of the polymer/nanoparticle interactions. Similar results are obtained with long coarse-grained chains on the cubic lattice [82].

Quite interestingly, SNND lattice simulations of filled PM or poly(oxyethylene) (POE) melts suggest that the chain size in the nanocomposites may be influenced by the mobility of the nanoparticles [84,85]. As previously explained, a peculiar aspect of these simulations is that the nanoparticles are represented by fully or partially collapsed chains. These model filler particles retain mobility in their internal degrees of freedom, and their centres of mass are also mobile. The results obtained for PM indicate that the mean-square radius of gyration of the matrix chains ($\langle s^2 \rangle_{matrix}$) is not changed much in the nanocomposites with respect to the value in the pure melt ($\langle s^2 \rangle_0$). The observed changes increase in absolute value with increasing filling density, but are relatively small even at very high concentrations. The radius of gyration is found to decrease when the number of units in the collapsed chains is equal to or larger than the number of units in the matrix chains, while a slight increase is observed when the number of units in the collapsed chains is smaller. For instance, $\langle s^2 \rangle_{matrix} \approx 0.9 \langle s^2 \rangle_0$ for a system with chains and particles of 58 beads at filling density as high as 60%, while $\langle s^2 \rangle_{matrix} \approx 1.1 \langle s^2 \rangle_0$ for a similar system with chains of 58 beads and particles of 14 beads. These results are obtained with mobile nanoparticles. However, by performing calculations in which the mobility of the nanoparticles is alternately suspended and resumed, it has been seen that the slight increase of $\langle s^2 \rangle_{matrix}$ observed for large chains and small nanoparticles is transformed in a slight decrease when the latter are immobilized. It is then concluded in Ref. [85] that the reduced or increased size of the matrix chains depends on whether they can completely adjust to the changing position of the nanoparticles or not. Such differences can be expected on the basis of the different behaviour of polymer chains in an "annealed" or "quenched" disordered environment, which has been demonstrated by both computer simulations and analytical calculations (see Ref. [132] for a review).

The results obtained in Ref. [85] for POE show much larger changes of chain size than for PM. For instance, a POE system gives $\langle s^2 \rangle_{matrix} \approx 1.8 \langle s^2 \rangle_0$ at 20% filling fractions. The large differences in the behaviour of these two polymers are not easily understood, but might be related to the fact that the

POE nanoparticles used in Ref. [85] are less collapsed and more permeable than the PM nanoparticles of Ref. [84]. Also, the former—unlike the latter—show some tendency to aggregate. More work is clearly required to clarify the origin of the different behaviour of the matrix chains in these two systems.

3.6. Arrangements of polymer chains and nanoparticles

The mutual arrangements of polymer chains and nanoparticles in a given nanocomposite system results from a complex interplay of several factors (size and shape of the nanoparticles, filling density, chain length and stiffness, interaction forces, etc.). In general, the polymer chains can be considered as sequences of interface segments (subchain segments totally running in the interface shell of a given particle), bridge segments (sequences of non-interface units with the two adjoining units in the interface shells of two different particles), loop segments (similar to bridge segments, but starting and ending in the interface shell of the same particle) and dangling terminal segments (Fig. 11). Comparing systems with large or small particles at the same overall volume fractions, we expect that the latter will contain more interface segments, shorter bridges, shorter dangling ends and many direct connections between interface segments (i.e., consecutive interface segments of two neighbouring particles without an intermediate bridge). This should lead to a stronger reinforcement effect.

The proportion of the various subchain segments and their average length have been studied as a function of the diameter of the nanoparticles and of the filling density in the coarse-grained simulations of Refs. [69,77,78], while the length of the bridge segments has been studied as a function of the distance between neighbouring nanoparticles and of the interaction strength between polymer units and nanoparticles in the SNND lattice simulations of Ref. [86].

Table 1 reports the values of selected parameters describing the mutual arrangements of chains and particles for four selected coarse-grained systems simulated in Refs. [69,77,78]. The various parameters are defined as follows:

- f_1 is the fraction of chain units in the interface shells of width 2σ surrounding the nanoparticles;
- f_2 is the fraction of chain units in the overlapping interface shells of adjacent nanoparticles;
- f_f is the fraction of free chains;
- N_i, N_b, N_l and N_t are the average number of interface, bridge, loop and terminal segments per chain, respectively, while L_i, L_b, L_l and L_t are their average length in terms of chain units;
- N_d is the average number of direct connections per chain;
- P_c is the average number of different interface shells visited by each chain;

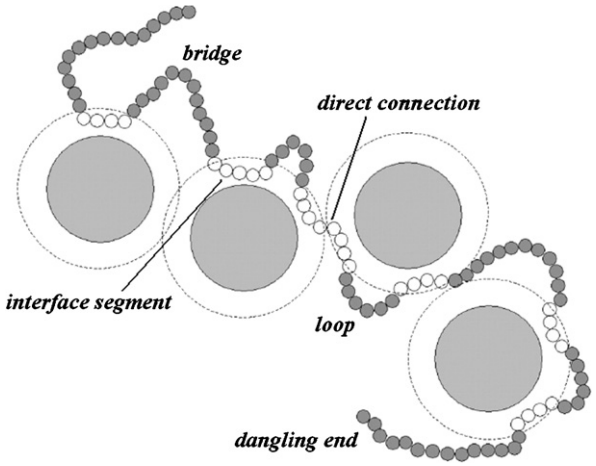

Fig. 11. Schematic representation of subchain segments. The dotted circles delimit the interface shells of the particles. Interface units are shown in white. Redrawn with permission from Vacatello [77], copyright (2002) of Wiley-VCH Verlag GmbH & Co. KGaA.

Table 1
Parameters chosen to describe the mutual arrangements of chains (100 units) and nanoparticles in Refs. [69,77,78]

	$D_{8,20}$	$D_{8,30}$	$D_{16,36}$	$D_{28,20}$
f_1	0.29	0.46	0.33	0.08
f_2	0.02	0.02	0.01	0
f_f	0.009	0	0.005	0.4
N_i	7.4	12	7.3	1.6
L_i	4.0	3.8	4.5	4.8
N_b	2.6	4.4	2.4	0.05
L_b	12	7.3	12	42
N_l	2.4	2.8	3.1	1.0
L_l	5.6	4.2	5.7	9.7
N_t	1.4	1.0	1.3	1
L_t	18	9	16	39
N_d	1.5	4.0	0.7	0
P_c	3.3	5.2	2.7	0.6
C_p	50	50	120	290

- C_p is the number of different chains visiting the interface shell of a given nanoparticle.

For each system, the first subscript indicates the diameter of the nanoparticles and the second subscript indicates the per cent volume fraction of filler.

Although these full density simulations are limited to relatively short chains of 100 units and relatively small nanoparticles, the systems in Table 1 cover a wide range of compositions. For instance, the fraction of interface units is as high as 50% in system $D_{8,30}$, while it is less than 10% in system $D_{28,20}$. Also, there are no free chains in the first case, while the free chains are as much as 40% in the second case. The simulations have been carried out with nanoparticles distributed at random, or with an ordered distributions of nanoparticles (this is the case of system $D_{28,20}$, in which the base cell contains one single nanoparticle), while the nanoparticles tend to form more or less large aggregates in real nanocomposites. Because of this and the adoption of a coarse-grained description, the numerical results obtained from these simulations are then better considered to refer to ideal systems, to be used as a reference when studying the behaviour of real nanocomposites. The same is obviously true for all other coarse-grained simulations performed up to now.

The results in Table 1 refer to the systems of short chains (100 units) and relatively small nanoparticles. When the chains are converted to phantom chains and at the same time the polymer–nanoparticle interactions are suitably adjusted to produce the correct density profiles (see Fig. 9 and the related discussion), the chain conformation and all parameters listed in Table 1 remain virtually unchanged [93]. Using this strategy, it is then possible to simulate much larger systems, containing many more nanoparticles and longer chains in the base cell.

Table 2 reports the values of the parameters of interest for some phantom chain systems with very large base cells containing chains of 2000 units and several nanoparticles distributed at random [94]. If the chain units are considered to be PM isodiametric units (see before), the molecular mass of the simulated chains is in the polymer range ($\approx 10^5$ amu). Parameters such as f_2 or N_d are negligible for large nanoparticles at realistic filling densities. As before, the first subscript indicates the diameter of the nanoparticles and the second subscript indicates the per cent volume fraction of filler.

Table 2
Parameters for phantom chain systems with long chains of 2000 units [26]

	$P_{28,05}$	$P_{28,20}$	$P_{50,05}$	$P_{50,20}$
f_1	0.017	0.075	0.010	0.042
f_f	0.31	0.001	0.61	0.07
N_i	7.6	33	4.1	18
L_i	4.5	4.5	4.7	4.6
N_b	0.66	6.6	0.13	1.8
L_b	350	145	400	275
N_l	6.2	25	3.6	16
L_l	35	22	41	31
P_c	1.1	4.7	0.48	2.0

The conclusions obtained from numerous systems with widely different compositions simulated at full density or with phantom chains may be summarized as follows:

(a) the average density of polymer units in a spherical shell between 0.8σ and 2σ from the surface of the nanoparticles in all full density systems is approximately $1.1\sigma^{-3}$ (i.e., 10% higher than in the unperturbed melt); considering that 0.8σ is the minimum distance found between chain units and surface of the nanoparticles, the fraction of interface units is given by $f_1 \approx 1.1(V_s/V_f)\varphi/(1-\varphi)-(f_2+f_3+\ldots)$, where V_s is the volume of the said shell, V_f is the volume of a nanoparticle and φ is the volume fraction of filler; f_2 and the other corrections are usually negligible;

(b) the length of the interface segments (L_i) increases with the diameter of the nanoparticles from the lowest value ≈ 3.5 when the latter are extremely small to the limiting value ≈ 5 for the same chains near infinitely extended two-dimensional surfaces [107]; for all investigated systems, L_i is well approximated by $L_i \approx 4.8-6.5\sigma/\sigma_f$, with σ_f the diameter of the filler nanoparticles;

(c) f_1 and L_i are independent of chain length, unless the chains are extremely short; once f_1 and L_i are known, the number of interface segments per chain is then given by $N_i \approx f_1 L_p/L_i$, where L_p is the chain length;

(d) in the rather naïve hypothesis that the chains can be considered as a spherical distribution of matter with radius proportional to their

unperturbed radius of gyration, P_c is expected to correspond to the average number of nanoparticles having centre within a sphere of diameter $\alpha R_g + \sigma_f + 4\sigma$ ($R_g \approx 0.65 {L_p}^{1/2}\sigma$ for the simulated chains); in all cases, it is well approximated by taking the adjustable parameter $\alpha = 1.7$;

(e) keeping with this approximation, the fraction f_f of free chains is expected to coincide with the probability that there are no nanoparticles centred inside a sphere of volume V^* around the centre of mass of a chain, or the probability of finding in the system of nanoparticles an empty sphere of volume V^*; this is given by $\exp[-\beta\varphi(V^*/V_f)/(\beta-\varphi)]$, where β is a constant between 0.64 and 0.74 (V_f/β is the volume excluded by each nanoparticle to the other nanoparticles);

(f) once P_c is known, C_p is given by $C_p = P_c N_p/N_f$, with N_p the total number of polymer chains and N_f the total number of nanoparticles in a given volume; therefore, $C_p = P_c(1-\varphi)V_f/(\varphi L_p \sigma^3)$.

Other simple expressions have been found in Refs. [77,78] relating number and length of bridge or loop segments to σ_f and φ for chains of 100 units. However, the dependence of these parameters on the chain length is far from being simple. For instance, N_b and N_l are expected to increase with L_p in a nearly linear way only for systems crowded with small nanoparticles, in which free chains and long dangling ends are practically absent. In all other cases, free chains and dangling ends are progressively converted to bridges and loops by increasing the chain length, the conversion rate depending on the values of σ_f and φ.

Another interesting result of the simulations is that chains and particles do form highly interconnected transient networks in all cases studied, including those with large particles and low filling density reported in Table 2. For instance, even though the average number of bridges *per chain* is as low as 0.13 in system $P_{50,05}$, the number of bridges *per particle* is anyway considerable, since each particle is in contact with $\approx$300 chains. See Ref. [94] for further discussion and quantitative expressions.

The relative abundance and length of the various kinds of chain sections has been studied in SNND simulations of Ref. [86] as a function of the distance between the surfaces of neighbouring nanoparticles and of the (attractive, neutral or repulsive) interactions between the polymer and nanoparticle beads. Since the simulated systems contain quite small nanoparticles placed at the nodes of an expanded close-packed array with filler volume fractions lower than 10%, a direct comparison between the numerical results reported in Ref. [86] and those of Refs. [69,77,78,93,94] cannot be made. In spite of all differences, including different definitions of the interface shells, the fraction of interface units and the fraction of free chains in the various systems simulated in Ref. [86] are given by $f_1 \approx 1.1(V_s/V_f)\varphi/(1-\varphi)$ (due to the low filling density and to the regular arrangement of the nanoparticles, f_2 is obviously zero here) and by $f_f \approx \exp[-\beta\varphi(V^*/V_f)/(\beta-\varphi)]$, in agreement with our previous expressions. Substantial agreement between the results of the first [77,78] and the second [86] sets of simulations is obtained also for the length of interface, loop and bridge segments.

An interesting observation of Ref. [86] is that the equilibrium distributions of the whole chains and of all the various subchain segments are practically unaffected by the repulsive, neutral or attractive nature of the polymer/nanoparticle interactions. This is consistent with the general idea that the overall equilibrium organization in these systems is mainly dictated by excluded volume effects. Note, however, that the picture can be quite different in cases in which strong polymer/filler interactions are localized in specific parts of the chains [69]. Not unexpectedly, the length distributions of the bridge and dangling end segments are found to change with changing the distance between neighbouring nanoparticles, while interface and loop segments are scarcely influenced by this parameter. Of course, increasing the distance between the surfaces of neighbouring nanoparticles of a given size leads to longer bridges and longer end segments. All the observed trends are in good agreement with the corresponding trends found in Ref. [77] for systems with randomly distributed nanoparticles of fixed diameter at various filling densities.

A second interesting aspect of the calculations in Ref. [86] is that the probability distributions of the bridge end-to-end distances in the simulated nanocomposites have been compared to the probability distributions for subchain segments of the same length in the pure melt. As the distance between the nanoparticle surfaces increases, the bridge end-to-end distribution is found to be shifted to higher distances and narrowed, which seems to imply that the bridges become more stretched and stiffer than the corresponding segments in the pure melt. This is

not the effect of a conformational perturbation due to the presence of the nanoparticles, but is an obvious consequence of the fact that a chain segment, to be defined as a bridge, has to cover the distance from the surface of a nanoparticle to the surface of a neighbouring nanoparticle. When this distance is significantly larger than R_g, bridges can be formed only by partly stretched segments [86]. The relevance of this effect to the stiffening of filled systems with respect to the pure melt has been questioned in Ref. [86] by remarking that significant stretching of the bridges is observed only for distances larger than $2R_g$, a situation in which the number of bridges per nanoparticle is small. Note, however, that the latter observation is based on systems with extremely small nanoparticles (diameter $\approx 3\sigma$) at volume fraction of filler less than 1%, while the number of bridges per nanoparticle is found to quite high in systems with large nanoparticles and long chains, even when the average distance between neighbouring nanoparticles is on the order of $2R_g$ or larger (see before, systems $P_{28,05}$ and $P_{50,05}$). Therefore, it appears that the consequences of the presence of stretched bridges on the stiffening of real filled systems have still to be assessed.

4. Molecular-level theories: equilibrium aspects

The two main theories currently applied to the study of liquid polymers—in particular polymer melts close to solid surfaces and polymer–nanoparticle "mixtures"—are the integral equation (also known as PRISM) and the DFT approaches. Our concise account of these theories is largely based on the reviews by Curro and Schweizer [97], by Heine et al. [98] and by Yethiraj [99]. These theories are important in the present context since they reproduce some of the structural features which have already been discussed in the previous part of this section devoted to MC and MD simulations (e.g., density oscillations close to a solid surface). Also, PRISM theory forms the basis of a thermodynamic analysis of the stability of nanoparticle dispersions in polymer melts [113,114].

As a general remark, the most successful implementations of these theories have concerned systems of hard chains. Thus, they capture quite well entropic effects related to chain packing constraints, either in bulk or close to a solid wall. Systems with strong attractive interactions are not modelled equally well, at least by the simplest versions of the theories. Even in these cases, however, there is often qualitative agreement with the simulations, so that PRISM and DFT approaches retain their usefulness as general interpretative tools.

4.1. Integral equation theories (PRISM)

The primary object in the investigation of polymeric liquids is the pair distribution function $g(r)$, representing the relative probability (compared to an ideal gas of non-interacting units at the same density) of finding a polymer unit, or a chain bead, at a distance r from another unit placed at the origin. The total correlation function is $h(r) = g(r)-1$, which is zero by construction for an ideal gas (i.e., in the absence of correlations).

Integral equation theories are based on the Ornstein–Zernike (OZ) equation [115]. This reads, for a monoatomic fluid interacting by a spherically symmetric potential:

$$h(r) = c(r) + \rho \int \mathrm{d}\boldsymbol{r}' c(\boldsymbol{r}') h(|\boldsymbol{r} - \boldsymbol{r}'|) \tag{1}$$

where ρ is the atom number density and $c(r)$ is the direct correlation function between two atoms. Eq. (1) effectively represents a definition of $c(r)$, and is based on the notion that the correlation between two atoms in a dense fluid is the result of their direct interaction [i.e., $c(r)$], but also of many-body effects represented by the convolution integral on the right-hand side. Eq. (1) is based on the statistical equivalence of the beads, i.e., the total correlation function reproduces itself after convolution with the direct correlation function. In reciprocal space the convolutions are transformed into simple products and the OZ equation reads

$$\hat{h}(k) = \hat{c}(k) + \rho \hat{c}(k) \hat{h}(k) \tag{2}$$

where the Fourier transforms are defined as

$$\hat{f}(k) = \int f(\boldsymbol{r})\, \mathrm{e}^{\mathrm{i}\boldsymbol{k}\boldsymbol{r}} \mathrm{d}^3\boldsymbol{r} = \frac{4\pi}{k} \int r f(r) \sin(kr)\, \mathrm{d}r \tag{3}$$

Iterative substitution of $h(r)$ or $\hat{h}(k)$ into the right-hand sides of (1) or (2) leads to an infinite series of terms corresponding to two-body, three-body, four-body…interactions. This infinite series must be truncated by application of an appropriate closure approximation. The simplest—but often quite effective for short-range interactions—closure is that of Percus and Yevick (PY):

$$c(r) = (1 - \mathrm{e}^{\beta u(r)}) g(r), \tag{4}$$

where $u(r)$ is the bead–bead interaction potential and $\beta = 1/k_BT$. Other closure approximations, such as the mean-spherical approximation (MSA) and the atomic hypernetted chain closure (HNC), may also be employed but the advantage of their application to polymer systems has been questioned [98].

The OZ equation may be extended to polymers if each chain is made to consist of N beads (all equivalent in the limit of large N for homopolymer) and the interaction potential is written as the sum of bead–bead interactions. The basic equations of PRISM theory are:

$$\hat{h}(k) = \hat{\omega}(k)\hat{c}(k)\hat{S}(k), \quad \hat{S}(k) = \hat{\omega}(k) + \rho\hat{h}(k), \tag{5}$$

where $\hat{\omega}(k)$ the single-chain structure factor and $\hat{S}(k)$ is the overall structure factor. In turn, $\hat{\omega}(k)$ is the Fourier transform of the intramolecular correlation function $\omega(r)$, defined as

$$\omega(r) = \frac{1}{N}\sum_{i=1}^{N}\sum_{j=1}^{N}\omega_{ij}(r) \tag{6}$$

Here $\omega_{ij}(r)$ is the probability that beads i and j are separated by a distance r. In the simplest version of the theory, $\omega(r)$ is pre-computed from a given polymer model (Gaussian or RIS chains, for example) and used as an input to Eq. (5), instead of being computed self-consistently with the intermolecular correlations. This simplification is justified by the Flory ideality hypothesis (unperturbed chain conformation in a polymer melt). The total correlation function $h(r)$ and its Fourier transform $\hat{h}(k)$ may be compared with simulation results or scattering experiments.

The logical scheme reported above has been extended to more complex cases. The case of nanoparticles in a polymer melt [113,114,116] will be dealt with shortly. The equations for polymer chains at a solid surface are derived from the PRISM theory for a two-component mixture of polymer chains and solid spherical particles, in the limit that the latter become infinitely diluted and infinitely large [99]. In this case two correlation functions need to be defined, both direct [$c(r)$ and $c_w(r)$] and total [$h(r)$ and $h_w(r)$]; the suffix w stands for "wall". The OZ equation analogous to Eq. (1) after replacement of the three-dimensional distance r with the perpendicular distance z from the surface, is

$$h_w(z) = 2\pi\int_0^{\infty} tS(t)\,\mathrm{d}t\int_{z-t}^{z+t} c_w(s')\,\mathrm{d}s' \tag{7}$$

Defining a one-dimensional Fourier transform by

$$\tilde{f}(k) = \frac{1}{2\pi}\int_{-\infty}^{+\infty} f(z)\,\mathrm{e}^{\mathrm{i}kz}\,\mathrm{d}z \tag{8}$$

and performing this transform on Eq. (7) we obtain

$$\tilde{h}_w(k) = \hat{S}(k)\tilde{c}_w(k), \tag{9}$$

an equation similar to Eq. (2) except that now we have both one- and three-dimensional Fourier transforms.

The wall–PRISM theory has been applied mainly to hard-chain models, close to a flat solid wall or between two surfaces. Depletion of chain sites close to the surface at low polymer densities and enhancement at high densities has been successfully described, and appears to be sufficiently accurate when the structure is dominated by repulsive interactions. This is illustrated by the top panel of Fig. 12, showing a comparison of density profiles from MC simulations and wall–PRISM calculations for hard flexible chains. Note, however, that the density oscillations at high packing fractions ($\eta = 0.45$) are not as accentuated as those from the MC simulations. The theory was also implemented for binary polymer blends, showing that stiffer and/or branched chains tend to segregate towards the surface compared to flexible/linear chains.

4.2. Density functional theory (DFT)

Unlike the integral equation theories based on the OZ approach, the DFT approach does not assume an intrinsically homogeneous statistical behaviour of the system under investigation. The strategy consists of minimizing the grand free energy with respect to the density distribution of the polymer fluid.

At a temperature T, the grand partition function Ξ of a monomatomic system is a function of: (i) the number of atoms n, (ii) the chemical potential per bead μ, related to the activity $\lambda = \exp(\beta\mu)$, (iii) the potential energy V_n from bead–bead interactions, (iv) the potential energy $\Phi_n = \sum_{i<n}\phi(\boldsymbol{r}_i)$ due to an external field (a surface, for example), $\boldsymbol{r}_i$ being the vector position of the ith bead. We have

$$\Xi = \sum_{n\geqslant 0}\frac{\lambda^n}{\Lambda^{3n}n!}\int \mathrm{e}^{-V_n/k_BT}\,\mathrm{e}^{-\Phi_n/k_BT}\,\mathrm{d}\boldsymbol{r}^n \tag{10}$$

Λ being a constant (thermal de Broglie wavelength). The grand free energy is

$$\Omega[\rho(\boldsymbol{r})] = -k_BT\,\ln\,\Xi \tag{11}$$

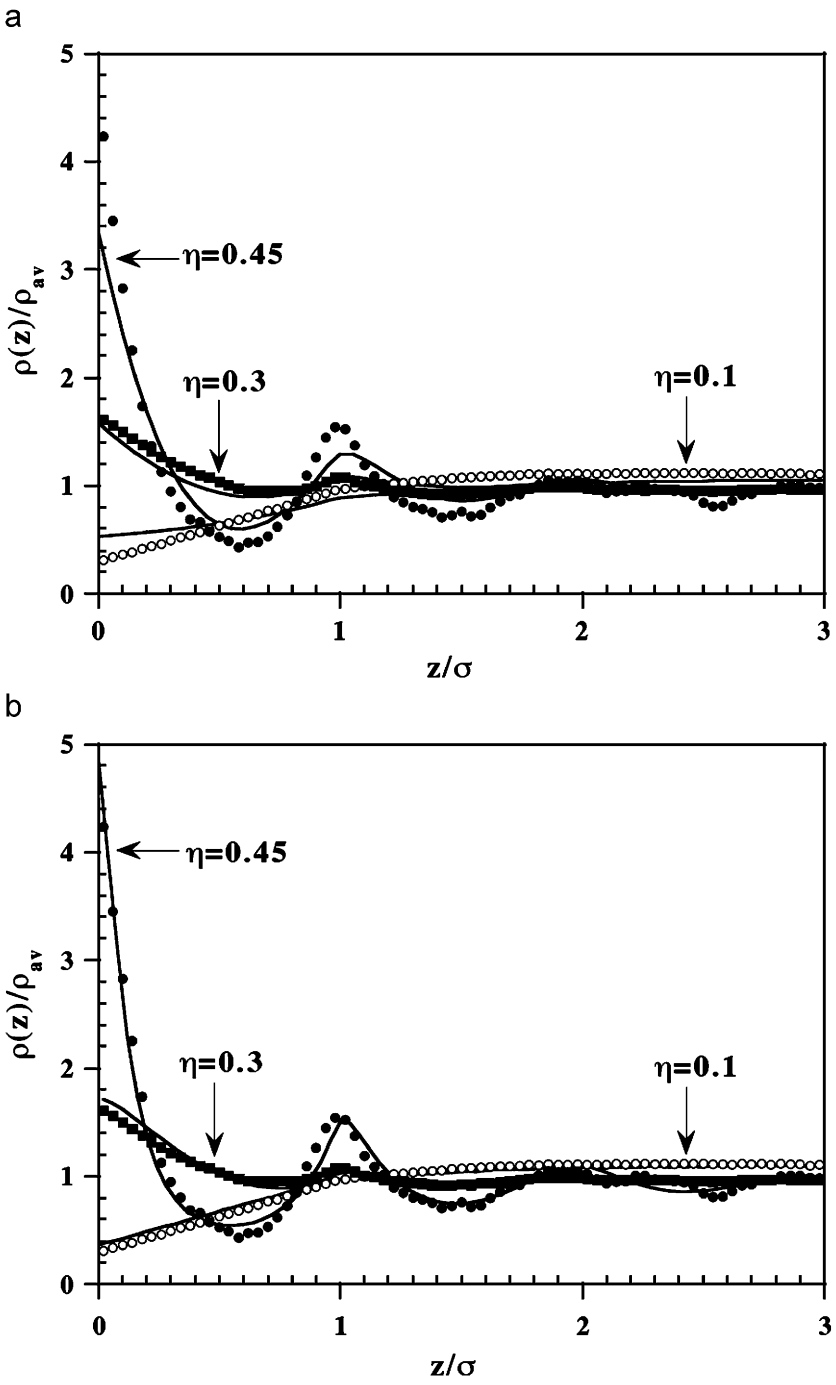

Fig. 12. Comparison of bead density profiles from MC simulations of hard flexible 20-mers (dots) and (a) wall–PRISM calculations, or (b) DFT calculations. Here η is the packing fraction, proportional to the number density of beads. Reproduced with permission from Yethiraj [99], copyright (2002) of John Wiley and Sons, Inc.

and the Helmholtz free energy is

$$F[\rho(\boldsymbol{r})] = \Omega + \int [\mu - \phi(\boldsymbol{r})]\rho(\boldsymbol{r})\,\mathrm{d}\boldsymbol{r} \tag{12}$$

where $\rho(\boldsymbol{r})$ is the individual bead density.

In a macromolecular system, both Ω and F may be regarded as functionals of the molecular density $\rho_M(\boldsymbol{R})$, where now the coordinates of all the beads in a chain have been collected as $\boldsymbol{R} = \{\boldsymbol{r}_1\boldsymbol{r}_2\ldots\boldsymbol{r}_N\}$. Formally, this density satisfies the

equilibrium condition:

$$\frac{\delta\Omega}{\delta\rho_M(\boldsymbol{R})} = 0 \tag{13}$$

Either free energy is usually expressed as the sum of an ideal contribution (e.g., $F_{ID}[\rho_M(\boldsymbol{R})]$) and an excess contribution accounting for bead–bead interactions ($F_{EX}[\rho(\boldsymbol{r})]$). The ideal gas functional for this molecular system is known exactly:

$$F_{ID}[\rho_M(\boldsymbol{R})] = k_B T \int \mathrm{d}\boldsymbol{R} \cdot \rho_M(\boldsymbol{R})[\ln\, \rho_M(\boldsymbol{R}) - 1] + \int \mathrm{d}\boldsymbol{R} \cdot \rho_M(\boldsymbol{R}) \cdot V(\boldsymbol{R}) \tag{14}$$

Eq. (14) contains a $3N$-dimensional integral over an intramolecular potential energy $V(\boldsymbol{R})$ expressing bonding constraints. This can be evaluated analytically (for the freely jointed case) or by means of single-chain MC simulations. The remaining problem consists of finding approximations for $F_{EX}[\rho(\boldsymbol{r})]$. Note that this has been written as a functional of an average bead density $\rho(\boldsymbol{r})$, which is already a substantial simplification compared to the molecular density $\rho_M(\boldsymbol{R})$. One approximation scheme, due to Hooper et al. [101], is based on an expansion in powers of the density truncated at the second order:

$$F_{EX}[\rho(\boldsymbol{r})] \approx -\frac{k_B T}{2} \int \mathrm{d}\boldsymbol{r}\, \mathrm{d}\boldsymbol{r}' \rho(\boldsymbol{r})\rho(\boldsymbol{r}')c(|\boldsymbol{r} - \boldsymbol{r}'|, \rho) \tag{15}$$

where $c(r)$ is the direct correlation function of the homogeneous polymer melt at the bulk density ρ and can be obtained, for example, from the PRISM theory. Another, more accurate theory involves an explicit separation of the excess free energy into a sum of hard-core and attractive terms, which are then approximated according to distinct criteria.

The DFT approach appears to be successful in describing the behaviour of hard chains at hard walls (depletion and enhancement effects). Thorough tests of the theory have been conducted by Yethiraj and Woodward [100]. The lower panel of Fig. 12 shows an almost perfect agreement between the DFT theory and MC simulations, at all densities.

In summary, both the Integral Equation and the DFT appear to be promising approaches to investigate polymer fluids. The latter is more accurate, but it also more computationally demanding. Comparatively little attention was devoted hitherto to the effect of the attractive part of the intermolecular potential on the wall–fluid and fluid–fluid behaviour of confined polymers. Accurate functionals exist for simple liquids and their extension to polymers should be interesting. Also, the development of more accurate closures should allow implementation of the wall–PRISM theory to more realistic systems [99].

4.3. Depletion interaction and phase separation

The polymer density plots in the vicinity of the surface of a particle (see Figs. 7, 8 and 12) show that the polymer chains are more tightly packed and presumably their dynamics is slower than in other regions of space. The chain entropic freedom is reduced even more strongly in the volume comprised between two particles, the more so the shorter the distance between their surfaces. This effect is especially large if the surface-to-surface distance is smaller than the chain radius of gyration. In this case the chains' internal degrees of freedom suffer an amplitude reduction and the chains try to escape from the restricted space. As a result the particles will be pushed against one another. The associated force, which is purely entropic, is known as the *depletion attraction*. In the following we shall limit our analysis to the assumption that the particles behave like *hard spheres*, as far as their direct interactions are concerned. Even in this case, the situation is quite complex since different scenarios may occur, depending on the strength of the polymer–particle interactions.

Using the PRISM integral equation approach, Hooper and Schweizer investigated the phase separation issue for systems of flexible polymer chains and spherical particles [113,114]. There are three relevant PRISM equations in the limit of "dilute" nanocomposites, describing polymer–polymer, polymer–particle and particle–particle correlations ("*pp*", "*pc*" and "*cc*" subscripts, repectively). In Fourier space, these read

$$h_{pp}(k) = \omega_p(k)c_{pp}(k)S_{pp}(k) \tag{16a}$$

$$h_{pc}(k) = c_{pc}(k)S_{pp}(k) \tag{16b}$$

$$h_{cc}(k) = c_{cc}(k) + \rho_p(k)c_{pc}^2(k)S_{pp}(k) \tag{16c}$$

Note that the solution of the polymer problem (16a) is used as an input to the polymer–particle problem (16b), and both of these enter the equation for the particle–particle problem (16c). The calculation of the particle–particle pair correlation

function is the central result of the theory. From this, it is straightforward to obtain a potential of mean force (PMF) describing the effective polymer-mediated interaction among a pair of particles:

$$W_{cc}(r) = -k_B T \ln[1 + h_{cc}(r)] \tag{17}$$

Representative plots of this PMF for different situations are depicted in Fig. 13. The answer depends on different parameters, such as the chain length (N), the ratio of monomer and particle diameters (d and D, respectively) and the form of the polymer–particle interaction potential. Labelling with r' the distance between the polymer bead and the surface of the particle ($r' = r - (D + d)/2$), the latter was modelled by

$$U_{pc}(\rho) = -\varepsilon_{pc} \exp\left[-\frac{r'}{\alpha d}\right] \tag{18}$$

where ε_{pc} is the polymer–particle energy at contact and α is a parameter characterizing the range of the potential ($\alpha = 0.5$ for a generic "van der Waals type" interaction, $\alpha = 0.25$ for a specific short-range "hydrogen bond like" interaction, $\alpha = 1.0$ for a longer-range interaction). As can be seen, several situations are possible. The extreme cases are represented by depletion attraction (case I) and fully repulsive interactions (case III), leading to poor or good particle dispersion. However, there are also interesting intermediate cases (II and IV), in which the PMF is characterized by several minima with a spacing of the order the monomer diameter. Physically, these correspond to different types of "bridging" configurations.

The same Authors also analysed the conditions for the stability of the polymer–particle mixture against phase separation (i.e., re-aggregation of the particles). They derived an effective one-component criterion for the boundaries of the spinodal phase diagram (particle volume fraction ϕ_c):

$$\phi_c \cong -\text{const.}\frac{B_{2,HS}}{B_{2,cc}} = -\text{const.}\overline{B}_2 \tag{19}$$

where $B_{2,HS}$ and $B_{2,cc}$ are the second virial coefficients for a pair of particles interacting by a hard-sphere potential and the PMF of Eq. (17), respectively:

$$B_{2,HS} = \frac{2\pi D^3}{3}, \quad B_{2,cc} = \frac{1}{2}\int [1 - e^{-\beta W_{cc}(r)}]\, d^3\boldsymbol{r}. \tag{20}$$

Taking the diameter ratio D/d in the range 10–24, the chain length $N = 100$ and different α

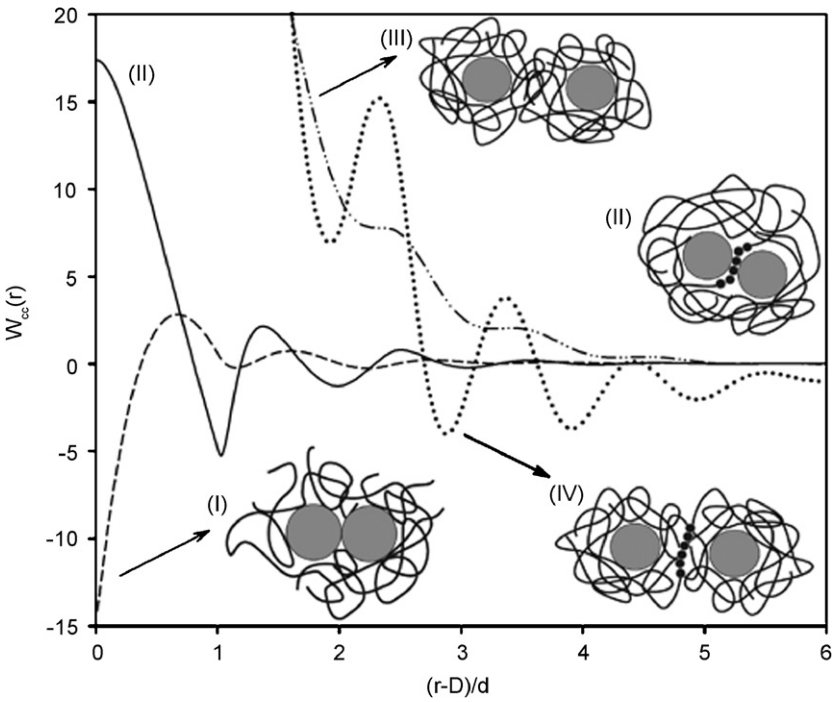

Fig. 13. Representative particle–particle PMF's, for diameter ratio $D/d = 16$ and chain length $N = 100$. Different situations arise for different choices of the α and ε_{pc} parameters [see Eq. (18)]: (I) contact aggregation, (II) bridging, (III) steric stabilization, and (IV) telebridging. Reproduced with permission from Hooper and Schweizer [114], copyright (2006) of the American Chemical Society.

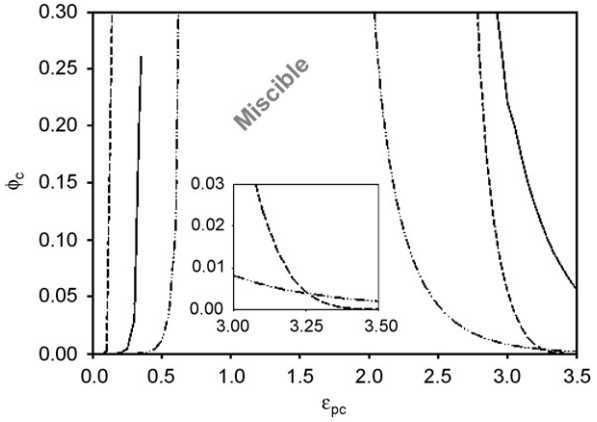

Fig. 14. Nanoparticle volume fraction at the spinodal for a hard-sphere system with $D/d = 16$ and $N = 100$, as a function of the polymer–particle interaction strength (ε_{pc}) and range ($\alpha = 0.25$ dash-dot-dot, $\alpha = 0.5$ solid, $\alpha = 1.0$ dash). The inset highlights a region where there is crossing of the phase boundaries for the systems with shortest- and longest-range attractions. Reproduced with permission from Hooper and Schweizer [114], copyright (2006) of the American Chemical Society.

parameters, the same Authors plotted the spinodal phase diagram against the contact strength ε_{pc} (see Fig. 14). For low values of $\varepsilon_{pc}(<0.05)$ we have separation of the particle-rich and of the polymer-rich phases as a result of the polymer-mediated depletion attraction. The same happens at large $\varepsilon_{pc}(>3)$, where the particle-rich phase is stabilized by tight inter-particle bridging due to the polymer chains strongly adhering to the particle surfaces. In this case, particles sterically stabilized with non-interpenetrating adsorbed polymer layers are embedded in a "crystallized" homopolymer matrix at relatively low volume fractions [113,114]. For intermediate ε_{pc}'s we have polymer/solvent miscibility within a single phase. Note that the high-concentration spinodal boundary varies non-monotonically with the interaction range (i.e., it is widest for the intermediate value $\alpha = 0.5$).

As pointed out by the Authors, these results are effectively obtained under the simplifying assumption that the particle-related contributions dominate, neglecting the explicit polymer–polymer contributions. As a consequence, a one-component system is effectively considered, where the particles interact via a polymer-mediated PMF. The corresponding normalized second virial coefficient $\overline{B}_2$ of the particle system is positive for single-phase miscibility, negative for phase separation. Also, we neglect any *direct* particle–particle attractions; these can modify the breadth of each transition region. Polymer chain length plays little role for weak monomer–particle attractions, in which case the depletion attraction dominates. However, we have a decrease of the effective inter-particle attraction with an increasing degree of polymerization.

In a recent paper on poly(ethylene glycol) (PEG) melts silica particles of 44 nm diameter, Anderson and Zukoski [116] show that the particles' dispersion is thermodynamically stable up to a polymer molecular weight $M_W = 80000$. These authors compare their experimental results with a suitable adaptation of the PRISM theory. They conclude that phase separation could be achieved only through modification of one or more key parameters ε_{pc}, α, D/d and N.

4.4. Polymer between parallel surfaces

If the particle size is sufficiently large compared with the particle–particle distance, the system may be effectively modelled by assuming parallel planar surfaces, their distance being much smaller than the transverse diameter. Thus the statistical-mechanical investigation of a polymer chain between planar surfaces can provide insights into the complex issue of a polymer (a melt or a solution) squeezed between two large particles, or confined within pores. While short-range chain packing effects are best addressed by the wall–PRISM and DFT approaches discussed previously, other features can be modelled by lattice models in view of their conceptual simplicity and mathematical handiness. Representative applications of the popular self-consistent-field (SCF) method can be found in Refs. [8,117,118]. Here, after a brief introduction, we shall illustrate two recent studies by two of us: compressed polymer networks [119] and polymer-mediated adhesion between two surfaces [120].

4.4.1. Single-polymer chains

The chain is regarded to be in an ideal phantom state, with a bead–surface attractive contact energy $\varepsilon<0$. Placing each chain on a cubic lattice model and describing the conformational statistics by a transfer matrix method, DiMarzio and Rubin [121] show that a very long (infinite) chain undergoes a second-order transition at the temperature T^* for which the energetic gain exactly compensates for the entropy loss of a bead contacting the wall ($\varepsilon/k_BT^* = -\ln 6/5 \cong -0.18$). At $T<T^*$ the chain beads are attracted to the walls, and repelled

at $T > T^*$. Interestingly, at $T = T^*$ the polymer fills uniformly the available space.

Using the DiMarzio–Rubin approach, Allegra and Colombo [122] derived the *partition coefficient* for chains of a contour length $L = Nl$ (N bonds of length l) to be either included or excluded from a slab with a width d between planar surfaces. Such a result, originally obtained by Casassa [123] for the hard-wall case ($T \gg T^*$), is useful to interpret size-exclusion chromatography results. As a remarkable effect, the bead density of a long chain ($L \gg L'$) is constant through the wall-to-wall slab width d, except in the immediate vicinity of the walls. In the hard-wall case ($\varepsilon = 0$) it is possible to show that the chain entrapment probability P is given by

$$P\left(\frac{R}{d}\right) = \exp\left(-\frac{\Delta G}{k_B T}\right) = \frac{8}{\pi^2}\sum_{p=1}^{\infty}\frac{1}{(2p-1)^2}\exp\left[-\frac{(2p-1)^2\pi^2 R^2}{d^2}\right] \quad (21)$$

where $R^2 = Nl^2/6$ is the mean-square radius of gyration of the unperturbed chain. ΔG is the *depletion free energy*. In the long-chain limit with $R^2/d^2 \gg 1$, the sum reduces to the first term and we have

$$\frac{\Delta G}{k_B T} \cong \frac{\pi^2 R^2}{d^2} = \frac{\pi^2}{6}\frac{Nl^2}{d^2} \quad (22)$$

This result, which agrees with scaling analyses [22], yields the entropic depletion free energy driving out of the slab a long polymer chain with N beads, $Nl^2 \gg d^2$. In the multi-chain case, Eq. (22) suggests that the depletion energy is simply proportional to the total polymer mass in the slab, assuming all the chains to be much longer than the slab width.

4.4.2. Polymer networks compressed between particles

In a filled cross-linked rubber two adjacent particles may be separated by a chain *network*, instead of separate chains. In order to understand the mechanical response under a change of the inter-particle distance, it is interesting to compare the cases where the particles are separated by (i) linear chains, (ii) a network with a two-dimensional topology, (iii) three-dimensional networks of variable topological thickness [119]. The two- and three-dimensional networks were assumed to have a square or cubic connectivity, respectively, and the are always regarded as phantom-like. The compression induced by a decrease of the inter-particle distance is mimicked by a harmonic potential $1/2Hx^2$ acting on each bead at a distance x from an average plane between the two particles. Of course, the larger H, the more compressed the network, the closer the particles. The model may be treated with a matrix approach and yields exact results as a function of the applied field strength H, in the long-chain limit. Although it does not account for the wall–chain interaction, the model suggests some interesting qualitative conclusions. First of all, it confirms that the mean-square radius of gyration of the two-dimensional network with equal chains increases logarithmically with the number of chains, whereas it goes to a finite limit in the three-dimensional case [124]. Fig. 15 shows the networks mean-square size along the direction of compression. We see that the three-dimensional network effectively behaves as a rigid particle with a fixed size, until a critical compression strength is reached. This conclusion strongly suggests that densely cross-linked polymer regions may be regarded as solid filler particles. Also, two large particles may not be able to come in contact if separated by a cross-linked polymer region.

4.4.3. Chains bound to parallel surfaces

Polymer chains may be grafted to the filler particles. The mechanical strength of this system depends on the statistics of the chains forming

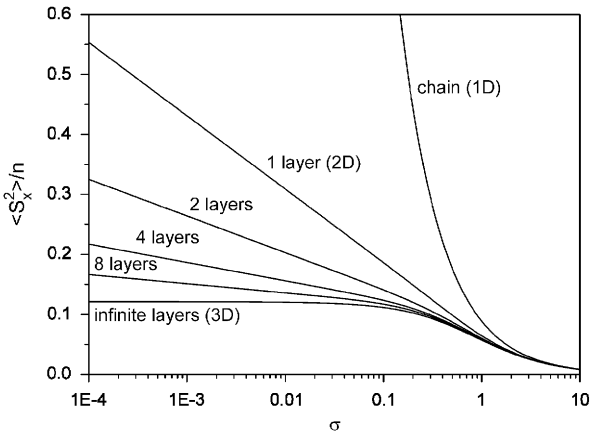

Fig. 15. Compression in a harmonic field of regular infinite networks of chains with n bonds of unit length. $\sigma = n\sqrt{H/12}$: compression parameter, in $k_B T$ units. $\langle S_X^2 \rangle$: mean-square radius of gyration of the network along the direction of compression. Reproduced with permission from Allegra and Raos [119], copyright (2002) of the American Institute of Physics.

bridges between the two particles/surfaces. This subject was investigated by two of us using the cubic lattice description, with the adoption of two different statistical models [120]. With "model A" we consider a controlled system of monodisperse polymer chains connecting parallel surfaces. Of course, obtaining such a "bridging brush" implies a delicate chemistry, because proper reacting groups must be placed at the chain ends and also on each surface before the chemical reaction. Conversely, with "model B" chains of different length are randomly attached to the surfaces, as it may happen in solvent- or melt-welding. The contour length of the loops and bridges formed by them is derived from an equilibrium distribution of a very long winding chain reversibly adsorbing on the surfaces, prior to (instantaneous) formation of irreversible polymer–surface bonds. In both cases the constraint of uniform polymer density through the slab width is fulfilled, by applying a small energetic premium on the monomers contacting the wall (e.g., $\varepsilon = -k_BT\ln(6/5)$ in the case of model *B* with an infinite chain). Fig. 16 shows that, within model *B*, the relative probability of chain strands returning to the same wall increases quickly with the slab width *n*, in qualitative agreement with experimental data.

Attention is focused on the elongational and the tangential moduli of both systems, respectively, k_{long} and k_{tan}. For typical chain lengths of $N = 40$ or 100 statistical segments (or beads) with length *l*, the average moduli with model A are larger than with model B except at very small slab widths *nl*

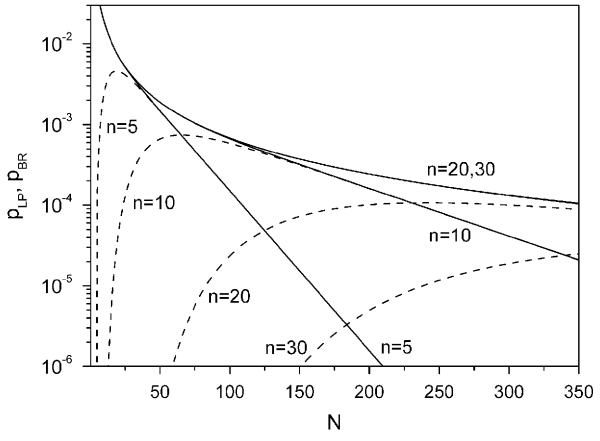

Fig. 16. Probabilities of existence of loops (solid lines) and bridges (dashed lines) of contour length *Nl*, for difference wall-to-wall separations *nl*. Reproduced with permission from Allegra and Raos [120], copyright (2003) of the American Institute of Physics.

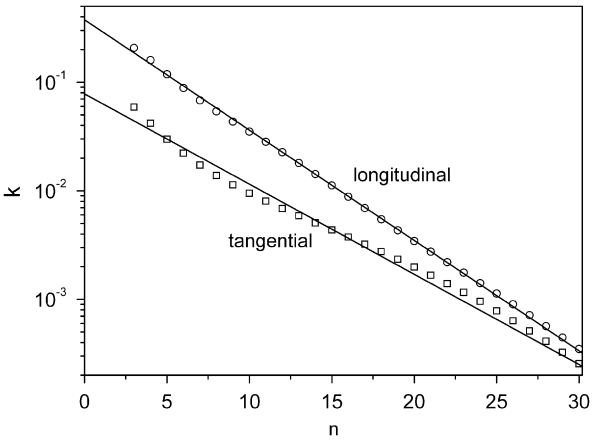

Fig. 17. Calculated tangential and longitudinal moduli for model B, as a function of the wall-to-wall distance *n*. Reproduced with permission from Allegra and Raos [120], copyright (2003) of the American Institute of Physics.

($n < 10$–20 segments, $l \approx 1$ nm). Besides, model A has the advantage that the moduli *increase* with *n* (for a fixed chain length), unlike with model *B*. As shown in Fig. 17, for model *B* the ratio k_{long}/k_{tan} tends to unity from above with increasing slab width, in agreement with expectation for a system of ideal, Gaussian chains.

It must be stressed that, in a dry polymer film, volume change represents an important additional contribution (on top of chain elasticity) to the effective elongational modulus k_{long}^{eff}, while in principle leaving k_{tan} unaffected. It can be computed from knowledge of the compressibility of the polymer (assuming that compressibility is unchanged on going from the bulk to a thin film). Alternatively, since a volume change can be envisaged as an intake or expulsion of voids (a very poor "solvent") it can be estimated by an additional Flory–Huggins-type term in the free energy [120]. This contribution is usually dominant. The longitudinal adhesion strength may be substantially controlled by polymer elasticity in two cases: (a) if the polymer chains connecting both walls are already rather stretched, or (b) when the polymer chains are surrounded by a good solvent communicating with an external reservoir.

5. Molecular-level simulations and theories: polymer dynamics at the interface

Overall, the behaviour of filled elastomers is governed by various length scales, such as the size of the particles and of their aggregates, the thickness

of the interfacial polymer shell close to the filler surfaces, and the average distance between the particles. The influence of the nanoparticles on the dynamic properties of the polymer matrix has been investigated with various methods in the MD simulations, with particular reference to the differences between polymer units located in the interface shells and those in the bulk.

The effects on T_g and on the dynamic properties of the chains due to the presence of the nanoparticles and to the interaction forces between polymer units and nanoparticles have been studied in Refs. [67,68] by calculating the radially averaged intermediate scattering function

$$F(q,t) = \frac{1}{NS(q)} \left\langle \sum_{j,k=1}^{N} e^{-i\mathbf{q}\cdot[\mathbf{r}_k(t)-\mathbf{r}_j(0)]} \right\rangle \tag{23}$$

normalized by the structure factor $S(q)$ for both attractive systems (with full monomer–nanoparticle LJ interactions) and non-attractive systems (only comprising the repulsive part of the LJ potential). The characteristic time for the decay of $F(q, t)$ has a local maximum at $q_0 \approx 7.08\,\mathrm{nm}^{-1}$, coinciding with the first maximum of $S(q)$. Plots of $F(q_0, t)$ at several temperatures for the systems studied indicate that at sufficiently low temperatures each system shows a two-step relaxation. Also, $F(q_0, t)$ does not fully decay to zero at low temperatures for the filled attractive system, indicating the presence of a very slow component of the relaxation. Relative to the unfilled system, the relaxation time is higher when the interactions between polymer and nanoparticle are attractive, the difference increasing with increasing T, and slightly smaller at low T for the non-attractive system, the difference increasing with decreasing T. Therefore, one expects T_g to be higher in the first case and lower in the second.

The local dynamics of the polymer units has also been studied as a function of their distance from the surface of the nanoparticle by plotting the self (incoherent) part of $F(q_0, t)$ for chain units initially in a given shell surrounding the nanoparticle. Example plots of $F_{self}(q_0, t)$ are shown in Fig. 18 for the attractive (a) and non-attractive (b) case. Fig. 18 shows that the relaxation of the chain units in the first few layers close to the nanoparticle is much slower than average for attractive interactions, while it is faster in the non-attractive systems. The slowing down observed for attractive interactions is much more pronounced in a further system simulated by doubling the attractive forces, to the

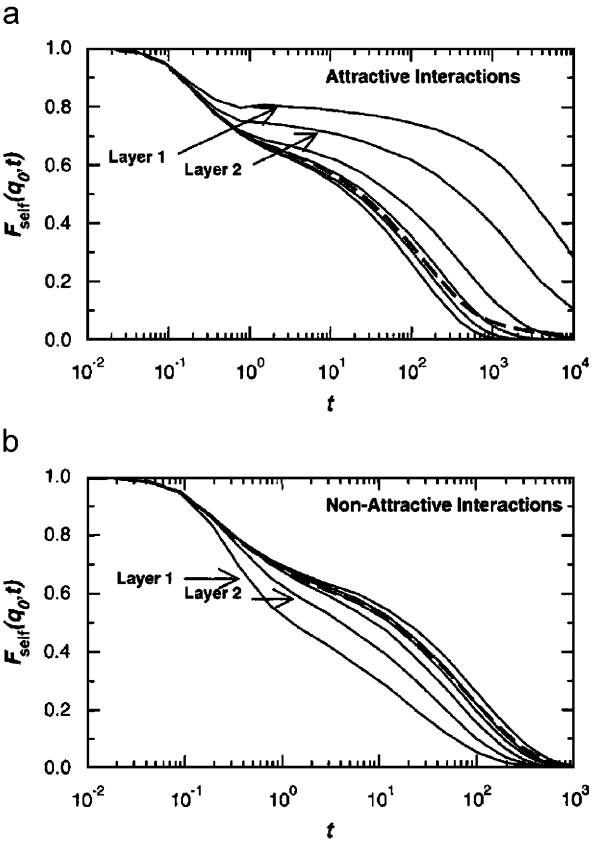

Fig. 18. $F_{self}(q_0, t)$ for the average of all chain units (dotted line) and decomposed into layers for: (a) attractive interactions and (b) non-attractive interactions at $T = 0.4$. The boundaries of the layers are defined to be the minima of the density. Reproduced with permission from Starr et al. [68], copyright (2002) of the American Chemical Society.

point that the chain units in the first shell do not relax in full on the time scale accessible to the simulations. It is concluded that the interactions between polymer and nanoparticles play a key role in controlling T_g and the local dynamics of nanocomposites.

This conclusion is confirmed by the results obtained in Ref. [70] studying similar systems of chains of 20 units or 10 units with attractive, neutral and repulsive interactions between chain units and nanoparticles (the repulsive case corresponds to the non-attractive case of Refs. [67,68]). Relative to the pure melt, the dynamic shear modulus and the viscosity are found in Ref. [70] to be strongly increased in the attractive case, less strongly increased for neutral systems and reduced for repulsive systems. In particular, the viscosity is found to increase or decrease monotonically with increasing the fraction of interface beads (i.e., beads

in the first two shells in contact with the nanoparticles), indicating that the overall effects are substantially due to modified dynamics of the polymer units within the interface shells. Further analyses show that the increased dynamics observed for repulsive systems can be explained by the lower density of chain units in the interface shells of these systems, while the strong slowing in the attractive systems is not simply due to densification effects. Also, the mean residence time of the chain units in the interface shells of attractive systems is only about twice that in neutral systems, suggesting that the dramatic slowing of the adsorption/desorption polymer in the attractive systems may be due to strongly co-operative effects. Consistent with these considerations, the mean-square displacement of the interfacial polymer units is found to be dramatically less in the attractive case with respect to the pure melt or neutral systems, indicating that the principal effect is due to increased barriers for the motion of the polymer units along the surface of the nanoparticles. The slowed dynamics with attractive nanoparticles is mainly attributed to the fact that the polymer units in the first interface shell feel the structure of the surface very strongly and are largely stuck in place [70]. This conclusion is consistent with the older finding that the strength of the interactions has little influence on the dynamics of polymers near structureless solid surfaces [110]. In this respect, the results obtained in Ref. [81] for the mean-square displacement of the methylene units in the presence of a silica nanoparticle are partly unclear, since the mobility is reduced close to the atomistic surface of the nanoparticle even though the simulated systems are repulsive (only the repulsive part of the LJ interactions is included). However, considering that the calculations are performed at very high pressures (4630 and 5000 bar) in order to obtain realistic densities and that the mobility of the interface units decreases with increasing the simulation pressure, it is not unlikely that such high pressures and the detailed atomistic nature of polymer and nanoparticle may mimic the effects of slightly attractive interactions. On the other hand, more recent coarse-grained MD calculations performed with longer chains (80 units) in Ref. [72] show that the mobility of the matrix chains is enhanced with repulsive interactions and reduced with strongly attractive interactions, although the surface of the simulated nanoparticles is perfectly smooth. The effect of strongly attractive interactions is attributed in Ref. [72] to a much higher barrier for monomer exchange between the first two interface shells, resulting in longer residence times of the polymer units in the first interface shell when the interactions are strongly attractive.

Smith et al. [126] investigated the behaviour of $F_{self}(q,t)$ for polymer melts between attractive surfaces, both in the assumption of a flat and of a regular surface structure. The observed behaviour is similar to that reported in Fig. 18(a). With the flat surface the probability distribution $P(R)$ of the bead self-displacement $R(t) = \langle |\boldsymbol{r}_k(t) - \boldsymbol{r}_k(0)| \rangle_k$ is close to Gaussian, as it is with the bulk melt. A reference index is defined as

$$\alpha_2(t) = \frac{3\langle R(t)^4 \rangle}{5\langle R(t)^2 \rangle^2} - 1 \tag{24}$$

that vanishes in the Gaussian case. Labelling as t_{max} the time corresponding to the maximum of $\alpha_2(t)$, in the structured case $\alpha_2(t_{max})$ is positive the more, the stronger is the attraction strength of the polymer beads to the surface centres (dynamic heterogeneity). For strong attractions a two-peak structure of $P(R)$ may appear. In conclusion, compared with the bulk melt, polymer dynamics between structured attractive surfaces is both slower and dynamically heterogeneous, meaning that not all the displacements $R(t)$ are equally probable "a priori". The slower dynamics and increasing heterogeneity with increasing strength of the polymer–surface attraction, especially evident for the structured surface, resemble behaviour observed for polymer melts with decreasing temperature, approaching the glass transition. In this respect we point out that, in comparison with the melt, the glassy state was suggested to be accompanied by more restricted rotational oscillations around the chain single bonds [127–129]. Considering that smaller oscillations favour a more ordered arrangement of the polymer beads, this theoretical result is consistent with the increasingly ordered bead structure at increasing attraction strength on the polymer layers close to the structured surface [68,126].

McCoy and Curro [125] have investigated the issue of the polymer glass transition in confined geometries starting from the assumption that its T_g may be approximated by that of a corresponding homogeneous bulk polymer at the same average density. The polymer density oscillations produced by a solid surface were described by the DFT method. The wall–(polymer bead) interaction

ranges from purely repulsive to strongly attractive. They showed that the difference ΔT_g between the glass temperature of the polymer film close to the wall and in the bulk changes from negative to positive on going from an air/polymer interface to strongly attractive surfaces. Also, ΔT_g changes linearly with $1/H$ for large distances H between parallel surfaces defining a slab wherein the polymer is included.

While McCoy and Curro [125] as well as others considered solid surfaces with simple geometries (flat or spherical), Vilgis has recently provided an overview of the reinforcement effects operating when the surfaces have a certain roughness, which can be described by a fractal model [21]. Equilibrium and dynamic properties of the adsorbed polymer chains were considered separately in [130,131]. By a variational calculation [51], they analyse the transition from a slightly deformed Gaussian polymer coil to an adsorbed localized conformation where the polymer size perpendicular to the surface does not depend on the chain length. Following earlier work by Baumgärtner and Muthukumar [132], they distinguish *space* heterogeneity on a rough surface, slightly affecting the localization transition, from *energetic* heterogeneity whereby the transition may be induced even at vanishing mean interaction strength.

For a certain strength of the filler activity the chain dynamics appears glassy, as only local motions are possible on a rough surface [131]. An approximate estimate of the shift of the polymer glass transition temperature is $\Delta T_g \propto \langle \Delta/b^3 \rangle^2$, where the parameter Δ represents the typical volume of holes on the surface, and b is the statistical segment length of the chain.

In a related investigation on the sliding friction of rubber networks on self-affine rough surfaces [133] Heinrich, Klüppel and Vilgis propose a dynamic theory for a ''Rouse slider'' on a Brownian surface, to describe the bulk polymer in the rubber–glass transition region. They obtain a bell-shaped dependence of the friction coefficient-proportional to the friction force for a constant applied load—vs. the logarithm of the friction velocity. The half-peak width is generally larger than two decades and increases with the number of sub-segments considered in the Rouse sliding model. It may be interesting to compare these results with those obtained by two of us [134] for the sliding friction between two polymer surfaces. A polymer with large rotational barriers around chain bonds was considered and results were obtained within a Rouse model of polymer dynamics, including internal viscosity [135]. In order to make the results applicable to the experimental data by Maeda et al. [136] on modified polystyrene, a single value of the wavelength specifying the undulations of the contacting surfaces was assumed. The half-peak width of the friction force vs. the relative velocity of the surfaces is about one decade, in agreement with the experimental data [136]. It tends to broaden for decreasing values of the rotational barriers, in some analogy with the results by Heinrich et al. (no internal viscosity) [133].

Features of these filler-induced changes to the polymer dynamics have been recently incorporated by Sarvestani and Picu [137] in a rheological model for polymeric melts with small particles. Here the particle–particle distance is on the order of the chain radius of gyration and the interaction of polymer and filler is assumed to be strong. This interaction is implicitly accounted for by an enhanced friction coefficient at selected chains sites. Thus the model is purely frictional in nature and the chain diffusion essentially takes place by reptation, to account for entanglement effects.

6. Overall viscoelastic response of polymer nanocomposites

6.1. Introduction

Most of the current theories and simulations of the overall viscoelastic response of polymer nanocomposites naturally fall into the mesoscopic regime. In a filled elastomer, this represents the length scale over which molecular details are averaged out, but the material cannot yet be considered as a homogeneous continuum. It is intermediate between the molecular and the macroscopic scales. The former is the traditional realm of the chemist intent on producing better materials by (for example) clever functionalization of the polymer or the nanoparticles, and it is also the subject of the molecular theories/simulations described in the previous sections. The latter belongs to the mechanical engineer interested in testing the final properties of a reinforced elastomer or in designing a tyre according to some given specifications. The mesoscale can be tentatively identified with the 10 nm–10 μm range, since this is the typical size of the particles, of their aggregates and their average separation at practical filler loadings.

A class of mesoscale models of filled rubber behaviour is essentially phenomenological in spirit. An example is the Kraus model [30]. Expressions for the in- and out-phase components of the complex modulus (μ' and μ'') are derived from kinetic equations for rates of breakup (R_b) and formation (R_f) of particle–particle "contacts". Strain dependence (i.e., the Payne effect) is modelled by assuming that these grow and decay as power laws of the strain γ:

$$R_b = k_b N\gamma^m, \quad R_f = k_f(N_0 - N)\gamma^{-m}, \tag{25}$$

where k_b and k_f are rate constants, N is the number of particle–particle contacts (N_0 in the unstrained state) and m is a constant. The in- and out-of-phase moduli (in excess over those of the unfilled network) are taken proportional to the number of existing contacts N and to the rate R_b, respectively. Kraus further assumed that, for a given amplitude and frequency, a steady state is always established with $R_b = R_f$. One of the results of the model is the identification of a characteristic or critical strain γ_c:

$$\gamma_c = \left(\frac{k_f}{k_b}\right)^{1/2m}. \tag{26}$$

Both the decay of μ' and the maximum of μ'' are predicted to occur around γ_c, in qualitative agreement with experiment. Heinrich, Vilgis and others investigated further and refined the basic Kraus model. These advances have been reviewed in Ref. [20]. One of the main results is that the m parameter entering (25) and (26), evaluated from experimental data for different elastomers and carbon blacks, always takes values in the range 0.5–0.6. An explanation for the apparent universality of this parameter was provided by Huber and Vilgis [18], who obtained $m = 0.66$ by a scaling analysis of the deformation of fractal fillers described by statistical parameters appropriate to the structure of common carbon blacks.

While the Kraus model and related approaches are interesting and instructive—and indeed useful by providing a theoretical framework for fitting experimental data—they also have shortcomings. They start by *assuming* that particle–particle interactions represent the most important contribution to reinforcement, and as a result they do not discriminate clearly among different reinforcement mechanisms. For example, it is conceivable that Eqs. (25) might also describe the kinetics of formation/breakup of polymer–filler interactions, rather than filler–filler bonds. Thus, the same mathematics could actually describe some rather different physics! For this reason, we believe that more rigorous approaches are required to achieve a firm understanding of reinforcement mechanisms. These models may contain adjustable parameters, but the physical significance of these parameters should be identified as clearly and as uniquely as possible. The remaining part of this section is devoted to this class of theories and simulations.

The basic starting point for most meso-scale theories of the mechanical properties of filled elastomers is represented by the Einstein relation for the enhancement of the viscosity (η) of a fluid by a dilute suspension of rigid spherical particles, or equivalently Smallwood's result for the increase in the shear modulus (μ) of an elastic solid by incorporation of a small fraction of hard spheres [138,139]:

$$\eta = \eta_0(1 + 2.5\phi), \quad \mu = \mu_0(1 + 2.5\phi), \tag{27}$$

where ϕ is the particle volume fraction, η_0/μ_0 are the properties of the fluid/matrix, and η/μ those of the suspension/composite.

The close similarity between Eq. (27) is not accidental. In fact, the viscous and the elastic problems are mathematically equivalent, since under appropriate limiting conditions (slow creeping flow and small deformations, incompressibility of the fluid and of the elastic matrix) there is a one-to-one correspondence between the Navier–Stokes equation of fluid flow and the Lamè equation of elasticity [138,139]. Further important assumptions at the basis of Eq. (27) are (a) the no-slip boundary condition for fluid flow, which translates into perfect adhesion at the rubber–filler interface in the elastic case, and (b) perfect mechanical homogeneity of the two phases. It is important to remark that, while incompressibility is always a good approximation for a polymer melt or network (the shear modulus is much smaller than the bulk one) and the limit of slow and small deformations leaves out several interesting phenomena (rubber is used for its high deformability, after all) but nonetheless may always be attained under appropriate experimental conditions, conditions (a) and (b) may or may not hold in a polymer nanocomposite. First of all, unlike conventional fluids, polymer melts may display a finite wall slip when sheared against a solid surface [140,141]. Intuitively, the no-slip condition is expected to hold at small deformations, especially for covalently bonded or strongly interacting polymers and particles, or

rough particle surfaces. A different problem arises in this case, however. We have already discussed the experimental and theoretical evidence for the existence of a glassy rubber shell surrounding reinforcing fillers such as carbon back. Thus the assumption of mechanical homogeneity of the two phases breaks down in this case.

It is also important to be aware of the fact that, even though the continuum picture should be roughly correct "on average", it is possible to envisage situations in which Eq. (27) will fail badly. For example, consider a polymer melt of linear chains with a zero shear modulus (at low frequencies), in which we disperse some nanoparticles. If the polymer chains can bind irreversibly to their surfaces (chemically or physically) and they are sufficiently long to form a substantial fraction of particle–particle bridges, the nanoparticles effectively become highly functional cross-links and we obtain a rubbery solid with a non-zero shear modulus [9,34,75]. Unfortunately, (27) always predicts $\mu = 0$ when $\mu_0 = 0$. Clearly, the continuum picture breaks down and the macromolecular nature of the matrix is essential in this case. We also point out that a *decrease* in viscosity produced by the dispersion of spherical particles was recently reported by Mackay et al. [142], for a special model system (cross-linked polystyrene nanospheres in a polystyrene melt). This is quite unexpected, since Eq. (27) and its generalizations to high concentrations (to be discussed below) always predict an increase of viscosity/modulus over those of the embedding medium. The reason for the behaviour are not fully understood, but a likely explanation is the plasticization of a layer of polystyrene melt close to the particles [142]. This is equivalent to a decrease of the viscosity and of the glass transition temperature. Therefore, now it is the assumption of homogeneity of the matrix phase, which seems to be invalid.

6.2. Micromechanical models

When we consider a cross-linked network, the matrix has a non-zero modulus and the continuum represents a reasonable starting point, also in view of the fact that the typical distance between neighbouring cross-links is much smaller than the average particle size (1–3 nm vs. 20–100 nm). Maintaining the equations of continuum mechanics as the basic starting point, several generalizations of Eq. (27) have been obtained. This "micromechanics" approach can be a mathematically sophisticated subject, but the final results are often expressed by simple equations. In fact, when confronted for example with a new set of experimental data, it makes sense to attempt a first-order interpretation using the continuum mechanics hypothesis, before going on to consider specific molecular models to explain possible deviations from the former. Thus, even though we do write down most of these formulae, we hope to do a good service by providing some relevant references and encourage the interested readers—particularly those with a polymer science background who might be unfamiliar with this topic—to approach them.

Analytical results have been obtained for the elastic moduli of the following model nanocomposites, in the limits of small deformations and dilute particle concentrations ($\phi \to 0$):

(a) The particles may be deformable and the matrix may have a non-zero compressibility (finite bulk modulus). This solution, which includes (27) as a special case, is probably too general for the case of particle-filled elastomers, but might be applied (for example) to the mechanical behaviour of a glassy or semi-crystalline polymer toughened with microscopic droplets of a rubbery polymer. See Ref. [138].

(b) The particles are perfectly rigid and the outer matrix deformable, but the two are separated by an interfacial shell of a different material of a certain thickness Δ [144]. This model is obviously relevant for the mechanical properties of the nanocomposites with a glassy polymer shell surrounding the particles. When this shell is much stiffer than the outer matrix, the main effect can be simply described by admitting that the particle radius R is replaced by an effective radius $(R+\Delta)$. In other words, the particle volume fraction ϕ becomes an effective volume fraction $\phi(R+\Delta)^3/R^3$. Of course, for a fixed shell thickness, this contribution becomes increasingly important as the particle size gets smaller.

(c) One possibility, which surprisingly has been worked out only very recently, is the generalization to the mechanical properties of a dilute suspension of perfectly rigid spheres in a model viscoelastic liquid (the so-called second-order fluid or SOF) [145]. An analytical solution is obtained perturbatively in the limit of "weak viscoelasticity" (i.e., for Deborah

number $De \to 0$). Under simple shear, both the real and imaginary components of the complex viscosity (or, equivalently, of the complex modulus) increase by a 2.5ϕ factor, as expected on the basis of (27). In addition, normal stress differences appear, and are given by

$$\langle N_1 \rangle = 2De(1 + 2.5\phi)$$
$$\langle N_2 \rangle = -De\left(2 + \frac{b}{4} + \frac{125 + 10b}{28}\phi\right) \tag{28}$$

where b is a dimensionless parameter entering the SOF constitutive equation. These results were supported by experimental as well as numerical data.

(d) Another possibility is the treatment of anisotropic particles such as prolate or oblate spheroids, i.e., whiskers or platelets in the limit of high/low aspect ratios. These may have a totally random orientation or have their axes aligned along a certain direction (producing in this case a composite with anisotropic properties). In the case of random orientation of hard particles in a soft matrix, both whiskers and platelets are more effective than spheres in enhancing the modulus, but the latter more so (for a given volume fraction). See Refs. [138,139].

(e) In a typical carbon black sample (there are actually several grades of carbon black), many near-spherical primary particles of radius $a_{CB} = 50$–100 nm's are fused to give branched, non-compact aggregates with average radius $R_{CB} \cong 0.1$ μm. Statistically, the structure of these aggregates can be described as "fractal". In particular, a_{CB} and R_{CB} are related by the following scaling law:

$$R_{CB} \approx a_{CB}N^{1/D} \quad \text{or} \quad N \approx (R_{CB}/a_{CB})^D \tag{29}$$

where N is the average number of primary particles within an aggregate and D is its "mass fractal dimension". For several carbon black grades $N \cong 10^2$ and $D \cong 2.4$–2.5 (i.e., significantly less than the value of 3 for compact objects). The rubbery material that penetrates the void space within the aggregates is shielded from any external deformation, in analogy with the hydrodynamic screening of the inner segments of a polymer coil in a dilute solution. In other words, a carbon black aggregate and the rubber occluded within its branches behave as a single, near-spherical solid object. Thus, while the true volume of the aggregate is $V \cong Na_{CB}^3$, its effective volume is $V_{\text{eff}} \cong R_{CB}^3$. At low volume fractions, Eq. (27) continues to hold, but with a rescaled or effective volume fraction:

$$\phi_{eff} \cong \phi\frac{R_{CB}^3}{Na_{CB}^3} \cong \phi\left(\frac{R_{CB}}{a_{CB}}\right)^{3-D} \cong \phi N^{(3-D)/D} \tag{30}$$

Clearly, $\phi_{eff} \gg \phi$ for large and highly branched aggregates ($N \gg 1$ and $D < 3$), thus producing a very significant increase of the elastic modulus. This simple argument about the reinforcement by fractal aggregates has been generalized also to high filler volume fractions by the application of scaling laws [143] or multiple scattering effective medium calculations [144]. These models generalize Eq. (30) by including also a connectivity exponent C (also known as spectral dimension) representing the degree of "branchedness" of an aggregate.

Another set of generalizations of Eq. (27) considers the behaviour at higher filler loadings (finite ϕ). If we limit ourselves to the simpler case of spherical particles, the effect of interparticle elastic interactions can be included in several ways:

(f) One possibility is to solve the mechanical problem of two spheres at finite distances, and then use these results to obtain a second-order correction. The result, first obtained by Batchelor and Green and then by Chen and Acrivos in a somewhat more general context, is

$$\mu = \mu_0(1 + 2.5\phi + 5.0\phi^2). \tag{31}$$

Note that the older Guth–Gold result with a 14.0 coefficient in place of 5.0 is still found frequently in the rubber literature, but is now known to be incorrect on theoretical grounds. The shortcoming of this approach is that (29), like (27) before it, is bound to become inaccurate at increasing volume fractions. The reason is that many-particle interactions (threefold or more) are neglected. As a consequence, the modulus can be seriously underestimated by (31). In fact, it predicts a finite value of it even as $\phi \to 1$, when μ should instead become infinite because of the assumption of perfectly rigid particles. A simple correction to (29) which remedies for this deficiency is [62,138]

$$\frac{\mu}{\mu_0} = \frac{1 + 0.5\phi}{1 - 2\phi} \tag{32}$$

This can be derived by a rational function (Padé) approximation to Eq. (31). It agrees with it to second order in ϕ, but it also diverges to infinity for $\phi \to 0.5$, which happens to be close to the maximum packing fraction for a random arrangement of monodisperse hard spheres [139]. Hence there is a certain justification for the divergence of μ at this particular value.

(g) A multiple scattering effective medium approach has been developed by Freed et al. [146–148]. As the name suggests, this approach considers the "scattering" of the elastic deformation field within the matrix by the surface of rigid particles embedded within it. It avoids the two-particle approximation by dealing with an infinite hierarchy of scattering events, but for mathematical simplicity it neglects any correlation in the relative positions of the particles (penetrable spheres). Tests of the theory against experimental results on some metallic/ceramic and polymer/glass composites support its general validity [148]. Huber and Vilgis have also used a similar formalism to derive expressions for the elastic modulus of an elastomer containing fractal fillers, but do not provide comparisons with experimental data [144]. Thus, tests on specific polymer–filler systems should be worthwhile, but to our knowledge this has not yet been attempted.

(h) A totally different approach, which in principle can be applied not just to composites with spherical inclusions but more generally to any sort of random heterogeneous material, consists of using information on the "*n*-point correlation functions" (statistical descriptors of the phase distribution inside a material) to define increasingly stringent bounds (i.e., lower and upper limits) on its elastic modulus. These correlation functions can be extracted from a theoretical model, from computer simulations, or from experimental characterization of a specific material (imaging by electron microscopy, for example). This approach is extensively reviewed in the book by Torquato [139]. It will not be discussed further, since we are not aware of any attempts to apply it to the specific case of filled elastomers.

(i) Finally, an approximate but "robust" approach consists of neglecting particle–particle correlations by invoking some kind of mean-field approximation. The most successful attempt in this sense is the "three-phase composite sphere model" by Christensen and Lo (CL) [138,149]. The essential idea is that the many-particle elastic problem is replaced by a simpler one, in which a single particle is coated with a spherical annulus of matrix phase (of radius chosen to produce the correct volume fraction ϕ), and this composite sphere is then embedded in an effective homogeneous medium representing the rest of the composite. The elastic modulus of this outer medium is identified with the overall effective modulus of the composite, and its value is the main objective of the whole calculation. The final result is a workable (but still too involved to be reported here, see also Ref. [150]) analytical expression for the elastic modulus, which retains its usefulness also at very large volume fractions. This is plotted in Fig. 19, alongside (31) and (32) for comparison. These three expressions agree up to $\phi \cong 0.2$. The CL solution is always bracketed by the other two and, unlike the Padé approximation (32), it diverges to infinity only when $\phi \to 1$. For this and other reasons, it is believed to be more accurate for a polydisperse system with a wide distribution of particle radii.

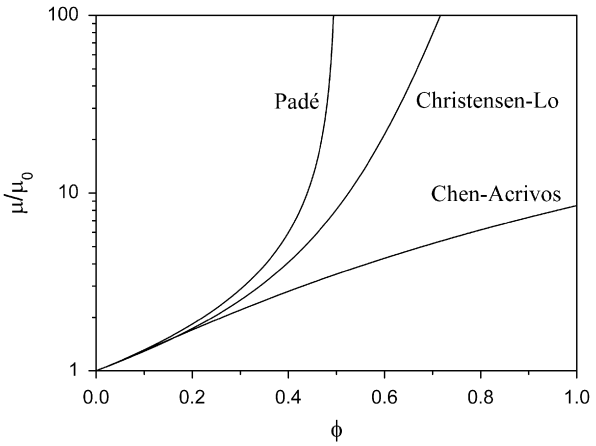

Fig. 19. Comparison of different formulae for elastic modulus of a composite with rigid spherical particles at volume fraction ϕ: Chen–Acrivos [Eq. (31)], Christensen–Lo [138,149,150] and Padé approximation [Eq. (32)].

Unfortunately, many of the previous generalization of (27) are mutually exclusive. It has generally proved difficult, if not altogether impossible, to obtain a closed analytical solution of the mechanical problem when two or more of features (a)–(e) are simultaneously included in the model, and a solution valid at high filler content is also

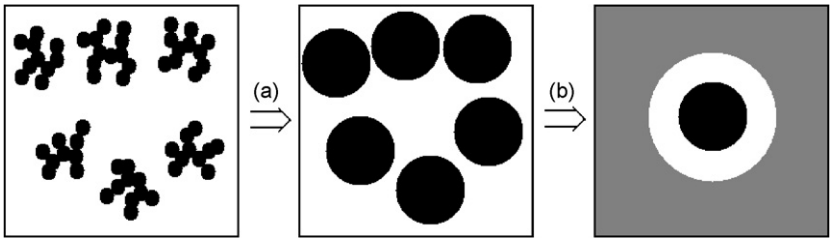

Fig. 20. Scheme for the calculation of the effective modulus [150]: (a) each branched filler aggregate is replaced by an effective sphere, with volume fraction $\phi_{eff} = f\phi$; (b) the many-sphere problem is replaced by the three-phase composite sphere model of Christensen–Lo.

sought [(f)–(i)]. As a result, one has to resort to either judicious approximations or numerical techniques in order to obtain quantitative results.

As an example of the approximations which may be introduced to deal with the combined effects of an interfacial glassy layer [point (b)], complex-shaped fillers [point (e)] and many-particle elastic interactions [points (f)–(i)], we briefly describe the work by one of us [150]. The essential elements are illustrated in Fig. 20. In essence, a difficult problem is factorized in two easy steps. In the first step, each branched filler aggregate is replaced by an effective sphere, at an effective volume fraction $\phi_{eff} = f\phi$. The f factor, which is the only adjustable parameter of the model, simultaneously accounts for the presence of a glassy shell of thickness Δ [see point (b)] and for the fractal structure of the filler [see point (e) and Eq. (30)]. In the second step, the elastic modulus of the system is calculated by replacing the complex many-particle problems by the three-sphere composite-sphere model of Christensen and Lo [see point (i)]. The effectiveness factor f is fixed by requiring that the experimental and theoretical moduli coincide at a single volume fraction.

The result is shown in Fig. 21, where we compare the experimental [26] and theoretical [150] values of the small-strain shear moduli for increasing amounts of N234 carbon black in a solution styrene–butadiene rubber matrix (SSBR) at 0 °C. The agreement is excellent up to 50 PHR, which corresponds to a filler volume fraction $\phi = 0.2$ and a tenfold increase in the modulus with respect to the unfilled matrix. Instead, the model overestimates the modulus above 60 PHR of filler. This is expected, since the replacement of the filler aggregates by effective spheres is a meaningful approximation only below the filler "overlap concentration" (defined in analogy with polymer solutions [22]). It is significant that, if we identify this overlap concentration with 60 PHR (i.e., the value of

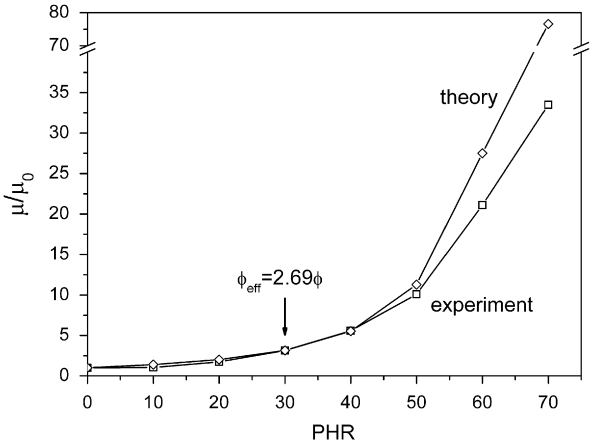

Fig. 21. Comparison of the experimental data (Ref. [26], see also Fig. 1) and theoretical prediction [150] for the small-strain elastic modulus of an SSBR rubber filled with N234 carbon black at 0 °C. The amount of filler is expressed in PHR units (grams of filler for 100 g of polymer).

loading at which the model starts to diverge from the experiment), we find that this corresponds to a value of effective volume fraction $\phi_{eff} \cong 0.6$. This is not too far above the maximum packing fraction of 0.5, for randomly dispersed monodisperse hard spheres. Also, the model fits equally well (or equally badly) the small-strain elastic moduli of the same composites at 70 °C. All that needs to be done is to adjust the effectiveness factor, from $f = 2.69$ at 0 °C to $f = 2.42$ at 70° (both are obtained from the moduli at 30 PHR). Qualitatively, the decrease in f is justified by the reduced thickness Δ of the glassy shell on going to higher temperatures.

The previous result is important not only because it offers a simple and accurate prediction of the small-strain modulus up to practical filler contents using a single adjustable parameter, but also for its implications on the interpretation of the reinforcement mechanism and the Payne effect. We recall that, in the "textbook" interpretation of

reinforcement, interparticle interactions are considered responsible for *both* the large values of the small-strain modulus *and* its drop at medium-large deformations. The fact that the elastic modulus can be extrapolated from low up to relatively high loadings without invoking additional reinforcement mechanisms such as Van der Waals interactions among the particles, means that these—although certainly present—are probably not so important after all. This immediately raises another interesting question: if interparticle interactions are negligible, what causes the drop in the modulus at medium-large strains? Several hypotheses have been put forward, but so far none has been scrutinized by rigorous theoretical or computational studies. We shall return to this point later on, after discussing a few more recent studies.

Gusev [151] has recently presented an interesting application of the finite-element method (FEM) [152–154] to obtain a numerical solution to a specific micromechanical model of a rubber matrix containing reinforcing filler particles. This particular study contains two important elements of novelty, compared to previous continuum mechanics approaches. First of all, unlike previous models, which considered a two-phase system formed by filler and polymer matrix with constant mechanical properties at their interior, Gusev adopts a three-phase model by introducing also a hard polymer shell of thickness Δ surrounding each particle. The mechanical properties of each phase are entirely determined by assigning the values of its three constitutive parameters (in-phase shear modulus μ', Poisson's ratio ν and loss factor $\tan\delta$). The thickness of the hard rubber shell is taken to be 0.04–0.12 times the particle radius, which corresponds to 2–6 nm for a typical radius of 50 nm. The second important element of Gusev's model is the adoption of a special filler morphology. Monodisperse spherical particles are positioned at the nodes of a diamond lattice in such a way that they almost touch each other (volume fraction 0.32). This is clearly unrealistic compared to the disordered experimental systems, but from a modelling perspective this choice helps to highlight the special role played by the polymer shells bridging closely spaced particles. After solving for the displacement field within the material undergoing a small macroscopic strain by the FEM method, it is possible to calculate both the overall μ'_{eff} and μ''_{eff} moduli of the composite, and to identify the contribution to these moduli from specific parts of it. The main result is that a 100-fold increase of both the storage and dissipative moduli can be readily achieved even with a very thin glassy shell. This should be compared with the modest four-fold increase of these moduli, computed for an analogous two-phase model with zero shell thickness and predicted also by the analytical solution of the three-phase model [138]. The second result is that most of the contribution to both moduli is highly localized within a very small fraction of material, in particular within the portions of the glassy shells bridging neighbouring particles.

6.3. Mesoscale bead-and-spring models and the electrostatic analogy

The continuum mechanics theories and FEM simulations discussed so far are based on the laws of linear elasticity and deal only with the range of small deformations. This is an obvious limitation, since we are ultimately interested in explaining the non-linear behaviour of filled elastomers at large deformations. Continuum mechanics theories and simulations methods can indeed be set up to treat this more general situation. See Refs. [155–159] for some entry points to this literature. Unfortunately, these approaches tend to highly specialized and mathematically involved and, most importantly, physical effects originating from the macromolecular nature of the matrix or from specific interactions at the rubber–filler interface are either neglected or obscured by the formalism.

An alternative attempt to achieve a substantial but physically sound simplification of the problem was made some time ago by two of us. It led to the formulation of a "mesoscopic bead-and-spring" (MBS) model of a rubber matrix filled with rigid spherical particles. As the name suggests, in this model the particles are represented by beads interacting by a certain potential, whereas the rubber matrix is effectively replaced by a set of harmonic springs connecting pairs of neighbouring particles. In other words, the total potential energy of the nanocomposite is written as

$$U(\boldsymbol{R}_1,\ldots,\boldsymbol{R}_N) = U_{int}(\boldsymbol{R}_1,\ldots,\boldsymbol{R}_N) + U_{el}(\boldsymbol{R}_1,\ldots,\boldsymbol{R}_N) \tag{33a}$$

$$U_{int}(\boldsymbol{R}_1,\ldots,\boldsymbol{R}_N) = \sum_{i<j}^{N} U_{ij}(|\boldsymbol{R}_i - \boldsymbol{R}_j|) \tag{33b}$$

$$U_{el}(\boldsymbol{R}_1,\ldots,\boldsymbol{R}_N)=\frac{1}{2}\sum_{i<j}^{N}K_{ij}(\boldsymbol{R}_i-\boldsymbol{R}_j)^2 \tag{33c}$$

Here, the $\boldsymbol{R}_i$ vector contains the coordinates of the centre-of-mass of particle i. For simplicity, in our simulations we have adopted a simple pairwise hard-core potential for the interaction between monodisperse spherical particles of diameter D:

$$U_{ij}(|\boldsymbol{R}_i-\boldsymbol{R}_j|)=\begin{cases}\infty & \text{for} \quad |\boldsymbol{R}_i-\boldsymbol{R}_j|\leqslant D\\ 0 & \text{for} \quad |\boldsymbol{R}_i-\boldsymbol{R}_j|>D\end{cases} \tag{34}$$

Note, however, that more general interaction potentials including an attractive tail for the van der Waals interactions among the particles could be easily implemented. This is a clear advantage over continuum mechanics approaches, which simply neglect all long-range interactions by writing the total energy as the space integral of the product of *local* stress and strain fields.

The other appealing feature of the MBS model is the simple and intuitive expression for the elastic energy entering Eq. (33). Note that the springs have zero equilibrium distance. This is consistent with the general theory of phantom polymer networks (viewing the particles as a special sort of highly functional, slowly fluctuating cross-links). The overall "collapse" of the spring network is prevented by enforcing the constant-volume constraint. With the appropriate choice of the force constants (see below), we find that the forces exerted on particle i by the neighbouring particles j add up to zero when the particles' coordinates are close to those used to assign their values (i.e., the positions "at cross-linking" almost coincide with the final equilibrium position). Incidentally, Long and Sotta [163] have recently proposed a similar model, but with some important differences. Instead of computing the force constants from the particle's initial positions, they simply set all the force constants to the same value (within a certain pre-defined cutoff distance). Also, their springs have a non-zero equilibrium length, which is identical for all pairs of connected particles.

The main problems associated with the MBS representation of the filled rubber elasticity may be summarized as follows:

(a) the question of how the elastic energy expression can be justified, and if this is so under which set of assumptions;
(b) the definition of a criterion or computational algorithm for the assignment of the values of the force constants K_{ij};
(c) whether the model is complex enough to capture the main phenomenology of rubber reinforcement and, if that is not the case, how it can be generalized so as to achieve this.

We will first discuss (a) and (b), and leave point (c) to the closing paragraphs of this section.

Concerning point (a), we have provided a justification for Eq. (33) by invoking an analogy between the mechanical behaviour of a polymer network inglobating perfectly rigid, non-rotating particles and the electrostatic problem of charged metallic particles separated by a dielectric medium. The analogy relates the following pairs of mechanical/electrostatic quantities:

$$\begin{aligned}&\text{force density } \boldsymbol{f} \Leftrightarrow \text{charge density } \rho\\ &\text{displacement } \boldsymbol{u} \Leftrightarrow \text{potential } \varphi\\ &2\times(\text{shear modulus}) \; 2\mu \Leftrightarrow \text{dielectric constant } \varepsilon\end{aligned} \tag{35}$$

Unlike the analogy between elastic and hydrodynamic problems—which is exact under certain limiting conditions (slow incompressible fluid flow, etc.)—this is only approximate. We originally derived it by comparing the rules for in-series and in-parallel combination of phantom polymer chains (mechanical problem) and of capacitors (electrostatic problem). However, it can also be justified by a continuum argument, without any reference to the macromolecular structure of the elastic matrix. Compare for example the displacement field produced by a point force and the electrostatic potential produced by a point charge at the origin [i.e., the Green's functions for $\boldsymbol{f}=\boldsymbol{F}\delta(\boldsymbol{r})$ and $\rho=Q\delta(\boldsymbol{r})$]:

$$\boldsymbol{u}(\boldsymbol{r})=\frac{(1+\boldsymbol{nn})}{8\pi\mu r}\boldsymbol{F} \tag{36a}$$

$$\varphi(\boldsymbol{r})=\frac{1}{4\pi\varepsilon r}Q \tag{36b}$$

where $\boldsymbol{1}$ is the identity matrix, $r=|\boldsymbol{r}|$ and $\boldsymbol{n}=\boldsymbol{r}/r$ [for simplicity we have specialized (36a) to the case of an incompressible material]. Note that both are long-range interactions, since they decay as r^{-1}.

The electrostatic analogy can be finalized to the specific case of rigid particles in a rubber matrix, by noting that all the points within the particles will

always undergo the same displacements, provided these are not allowed to rotate (probably not a critical assumption in the case of spherical fillers). According to Eq. (35) this corresponds to a constant electrostatic potential within the particles. Alternatively, a perfectly rigid particle has an infinite shear modulus, which corresponds to an infinite dielectric constant. By either argument, we see that the rigid particles correspond to conductors in the electrostatic model. It can then be shown [160–162] that the quadratic expression for the electrostatic energy of a systems of N conductors at potential φ_i.

$$U = \frac{1}{2}\sum_{i,j=1}^{N} C_{ij}\varphi_i\varphi_j \tag{37}$$

almost directly translates into the elastic energy (33c) (the derivation exploits the "full screening" condition $C_{ii} = -\sum_{j\neq i} C_{ij}$, which is achieved in the limit of an infinite system). The K_{ij} force constants of the mechanical problem are simply related to the C_{ij} induction coefficients of the electrostatic one:

$$K_{ij} = K_{ji} = -C_{ij} = -C_{ji} \quad (i \neq j) \tag{38}$$

Their relationship can also be appreciated by comparing the following linear relationships between particle charges/potentials and forces/displacements:

$$Q_i = \sum_{j=1}^{N} C_{ij}\varphi_j \tag{39a}$$

$$\boldsymbol{F}_i = -\sum_{j=1}^{N} K_{ij}\Delta\boldsymbol{u}_j \tag{39b}$$

Incidentally, we point out that a related electrostatic analogy has been invoked with similar justifications by Douglas et al. [164] to compute the translational diffusion coefficient of complex-shaped nanoparticles in a viscous fluid (the single-particle hydrodynamic radius corresponds to the electrostatic capacity in this case).

The electrostatic analogy also provides an answer to point (b), by establishing a route for the determination of the force constants. According to (38), these are essentially the induction coefficients for a system of conductors, placed at the particle positions "at the time of cross-linking" (which is assumed to be instantaneous). These are obtained from the solution of the linear system (39a), using a multipole representation for the (inhomogeneous) charge distribution at the particle surfaces and the electrostatic field produced by them. An example of the results obtained in this way is given in Fig. 22, for a systems of randomly dispersed spherical particles at volume fraction $\phi = 0.1$. It can be seen that the individual force constants decay in a roughly exponential way with the interparticle distance (where the "screening length" diminishes with ϕ), but there is also a certain scatter in the force constants arising from the details of the local particle environments (neighbouring third particles).

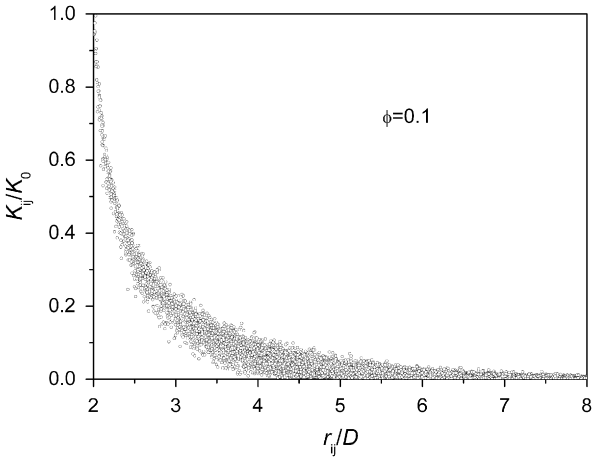

Fig. 22. Dependence of the pairwise force constants of the MBS model on the interparticle distance at cross-linking, for a system of randomly dispersed hard spheres at volume fraction $\phi = 0.1$. D and K_0 are the particle diameter and a normalizing force constant, proportional to the product of matrix modulus and particle diameter. Redrawn with permission from Raos et al. [161], copyright (2002) of Elsevier Ltd.

The force constants and the induction coefficients have one further interesting interpretation. This arises from yet another analogy, between the Poisson equation of electrostatics and the steady-state diffusion equation:

$$\nabla^2\varphi = -\frac{\rho}{\varepsilon} \tag{40a}$$

$$\nabla^2 n = -\frac{\sigma}{D} \tag{40b}$$

where n is the concentration of Brownian particles undergoing diffusion (let us call them RWs, for Random Walkers), σ is the local rate of creation or annihilation (depending on the sign) of RW's, and D is the local diffusion coefficient. Thus, (35) may be complemented by the *exact* correspondence rules:

creation/annihil. rate $\sigma \Leftrightarrow$ charge density ρ

concentration $n \Leftrightarrow$ potential φ

diffusion coeff. $D \Leftrightarrow$ dielectric constant ε (35b)

In the diffusion problem, the rigid/conducting particles correspond to regions of space with an infinite (or very large) diffusion coefficients. The RW concentration is constant within these regions. Let us also assume that the RW's are created/annihilated only at the surface of these particles (in analogy with the change distribution of conductors). Then (39a) and (39b) translate into:

$$S_i = \sum_{j=1}^{N} C_{ij} n_j \tag{39c}$$

where n_j is the RW concentration within particle j, S_i is the overall rate of RW creation/annihilation on the surface of particle i, and the C_{ij}'s are identical to the induction coefficients, but with a different interpretation. A little reflection shows that their absolute values are proportional to the probability that a RW created at i diffuses until reaching another particle j, at which point it is annihilated. Thus, because of the one-to-one mapping between random diffusion problems and the statistics of phantom chains, the C_{ij}'s are also proportional to the number of polymer bridges connecting the two particles. In principle, their values could be obtained from simulations of long phantom chains, similar to those described in the first part of this review.

The small-strain elastic moduli under shear or elongation can be readily calculated by taking the appropriate second derivative of the energy (33a), assuming a constant volume, affine particle displacements and neglecting particle–particle interactions for the moment. The overall soundness of the MBS model and the reliability of the force constants associated with it through Eq. (38) is demonstrated by the fact that the dependence of the elastic modulus on particle volume fraction is consistent with Eq. (27) and its extensions [our data for $\phi \leqslant 0.3$ are nicely fitted by $\mu/\mu_0 = 1 + 2.5\phi + 5.0\phi^2 + 14.0\phi^3$]. Also, as already remarked above, the particle positions which minimize the elastic energy are very close to those "at cross-linking" (i.e., the coordinates used in the solution of the electrostatic problem).

The behaviour of the MBS models at large deformations—including also the effect of interparticle interactions (33b)—can be studied by any of the standard particle-based simulation methods. We used a Monte Carlo procedure, in which random single-particle displacements are alternated with collective stretching/compression moves whose acceptance depends on an applied external force (thus, they are essentially constant-stress MC simulations). Our MC simulations, demonstrated that the equilibrium stress–strain curves of the filled networks closely follow the same law of the reference embedding matrix (unfilled phantom network), as if the particle–particle interactions were absent:

$$\sigma = \mu(\lambda - \lambda^{-2}) \tag{40}$$

Also, this result is substantially independent of amount of particle fluctuations about their equilibrium positions (their mean-square displacements are proportional to the absolute temperature and inversely proportional to the force constants, which depend in turn on the product of particle radius and matrix modulus). This is quite unexpected, since we do observe large deviations from affinity produced by the hard-core interactions (34) among the particles, due to their "collisions" perpendicularly to the direction of stretching. A different, more complex deformation mode might highlight more clearly the effect of particle non-affinity on the stress–strain curves, but we did not explore this possibility.

Long and Sotta [163] simulated the dynamical behaviour of their MBS system under oscillatory shear by a simplified dissipative particle dynamics (DPD) method (in fact, because of these simplifications it is more similar to conventional Brownian dynamics (BD)). Their computational experiments evidence elastic as well as plastic behaviour at large deformations. The plastic deformations are associated with permanent or very slow-healing changes in the structure of the material, which they identify with irreversible non-affine particle displacements produced by the unlocking of jammed particle configurations. Clearly, this is in contradiction with our own findings, in which the stress–strain curves are almost trivial and perfectly reversible. However, it is also true that while the basic physical models are similar, their results are not directly comparable to our own, due to a number of important details such as the differences in the representation of the elastic forces and to the different simulation method employed. More work is clearly required to reconcile these two sets of results.

Finally, we come to discuss point (c), which we had anticipated, namely whether the MBS model is complex and general enough to deal with the essential features of rubber reinforcement. The apparent disagreement between our own and the Long–Sotta flavours of it means that it is probably

premature to draw any definite conclusion, but we attempt anyway a brief discussion. The greatest strength of the MBS model is that, with the right choice of the force constants, it can reproduce one basic continuum mechanics result (the ϕ-dependence of the modulus) and extend it to large deformations with a conceptually simple machinery. Dealing with more general deformation modes or possibly anisotropic particles undergoing rotations might require the introduction of tensorial force constant $\boldsymbol{K}_{ij}$, in place of scalar ones K_{ij}. Obviously, the electrostatic analogy is no longer of use in this case, but one should probably go through the FEM solution of the full elastic problem to obtain the $\boldsymbol{K}_{ij}$'s (see for example [165]).

We have also seen that even the most accurate micromechanics results generally fail to reproduce some basic phenomenology of reinforcement, unless adjustable parameters or additional assumptions are introduced (see e.g., [150,151]). The same criticism could thus be extended to the MBS formulations explored so far. The fact that the filled rubber modulus decreases while that of the unfilled rubber matrix increases with temperature, means either that the assumption of phase homogeneity must be given up (because of the glassy rubber shell) or some important enthalpic contribution is at work, in addition to the entropic elasticity of the polymer network. Enthalpic elasticity could be introduced in the form of a more realistic particle–particle interaction model, including attractive or even tangential (i.e., friction) forces, in addition to the excluded-volume interaction (34). The effect of the glassy shell and the finite extensibility of the polymer chains could be modelled by non-linear elastic springs. Finally, the history- and strain-dependence of the material properties (Mullins and Payne effects) might be partly explained by the particle jamming/unjamming phenomena which have already been observed in the version of the MBS model by Long and Sotta, but might also require admitting some history-dependence of the force constants themselves. Of course, there are also potential disadvantages in carrying out this programme, since some of these corrections would be necessarily empirical and they would imply a loss in the appealing simplicity of the original model.

6.4. Non-equilibrium molecular dynamics simulations

We finally turn to the simulation schemes in which the macromolecular nature of the matrix material is explicitly taken into account. There are two main approaches to the calculation of the viscosity (or the elastic modulus) of a molecular system [64,166]. The first one involves the evaluation of the time-integral of the stress autocorrelation function from a conventional equilibrium MD simulation (Green–Kubo relation):

$$\eta_0 = \frac{V}{k_B T}\int_0^\infty \langle \sigma_{\alpha\beta}(t)\sigma_{\alpha\beta}(0)\rangle \, \mathrm{d}t \quad (\alpha\beta = xy, xz, yz). \tag{41}$$

The instantaneous value of the stress tensor is the sum of a kinetic (ideal gas) term and a virial term for the pairwise interactions among all the atoms:

$$\sigma_{\alpha\beta} = \frac{1}{V}\left\{\sum_i m_i v_{i\alpha} v_{i\beta} + \sum_{i<j} r_{ij\alpha} f_{ij\beta}\right\}. \tag{42}$$

The other approach, usually called non-equilibrium molecular dynamics (NEMD) [166], requires the explicit application of a shear velocity profile through the so-called Lees–Edwards or "sliding bricks" boundary conditions:

$$\langle v_x(z)\rangle = \dot{\gamma} z \tag{43a}$$

where $\dot{\gamma}$ is the (constant) shear rate. Much as in an actual experiment, the steady-state viscosity then is obtained by recording the average stress and computing the ratio:

$$\eta = \frac{\langle \sigma_{xz}\rangle}{\dot{\gamma}} \tag{44}$$

Thermostatting is a crucial issue in NEMD simulations, since mechanical work is continuously fed into the system through the applied shear field (43), and therefore heat has to be removed by the MD thermostat in order to keep the temperature stable.

These two approaches to the viscosity of homopolymer melts have been pursued by Kumar and coworkers [167] and by Kröger and Hess [168], respectively. Applications to filled nanocomposites have been given by Smith et al. [70] and by Sen et al. [75] using the equilibrium Green–Kubo approach, and by Kairn et al. [74], Pryamitsyn and Ganesan [170] and Raos et al. [171] using variants of the NEMD method. A detailed comparison of the methods has been presented by Vladkov and Barrat [169] for homopolymer melts. We are not aware of a similar comparison for polymer nanocomposites, but some general rules about their relative strengths and weaknesses can already be drawn. The Green–Kubo relations provide an estimate of the viscosity

as a simple by-product of a standard MD simulation. However, only the linear response can be obtained in this way (zero-shear viscosity η_0). The non-equilibrium approach mimics closely the actual rheological experiments and allows to explore also the non-linear regime (e.g., shear-thinning at high deformation rates). A separate simulation is required for different shear rates (and amplitudes), and there can be large uncertainties on the zero-shear viscosity due to the small values of the stress at low shear rates ($\eta \to \eta_0$ for $\dot{\gamma} \to 0$). Very long simulations are generally required to obtain reliable statistics by either method, sadly confirming the general observation that "there are no free lunches".

Having already presented some results from the equilibrium simulations in Sections 3 and 5 [70,75], here we concentrate on the discussion of the NEMD studies. Kairn et al. [74] adopted a flexible chain model with 20 LJ sites of diameter σ, with a rms radius of gyration $R_g = 2.219\sigma$. The particles have a diameter $d = 2.2254\sigma$, i.e., roughly equal to the average chain radius and only twice the size of a chain monomer, and have a range of volume fractions up to 0.30. All interactions among the monomers and the particles are purely repulsive, being truncated at the minimum of the LJ potential. These authors observe a plateau in the effective viscosity at low shear rates (smaller than the inverse of the Rouse relaxation time of the matrix chains) and shear thinning at higher rates. Both the zero-shear viscosities and the rate of shear thinning increase with filler content, in qualitative agreement with several experiments and continuum mechanics predictions. Quantitatively, the amount of this viscosity increase is not as large as expected. The authors identify at least two possible reasons for the relative modest effect of the particles. The first one is that the repulsive nature of all the interactions. Also Smith et al. [70] had shown that a system with repulsive polymer–filler interactions has a lower zero-shear viscosity than one with attractive interactions, other things being equal. The second reason is the very small size of the particles: if these were only slightly smaller, equal to individual chain beads, they would behave as solvent molecules or plasticizers. Hence, the particle radius chosen by Kairn et al. [74] is likely to fall within a cross-over region, between a solvent-like regime (viscosity decreases with particle content) and a filler-like regime (viscosity increases with particle content). These results might also be relevant to explain the non-Einstein-like behaviour described by Mackay et al. [142].

Pryamitsyn and Ganesan [170] and Raos et al. [171] independently adopted the DPD method [172,173] to conduct their simulations. DPD differs from other coarse-grained methods in two respects: type of interaction potentials and the use of a particular thermostat (incorporated in the MD equations of motion). The DPD beads interact by purely repulsive and very soft potentials (the interaction energy has a finite positive value at zero distance). As a consequence, in DPD it is possible to use relatively long time steps, and equilibrations is particularly easy. On the other hand, there are also potential disadvantages: the DPD model shows no glass transition even at low temperatures, and there are no entanglements among the polymer chains since these may pass freely through each other. The DPD method also uses a special sort of thermostat, which is apparently similar to BD because it involves a combination of friction and stochastic forces. Unlike BD, it has the important property of being "Galileian invariant" or "momentum conserving", which makes it particularly suitable for non-equilibrium simulations. In one set of simulations, the polymer matrix is a melt of linear chains of $N_p = 8$–96 beads [170], whereas in the other work the matrix is a fully cross-linked network [171]. Both probe the viscoelastic response of the nanocomposites by oscillatory shear NEMD simulation, in which (43a) is replaced by

$$\langle v_x(z,t)\rangle = z\gamma_0\omega\,\cos(\omega t) \tag{43b}$$

where γ_0 and ω are the amplitude and angular frequency, respectively. Results are presented in terms of the in- and out-of-phase components of the shear modulus (μ' and μ''), representing elastic and dissipative effects, and their ratio $\tan\delta = \mu''/\mu'$.

In their simulations, Pryamitsyn and Ganesan [170] report evidence of both particle-induced distortions of the strain field (i.e., generic hydrodynamic effects, captured also by continuum mechanics) and modifications of the intrinsic polymer-relaxation dynamics (included in the DPD equations through and enhanced polymer–particle friction coefficient). These results are somewhat expected, on the basis of our previous discussion of other simulations. The most interesting aspect of their results is the identification at high particle loadings (volume fraction $\phi = 0.5$) of: (a) a low-frequency plateau in the elastic modulus, indicative of solid-like behaviour even in the absence of

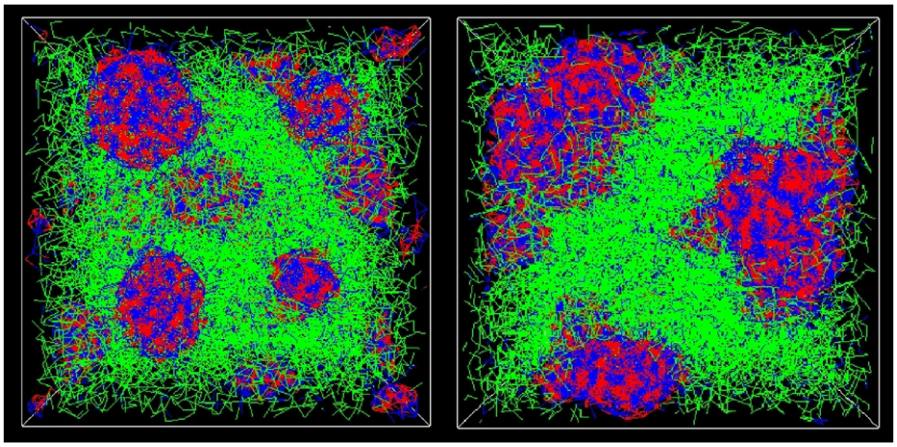

Fig. 23. Fully dispersed (left) and fully aggregated (right) morphologies of filler particles at $\phi = 0.2$ investigated in the DPD simulations of Ref. [171]. The polymer matrix is pictured in green. The particles are pictured in red and blue, corresponding to different types of filler atoms (chemically heterogeneous particles were considered in a subset of the simulations).

polymer cross-links, and (b) a very large enhancement of μ' at this plateau, compared to low particle loadings (by one, sometimes almost two orders of magnitude). These authors ruled out the former two effects (hydrodynamic and polymer–particle interactions) as the main source of reinforcement in this case. Instead, they identified particle jamming as the main contribution at such high loadings. Indeed, $\phi = 0.5$ is very close to the critical volume fraction for the observation of a glass transition in a system of monodisperse hard spheres [139]. There is also a close analogy between this conclusion and those of Long and Sotta, obtained with their bead-and-spring model [163]. As a note of caution, however, we also point out that these simulations were obtained at relatively high frequencies. Since jamming and the glass transition are rate-dependent phenomena, it would clearly be desirable to confirm these conclusions using slower deformation cycles.

In search of an explanation for the Payne effect, Raos et al. [171] explicitly explored the strain-dependence of the elastic response of a filled, cross-linked network. Thus, they conducted their simulations at γ_0 values comprised between 0.025 and 0.80 (i.e., 2.5% and 80%) and two different frequencies. The simulations considered systems with different morphologies, between the fully dispersed to the fully aggregates extremes (see Fig. 23), always keeping the particle volume fraction at $\phi = 0.2$. Particle jamming phenomena should be unimportant at this loading level. The relative strength of the polymer–filler interactions was also changed in some simulations, thus producing different effective particle–particle interactions.

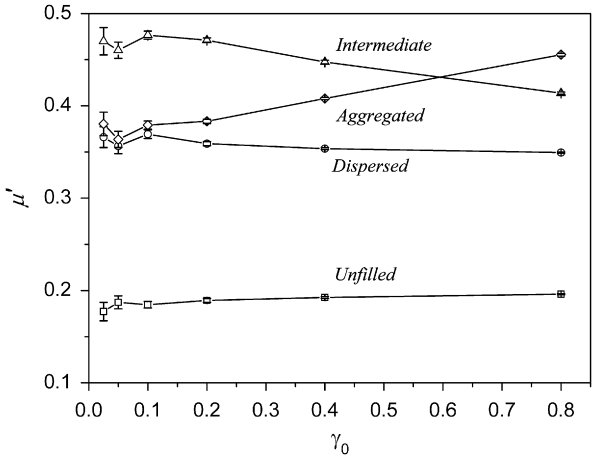

Fig. 24. In-phase shear moduli as a function of shear amplitude, from DPD simulation of filled networks with different degrees of particle dispersion. The "dispersed" and "aggregated" systems correspond to those represented in Fig. 23. The shear frequency is $\nu = 2\pi\omega = 10^{-4}$ (in reduced "DPD units"). Redrawn with permission from selected data in Ref. [171], copyright (2006) of the American Chemical Society.

Representative results from these simulations are given in Fig. 24, containing the effective strain-dependent moduli μ' as a function of the maximum strain amplitude γ_0, for systems with different degrees of particle aggregation. The reference unfilled network has a fully linear response, resulting in a strain-independent modulus. This agrees with all the experimental observations. Also the system with fully dispersed spherical particles has a

strain-independent modulus. Their ratio, equal to about 1.9, is close to the prediction of the Christensen–Lo or other continuum mechanics models [138], for spherical fillers at $\phi = 0.2$. The fully aggregated system has virtually the same small-strain modulus as the fully dispersed one. This can be understood by recognizing that we now have a sample with compact quasi-spherical *aggregates*, which at small strains behave as single quasi-spherical *particles*. At larger strains, instead, these aggregates can be substantially deformed or possibly even broken. This produces a significant (and quite unexpected) non-linear response that we might define anti-Payne: the effective modulus is an increasing function of deformation, so that we have a strain-hardening material. A behaviour resembling the conventional Payne effect is observed for intermediate morphologies, in which the particles form more loosely connected, somewhat open and branched clusters. The small-strain modulus is significantly larger (by a 2.5 factor over the unfilled network) and this modulus decays with increasing deformation amplitude (strain softening). Note, however, that the agreement with experiment is only qualitative: the decay of the modulus is modest (−10%, roughly) compared to the order-of-magnitude drop described in Section 2.

The main conclusion emerging from these simulations [171], is that particle–particle interactions can indeed produce a certain non-linearity in the response of a filled polymer network. However, both the sign and the magnitude of these non-linearities do not seem to agree with the hypothesis that these interactions dominate the elasticity of these materials, as implied by the original interpretation by Payne and the subsequent Kraus model (including its generalizations). Some additional features, such as entanglements, glassy dynamics, finite chain extensibility or bonding/debonding mechanisms at the rubber filler interface will probably need to be included within the model, in order to capture fully these non-linearities.

7. Conclusions and perspectives

The field of polymer-based nanocomposites is currently undergoing an explosive growth, involving both an improvement of "classic" properties (elasticity, toughness) and a development of multifunctional materials for entirely new applications (photovoltaic devices, for example) [4]. Our own interest in polymer nanocomposites was originally motivated by the need to understand the origin of reinforcement of elastomers by active fillers, such as carbon black and silica. This is a long-standing problem, which has gained new impetus from the combination of experimental, theoretical and computational efforts.

Reinforcement actually involves both a substantial increase in the elastic modulus at small strains (linear regime) and a dramatic non-linear response of the material at medium-large strains. For a long time, discussions on the interpretation of these effect have revolved about the relative importance of particle–particle and polymer–particle interactions [1,20,23,31]. It seems that we are at last approaching a consensus, at least on the mechanisms of the small-strain linear response. Good adhesion of the polymer at the filler surface is certainly important to achieve good mechanical properties. Strong polymer–particle interactions can actually produce a shell of glassy polymer (sometimes a few nm's thick), which significantly enhances the "effective" filler volume fraction compared to the "true" one when the particles are nano-sized [26,35]. This shell and the polymer dynamics within it have also been studied theoretically and computationally. On a smooth surface (flat or spherical), an increase of the glass transition can be justified by an enhanced average density of the polymer segments, within a few bead diameters from it [67–70,80,99,125]. A rough surface may disrupt this orderly packing of segments, but an increase in T_g may still arise from the kinetic trapping of the chains within holes of suitable size [21,131].

Our emphasis on the polymer–particle interface does not imply that particle–particle interactions are unimportant. Quite the opposite. However, they are probably different from the "direct" interactions originally envisaged by Payne, because they are actually *effective* interactions transmitted and mediated by the intervening polymer [113]. While in a small-molecule liquid an increase of matrix–particle interactions necessarily decreases particle–particle interactions (it is easier to separate two particles if the surrounding liquid wets them), in a polymeric liquid matrix–particle interactions may actually strengthen particle–particle interactions through the formation of bridging chains. This simple qualitative concept has been demonstrated by a calculation of the potential of mean force between two particles in an polymeric liquid and the corresponding phase diagram, showing that a stable

dispersion is achieved only if the polymer–particle interaction is neither too large not too small [114].

Today, the heat of the argument seems to have shifted to a different level, namely about the "right" level of coarseness in the description. In other words, whether molecular or continuum models are more appropriate. To a certain extent, this is a matter of taste and people have taken sides on the basis of their previous cultural background (e.g., polymer science or mechanical engineering), rather than solid scientific evidence. One of the aims of this review was to stimulate the discussion by starting to fill up a cultural gap, without trying to identify a "winner" of the argument. A macromolecular picture is certainly necessary in the case of nanoparticle dispersions in polymer melts. The liquid-to-solid-like transition observed in these systems, including its dependence on particle concentration and polymer molecular weight, can be explained in a simple way only by admitting the formation of long-lived polymer bridges connecting two particles [32,34,37]. Such bridges have indeed been observed and their statistics studies also by computer simulation [77,82]. Note, however, that polymer bridges are ill-defined in a fully cross-linker polymer matrix, so that a simpler multiphase continuum picture (filler, elastomer and interfacial shell) may be preferable in this case [35,151]. From a computational (i.e., rather pragmatic) point of view, it may be that in the end it will be necessary to take an entirely different approach [162] or exploit the best of both worlds, by interfacing MD or MC simulations of the rubber–filler interface with a FEM description of the bulk polymer region away from it. At the time of writing, unfortunately, no one quite knows how to set up and carry out such multi-scale simulations in a general and reliable way.

While there is a certain consensus on the mechanisms of reinforcement at small strains, the interpretation of strain softening at large deformations (Payne effect) is still a largely open problem, even though several interesting suggestions have been put forward [33,36,37]. The application of both molecular- and continuum-level simulations is not straightforward in this case. Non-equilibrium molecular dynamics simulations of coarse-grained models have already provided some insights [74,170,171]. However, the models used so far are still too simple to reproduce the main effects. Thus, they need to be modified and made more realistic by introducing new features (roughness of the particles or possibility of detachment of polymer chains from their surfaces, for example). All this has to be done carefully, to keep the problem tractable and the results interpretable. It might also be necessary to address more fundamental problems in molecular simulations, such as testing and perhaps devising better thermostats for non-equilibrium dynamics to avoid possible artefacts.

In summary, theory and simulation have recently played an important role within the field of polymer-based nanocomposites. We hope to have shown that there are still plenty of interesting problems and open challenges waiting to be taken up. Progress will be possible through an even closer integration of experiment, theory and computational approaches.

Acknowledgements

GA and GR thank M. Galimberti for useful discussions. They acknowledge financial support from MIUR (PRIN2005 and PRIN2006 programs) and by the Cariplo Foundation.

References

[1] Kraus G, editor. Reinforcement of elastomers. New York, NY: Interscience Publishers; 1965.
[2] Krishnamoorti R, Yurekli K. Rheology of polymer layered silicate nanocomposites. Curr Opin Coll Interface Sci 2001;6:464–70.
[3] Schmidt G, Malwitz MM. Properties of polymer–nanoparticle composites. Curr Opin Coll Interface Sci 2003;8:103–8.
[4] Mark JE. Some novel polymeric nanocomposites. Acc Chem Res 2006;39:881–8.
[5] (a) Balazs A, Emrick T, Russell TP. Nanoparticle polymer composites: where two small worlds meet. Science 2006;314:1107–10;
(b) Vaia AR, Maguire JF. Polymer nanocomposites with prescribed morphology: going beyond nanoparticle-filled polymers. Chem Mater 2007;19:2736–51;
(c) Glotzer SC, Solomon MJ. Anisotropy of building blocks and their assembly into complex structures. Nat Mater 2007;6:557–62;
(d) Böker A, He J, Emrick T, Russell TP. Self-assembly of nanoparticles at interfaces. Soft Matter 2007;3:1231–48.
[6] Ha Y-H, Kwon Y, Breiner T, Chan EP, Tzianetopoulou T, Cohen RE, et al. An orientationally ordered hierarchical exfoliated clay-bock copolymer nanocomposite. Macromolecules 2005;38:5170–9.
[7] Liff SM, Kumar N, McKinley GH. High-performance elastomeric nanocomposites via solvent-exchange processing. Nat Mater 2007;6:76–83.
[8] Balazs AC, Singh C, Zhulina E, Lyatskaya Y. Modeling the phase behavior of polymer/clay nanocomposites. Acc Chem Res 1999;32:651–7.

[9] Salaniwal S, Kumar SK, Douglas JF. Amorphous solidification in polymer–platelet nanocomposites. Phys Rev Lett 2002;89. [258301-1/4].
[10] Thompson RB, Ginzburg VV, Matsen MW, Balazs AC. Predicting the mesophases of copolymer–nanoparticles composites. Science 2001;292:2469–72.
[11] Reister E, Fredrickson GH. Nanoparticles in a diblock copolymer background: the potential of mean force. Macromolecules 2004;37:4718–30.
[12] Schultz AJ, Hall CK, Genzer J. Computer simulation of block copolymer/nanoparticle composites. Macromolecules 2005;38:3007–16.
[13] Pryamitsyn V, Ganesan V. Strong segregation theory of block copolymer–nanoparticle composites. Macromolecules 2006;39:8499–510.
[14] Kim BJ, Fredrickson GH, Hawker CJ, Kramer EJ. Nanoparticle surfactants as a route to block copolymer morphologies. Langmuir 2007;23:7804–9.
[15] Guenes S, Neugebauer H, Sariciftci NS. Conjugated polymer-based organic solar cells. Chem Rev 2007;107: 1324–38.
[16] (a) Haraguchi K, Takehisha T. Nanocomposite hydrogels: a unique organic–inorganic network structure with extraordinary mechanical, optical and swelling–deswelling properties. Adv Mater 2002;14:1120–4;
(b) Huang T, Xu H, Jiao K, Zhu L, Brown HR, Wang H. A novel hydrogel with high mechanical strength: a macromolecular microsphere composite gel. Adv Mater 2007;19:1622–6.
[17] Lodge TP, Muthukumar M. Physical chemistry of polymers: entropy, interactions and dynamics. J Phys Chem 1996;100:13275–92.
[18] Huber G, Vilgis TA. Universal properties of filled rubbers: mechanisms for reinforcement on different length scales. Kautsch Gummi Kunstst 1999;52:102–7.
[19] Heinrich G, Klüppel M, Vilgis TA. Reinforcement of elastomers. Curr Opin Solid State Mater Sci 2002;6: 195–203.
[20] Heinrich G, Klüppel M. Recent advances in the theory of filler networking in elastomers. Adv Polym Sci 2002;160: 1–44.
[21] Vilgis TA. Time scales in the reinforcement of elastomers. Polymer 2005;46:4223–9.
[22] de Gennes PG. Scaling concepts in polymer physics. Ithaca, NY: Cornell University Press; 1979.
[23] Medalia AI. Effect of carbon black on dynamic properties of rubber vulcanizates. Rubber Chem Technol 1978;51: 437–523.
[24] Wolff S. Chemical aspects of rubber reinforcement by fillers. Rubber Chem Technol 1996;69:325–46.
[25] Donnet J-B. Black and white fillers and tire compound. Rubber Chem Technol 1998;71:323–41.
[26] Wang MJ. Effect of polymer–filler and filler–filler interactions on dynamic properties of filled vulcanizates. Rubber Chem Technol 1998;71:520–89.
[27] Leblanc JL. Rubber–filler interactions and rheological properties in filled compounds. Prog Polym Sci 2002;27: 627–87.
[28] Gersappe D. Molecular mechanisms of failure in polymer nanocomposites. Phys Rev Lett 2002;89. [058301-1/4].
[29] Israelachvili JN. Intermolecular and surface forces. 2nd ed. New York: Academic Press; 1991.
[30] Kraus G. Mechanical losses in carbon black filled rubbers. J Appl Polym Sci: Appl Polym Symp 1984;39:75–92.
[31] Maier PG, Göritz D. Molecular interpretation of the Payne effect. Kautsch Gummi Kunstst 1996;49:18–21.
[32] Yurekli K, Krishnamoorti R, Tse MF, McElrath KO, Tsou AH, Wang H-C. Structure and dynamics of carbon black-filled elastomers. J Polym Sci B: Polym Phys 2001;39: 256–75.
[33] Sternstein SS, Zhu A-J. Reinforcement mechanism of nanofilled polymer melts as elucidated by nonlinear viscoelastic behavior. Macromolecules 2002;35:7262–73.
[34] Zhang Q, Archer LA. Poly(ethylene oxide)/silica nanocomposites: structure and rheology. Langmuir 2002;18: 10435–42.
[35] Berriot J, Montes H, Lequeux F, Long D, Sotta P. Evidence for the shift of the glass transition near the particles in silica-filled elastomers. Macromolecules 2002;35: 9756–62.
[36] Montes H, Lequeux F, Berriot J. Influence of the glass transition temperature gradient on the nonlinear viscoelastic behaviour in reinforced elastomers. Macromolecules 2003;36:8107–18.
[37] Zhu Z, Thompson T, Wang S-Q, von Meerwall ED, Halasa A. Investigating linear and nonlinear viscoelastic behavior using model silica-particle-filled polybutadiene. Macromolecules 2005;38:8816–24.
[38] Ramier J, Gauthier C, Chazeau L, Stelandre L, Guy L. Payne effect in silica-filled syrene–butadiene rubber: influence of surface treatment. J Polym Sci B: Polym Phys 2007;45:286–98.
[39] Friedlander SK, Ogawa K, Ullman M. Elastic behavior of nanoparticle chain aggregates: a hypothesis for polymer–filler behaviour. J Polym Sci B: Polym Phys 2000;38: 2658–65.
[40] Bandyopadhyaya R, Rong W, Friedlander SK. Dynamics of chain aggregates of carbon nanoparticles in isolation and in polymer films: implications for nanocomposite materials. Chem Mater 2004;16:3147–54.
[41] Rong W, Ding W, Mädler L, Ruoff RS, Friedlander SK. Nano Lett 2006;6:2646–55.
[42] Dannenberg EM. Bound rubber and carbon black reinforcement. Rubber Chem Technol 1986;59:512–24.
[43] Hamed GR, Hatfield S. On the role of bound rubber in carbon black reinforcement. Rubber Chem Technol 1989;62:143–56.
[44] Meissner B. Bound rubber and elastomer–filler interaction. Rubber Chem Technol 1995;68:297–310.
[45] Catellano M, Conzatti L, Turturro A, Costa G, Busca G. Influence of the silane modifiers on the surface thermodynamic characteristics and dispersion of the silica into elastomer compounds. J Phys Chem B 2007;111:4495–502.
[46] Schröder A, Klüppel M, Schuster RH. Characterization of the surface activity of carbon black and its relation to polymer–filler interaction. Macromol Mater Eng 2007;292: 885–916.
[47] Tsagaropoulos G, Eisenberg A. Direct observation of two glass transitions in silica-filled polymers. Implications for the morphology of random ionomers. Macromolecules 1995;28:396–8.
[48] Arrighi V, Higgins JS, Burgess AN, Floudas G. Local dynamics of PDMS in the presence of reinforcing filler particles. Polymer 1998;39:6369–76.

[49] Litvinov VM, Steeman PAM. EPDM–carbon black interactions and the reinforcement mechanisms, as studied by low-resolution ^{1}H NMR. Macromolecules 1999;35:4356–64.
[50] Litvinov VM, Barthel H, Weis J. Structure of a PDMS layer grafted onto a silica surface studied by means of DSC and solid-state NMR. Macromolecules 2002;35:4356–64.
[51] Simonutti R, Comotti A, Negroni F, Sozzani P. ^{13}C and ^{29}Si solid-state NMR of rubber–silica composite materials. Chem Mater 1999;11:822–8.
[52] Berriot J, Lequeux F, Monnerie L, Montes H, Long D, Sotta P. Filler–elastomer interaction in model filled rubbers, a ^{1}H NMR study. J Non-Cryst Sol 2002;307–310:719–24.
[53] Rittigstein P, Priestley RD, Broadbelt LJ, Torkelson JM. Model polymer nanocomposites provide an understanding of confinement effects in real nanocomposites. Nat Mater 2007;6:278–82.
[54] Alcoutlabi M, McKenna GB. Effects of confinement on material behaviour at the nanometer size scale. J Phys Condens Matter 2005;17:R461–524.
[55] Tscheschel A, Lacayo J, Stoyan D. Statistical characterization of TEM images of silica-filled rubber. J Microsc 2005;217:75–82.
[56] Rharbi Y, Cabane B, Vacher A, Janicot M, Boué F. Modes of deformation in a soft/hard nanocomposite: a SANS study. Europhys Lett 1999;46:472–8.
[57] Ehrburger-Dolle F, Hindermann-Bischoff M, Livet F, Bely F, Rochas C, Geissler E. Anisotropic ultra-small-angle X-ray scattering in carbon black filled polymers. Langmuir 2001;17:329–34.
[58] (a) Oberdisse J. Aggregation of colloidal nanoparticles in polymer matrices. Soft Matter 2006;2:29–36;
(b) Schaefer DW, Justice RS. How nano are nanocomposites? Macromolecules 2007;40:8501–17.
[59] Oberdisse J, Hine P, Pyckout-Hintzen W. Structure of interacting aggregates of silica nanoparticles in a polymer matrix: small-angle scattering and reverse Monte Carlo simulations. Soft Matter 2007;3:476–85.
[60] Le Diagon Y, Mallarino S, Fretigny C. Particle structuring under the effect of an uniaxial deformation in soft/hard nanocomposites. Eur Phys J E 2007;22:77–83.
[61] Nakatani AI, Chen W, Schmidt RG, Gordon GV, Han CC. Chain dimensions in polysilicate-filled poly(dimethyl siloxane). Polymer 2001;42:3713–22.
[62] Botti A, Pyckout-Hintzen W, Richter D, Urban V, Straube E. A microscopic look at the reinforcement of silica-filled rubbers. J Chem Phys 2006;124. [174908-1/5].
[63] Mackay ME, Tuteja A, Duxbury PM, Hawker CJ, Van Horn B, Guan Z, et al. General strategies for nanoparticle dispersion. Science 2006;311:1740–3.
[64] Allen MP, Tildesley DJ. Computer simulation of liquids. Oxford and New York: Oxford University Press; 1987.
[65] Frenkel D, Smit B. Understanding molecular simulation. San Diego and London: Academic Press; 1996.
[66] Attig N, Binder K, Grubmüller H, Kremer K, editors. Computational soft matter: from synthetic polymers to proteins. Jülich: NIC Series; 2004 ⟨http://www.fz-juelich.de/nic-series/volume23⟩.
[67] Starr FW, Schroder TB, Glotzer SC. Effects of a nanoscopic filler on the structure and dynamics of a simulated polymer melt and the relationship to ultrathin films. Phys Rev E 2001;64:021802.
[68] Starr FW, Schroder TB, Glotzer SC. Molecular dynamics simulation of a polymer melt with a nanoscopic particle. Macromolecules 2002;35:4481–92.
[69] Vacatello M. Monte Carlo simulations of polymer melts filled with solid nanoparticles. Macromolecules 2001;34:1946–52.
[70] Smith GD, Bedrov D, Li L, Byutner O. A molecular dynamics simulation study of the viscoelastic properties of polymer nanocomposites. J Chem Phys 2002;117:9478–89.
[71] Hooper JB, Schweizer KS, Desai TG, Koshy R, Keblinski P. Structure, surface excess and effective interactions in polymer nanocomposite melts and concentrated solutions. J Chem Phys 2004;14:6986–97.
[72] Desai T, Keblinski P, Kumar SK. Molecular dynamics simulations of polymer transport in nanocomposites. J Chem Phys 2005;122:134910.
[73] Starr FW, Douglas JF, Glotzer SC. Origin of particle clustering in a simulated polymer nanocomposites and its impact on rheology. J Chem Phys 2003;119:1777–88.
[74] Kairn T, Daivis PJ, Ivanov I, Bhattacharya SN. Molecular-dynamics simulation of model polymer nanocomposites rheology and comparison with experiment. J Chem Phys 2005;123:194905.
[75] Sen S, Thomin JD, Kumar S, Keblinski P. Molecular underpinnings of the mechanical reinforcement in polymer nanocomposites. Macromolecules 2007;40:4059–67.
[76] Vacatello M. Chain dimensions in filled polymers: an intriguing problem. Macromolecules 2002;35:8191–3.
[77] Vacatello M. Molecular arrangements in polymer-based nanocomposites. Macromol Theory Simul 2002;11:757–65.
[78] Vacatello M. Predicting the molecular arrangements in polymer-based nanocomposites. Macromol Theory Simul 2003;12:86–91.
[79] Zhang Q, Archer LA. Monte Carlo simulation of structure and nanoscale interactions in polymer nanocomposites. J Chem Phys 2004;121:10814–24.
[80] Papakonstantopoulos GJ, Yoshimoto K, Doxastakis M, Nealey PF, de Pablo JJ. Local mechanical properties of polymeric nanocomposites. Phys Rev E 2005;72:031801.
[81] Brown D, Mélé P, Marceau S, Albérola ND. A molecular dynamics study of a model nanoparticle embedded in a polymer matrix. Macromolecules 2003;36:1395–406.
[82] Ozmusul MS, Picu CR, Sternstein SS, Kumar SK. Lattice Monte Carlo simulations of chain conformations in polymer nanocomposites. Macromolecules 2005;38:4495–500.
[83] Huang J, Mao Z, Qian C. Dynamic Monte Carlo study on the polymer chain in random media filled with nanoparticles. Polymer 2006;47:2928–32.
[84] Lin H, Erguney F, Mattice WL. Collapsed chains as models for filler particles in a polymer melt. Polymer 2005;46:6154–62.
[85] Erguney FM, Lin H, Mattice WL. Dimensions of matrix chains in polymers filled with energetically neutral nanoparticles. Polymer 2006;47:3689–95.
[86] Dionne PJ, Ozisik R, Picu CR. Structure and dynamics of polyethylene nanocomposites. Macromolecules 2005;38:9351–8.
[87] Dionne PJ, Picu CR, Ozisik R. Adsorption and desorption dynamics of linear polymer chains to spherical

nanoparticles: a Monte Carlo investigation. Macromolecules 2006;39:3089–92.
[88] Kloczkowski A, Sharaf MA, Mark JE. Molecular theory for reinforcement in filled elastomers. Comput Polym Sci 1993;3:39–45.
[89] Sharaf MA, Kloczkowski A, Mark JE. Simulations of the reinforcement of elastomeric poly(dimethylsiloxane) by filler particles arranged on a cubic lattice. Comput Polym Sci 1994;4:29–39.
[90] Yuan QW, Kloczkowski A, Mark JE, Sharaf MA. Simulations of the reinforcement of poly(dimethylsiloxane) by randomly distributed filler particles. J Polym Sci—Part B: Polym Phys 1996;34:1647–57.
[91] Sharaf MA, Kloczkowski A, Mark JE. Monte Carlo simulations of reinforcement of an elastomer by oriented prolate particles. Comput Theor Polym Sci 2001;11:251–62.
[92] Sharaf MA, Kloczkowski A, Sen TZ, Jacob KI, Mark JE. Filler-induced deformations of amorphous polyethylene chains. The effects of the deformations on elastomeric properties, and some comparison with experiments. Eur Polym J 2006;42:796–806.
[93] Vacatello M. Phantom chain simulations of polymer–nanofiller systems. Macromolecules 2003;36:3411–6.
[94] Vacatello M. Phantom chain simulations of realistically sized polymer-based nanocomposites. Macromol Theory Simul 2006;15:303–10.
[95] Curro JG, Schweizer KS, Grest GS, Kremer K. A comparison between integral equation theory and molecular dynamics simulations of dense flexible polymer liquids. J Chem Phys 1989;91:1357–64.
[96] Honnell KG, Curro JG, Schweizer KS. Local structure of semiflexible polymer melts. Macromolecules 1990;23: 3496–505.
[97] Schweizer KS, Curro JG. Integral equation theories of the structure, thermodynamics and phase transitions of polymer fluids. Adv Chem Phys 1997;98:1–142.
[98] Heine DR, Grest GS, Curro JG. Structure of polymer melts and blends: comparison of integral equation theory and computer simulation. Adv Polym Sci 2004;176:211–50.
[99] Yethirajm A. Polymer melts at solid surfaces. Adv Chem Phys 2002;121:89.
[100] Yethiraj A, Woodward CE. Monte Carlo density functional theory of nonuniform polymer melt. J Chem Phys 1995;102:5499–505.
[101] Hooper JB, McCoy JD, Curro JG. Density functional theory of simple polymers in a slit pore. I. Theory and efficient algorithm. J Chem Phys 2000;112:3090–3.
[102] Kremer K, Grest GS. Dynamics of entangled linear polymer melts: a molecular-dynamics simulation. J Chem Phys 1990;92:5057–86.
[103] Flory PJ, Yoon DY, Dill KA. The interphase in lamellar semicrystalline polymers. Macromolecules 1984;17:862–8.
[104] Rapold RF, Mattice WL. New high-coordination lattice model for rotational isomeric state polymer chains. J Chem Soc—Faraday Trans 1995;91:2435–41.
[105] Rapold RF, Mattice WL. Introduction of short and long range energies to simulate real chains on the 2nnd lattice. Macromolecules 1996;29:2457–66.
[106] Doruker P, Mattice WL. Reverse mapping of coarse grained polyethylene chains from the second nearest neighbour diamond lattice to an atomistic model in continuous space. Macromolecules 1997;30:5520–6.
[107] Vacatello M. Monte Carlo simulations of the interface between polymer melts and solids. Effects of chain stiffness. Macromol Theory Simul 2001;10:187–95.
[108] Vacatello M. Monte Carlo simulations of polymers in nanoslits. Macromol Theory Simul 2004;13:30–5.
[109] Flory PJ. Statistical mechanics of chain molecules. New York: Wiley; 1989.
[110] Matsuda T, Smith GD, Winkler RG, Yoon DY. Stochastic dynamics simulations of *n*-alkane melts confined between solid surfaces: influence of surface properties and comparison with Scheutjens–Fleer theory. Macromolecules 1995;28:165–73.
[111] Vacatello M. Unpublished, 2004.
[112] Klein J. Surface interactions with adsorbed macromolecules. J Colloid Interface Sci 1986;111:305–13.
[113] Hooper JB, Schweizer KS. Contact aggregation, bridging and steric stabilisation in dense polymer–particle mixtures. Macromolecules 2005;38:8858–69.
[114] Hooper JB, Schweizer KS. Theory of phase separation in nanocomposites. Macromolecules 2006;39:5133–42.
[115] Hansen JP, McDonald IR. Theory of simple liquids. New York, NY: Academic Press; 1986.
[116] Anderson BJ, Zukoski CF. Nanoparticle stability in polymer melts as determined by particle second virial measurements. Macromolecules 2007;40:5133–40.
[117] Evers OA, Scheutjens JMHM, Fleer GJ. Statistical thermodynamics of block copolymer adsorption. 1. Formulation of the model and results for the adsorbed layer structure. Macromolecules 1990;23:5221–33.
[118] Daoulas KCh, Theodorou DN, Harmandaris VA, Karayiannis NCh, Mavrantzas VG. Self-consistent-field study of compressible semiflexible melts adsorbed on a solid substrate and comparison with atomistic simulations. Macromolecules 2005;38:7134–49.
[119] Allegra G, Raos G. Confined polymer networks: the harmonic approach. J Chem Phys 2002;116:3109–18.
[120] Allegra G, Raos G, Manassero C. Polymer-mediated adhesion: a statistical approach. J Chem Phys 2003;119:9295–307.
[121] DiMarzio EA, Rubin RJ. Adsorption of a chain polymer between two plates. J Chem Phys 1971;55:4318–36.
[122] Allegra G, Colombo E. Polymer chain between attractive walls: a second-order transition. J Chem Phys 1993;98: 7398–404.
[123] Casassa EF, Tagami Y. An equilibrium theory for exclusion chromatography of branched and linear polymer chains. Macromolecules 1969;2:14–26.
[124] Ronca G, Allegra G. Contraction effects in ideal networks of flexible chains. J Chem Phys 1975;63:4104–9.
[125] McCoy JD, Curro JG. Conjectures on the glass transition of polymers in confined geometries. J Chem Phys 2002;116:9154–7.
[126] Smith GD, Bedrov D, Borodin O. Structural relaxation and dynamic heterogeneity in a polymer melt at attractive surfaces. Phys Rev Lett 2003;90. [226103-1/4].
[127] Allegra G, Bignotti F, Gargani L, Cociani M. Glass transition in polymers: freezing of molecular oscillations. Macromolecules 1990;23:5326–34.
[128] Allegra G, Caccianotti L, Fusco R. Glass temperature of ethylene/propylene copolymers: an application of the pseudostereochemical equilibrium approach. Macromolecules 1999;31:5487–94.
[129] Gibbs JH, DiMarzio EA. Nature of the glass transition and the glassy state. J Chem Phys 1958;28:373–83.

[130] Huber G, Vilgis TA. Polymer adsorption on heterogeneous surfaces. Eur Phys J B 1998;3:217–23.
[131] Migliorini G, Rostiashvili VG, Vilgis TA. Polymer chain in a quenched random medium: slow dynamics and ergodicity breaking. Eur Phys J B 2003;33:61–73.
[132] Baumgärtner A, Muthukumar M. Polymers and disordered media. Adv Chem Phys 1996;94:625–708.
[133] Heinrich G, Klüppel M, Vilgis TA. Evaluation of self-affine surfaces and their implication for frictional dynamics as illustrated with a Rouse material. Comput Theor Polym Sci 2000;10:53–61.
[134] Allegra G, Raos G. Sliding friction between polymer surfaces: a molecular interpretation. J Chem Phys 2006;124:144713.
[135] Allegra G. Internal viscosity in polymer chains: a critical analysis. J Chem Phys 1986;84:5881–90.
[136] Maeda N, Chen N, Tirrell M, Israelachvili JN. Adhesion and friction mechanisms of polymer-on-polymer surfaces. Science 2002;297:379–82.
[137] Sarvestani AS, Picu CR. A frictional molecular model for the viscoelasticity of entangled polymer nanocomposites. Rheol Acta 2005;45:132–41.
[138] Christensen RM. Mechanics of composite materials. New York: Dover Publishing; 2005.
[139] Torquato S. Random heterogeneous materials. Berlin: Springer; 2002.
[140] Léger L, Raphaël E, Hervet H. Surface-anchored polymer chains: their role in adhesion and friction. Adv Polym Sci 1999;138:185–225.
[141] Granick S, Zhu Y, Lee H. Slippery questions about complex fluids flowing past solids. Nat Mater 2003;2:221–7.
[142] Mackay ME, Dao TT, Tuteja A, Ho DL, Van Horn B, Kim HC, et al. Nanoscale effects leading to non-Einstein-like decrease in viscosity. Nat Mater 2003;2:762–6.
[143] Witten TA, Rubinstein M, Colby RH. Reinforcement of rubber by fractal aggregates. J Phys II France 1993;3:367–83.
[144] Huber G, Vilgis TA. On the mechanism of hydrodynamic reinforcement in elastic composites. Macromolecules 2002;35:9204–10.
[145] Greco F, D'Avino G, Maffettone PL. Stress tensor of a dilute suspension of spheres in a viscoelastic liquid. Phys Rev Lett 2005;95. [246001-1/4. Erratum: ibid. 2007;98:109904].
[146] Freed KF, Muthukumar M. On the Stokes problem for a suspension of spheres at finite concentrations. J Chem Phys 1978;68:2088–96.
[147] Jhon MS, Metz RJ, Freed KF. Effective medium theory for elastic matrix composites containing dispersed particulates. J Stat Phys 1988;52:1325–42.
[148] Mondescu RP, Muthukumar M. Effective elastic moduli of a composite containing rigid spheres at nondilute concentrations: a multi scattering approach. J Chem Phys 1999; 110:1123–37.
[149] Christensen RM, Lo KH. Solutions for the effective shear properties in three phase sphere and cylinder models. J Mech Phys Solids 1979;27:315.
[150] Raos G. Application of the Christensen–Lo model to the reinforcement of elastomers by fractal fillers. Macromol Theory Simul 2003;12:17–23.
[151] Gusev AA. Micromechanical mechanism of reinforcement and losses in filled rubbers. Macromolecules 2006;39:5960–2.
[152] Zienkiewicz OC, Taylor RL. The finite element method the basis, 5th ed., vol. 1, Woburn, MA: Butterworth-Heinemann; 2000.
[153] Zienkiewicz OC, Taylor RL, The finite element method solid mechanics. 5th ed., vol. 2. Woburn, MA: Butterworth-Heinemann; 2000.
[154] Gusev AA. Numerical identification of the potential of whisker- and platelet-filled polymers. Macromolecules 2001;34:3081–93.
[155] Ogden RW. Non-linear elastic deformations. New York: Dover; 1997.
[156] Ponte Castañeda P, Suquet P. Nonlinear composites. Adv Appl Mech 1998;34:171–302.
[157] Ponte Castañeda P, Tiberio E. A second-order homogenization procedure in finite elasticity and applications to black-filled elastomers. J Mech Phys Solids 2000;48:1389–411.
[158] Lion A, Kardelky C. The Payne effect in finite viscoelasticity: constitutive modelling based on fractional derivatives and intrinsic time scales. Int J Plast 2004;20: 1313–45.
[159] Drozdov AD, Dorfmann A. A micro-mechanical model for the response of filled elastomers at finite strains. Int J Plast 2003;19:1037–67.
[160] Allegra G, Raos G. Rigid particles in an elastic polymer network: an electrical-analog approach. J Chem Phys 1998;109:3285–92.
[161] Raos G, Allegra A, Assecondi L, Croci C. Rigid filler particles in a rubber matrix: effective force constants by multipolar expansion. Comput Theor Polym Sci 2000;10:149–57.
[162] Raos G, Allegra G. Mesoscopic bead-and-spring model of hard spherical particles in a rubber matrix. Hydrodynamic reinforcement. J Chem Phys 2000;113:7554–63.
[163] Long D, Sotta P. Nonlinear and plastic behavior of soft thermoplastic and filled elastomers studied by dissipative particle dynamics. Macromolecules 2006;39:6282–97.
[164] Mansfield ML, Douglas JF, Irfan S, Kang E-H. Comparison of approximate methods for calculating the friction coefficient of and intrinsic viscosities of nanoparticles and macromolecules. Macromolecules 2007;40:2575–89.
[165] Gusev AA. Finite element mapping for spring network representations of the mechanics of solids. Phys Rev Lett 2004;93. 034302-1/4.
[166] Evans DJ, Morris GP. Statistical mechanics of nonequilibrium liquids. New York, NY: Academic Press; 1990.
[167] Sen S, Kumar SK, Keblinski P. Viscoelastic properties of polymer melts from equilibrium molecular dynamics simulations. Macromolecules 2005;38:650–3.
[168] Kröger M, Hess S. Rheological evidence for a dynamical crossover in polymer melts via nonequilibrium molecular dynamics. Phys Rev Lett 2000;85:1128–31.
[169] Vladkov M, Barrat J-L. Linear and nonlinear viscoelasticity of a model unentangled polymer melt: molecular dynamics and Rouse modes analysis. Macromol Theory Simul 2006;15:252–62.
[170] Pryamitsyn V, Ganesan V. Origins of linear viscoelastic behavior of polymer–nanoparticle composites. Macromolecules 2006;39:844–56.
[171] Raos G, Moreno M, Elli S. Computational experiments on filled rubber viscoelasticity: what is the role of particle–particle interactions? Macromolecules 2006;39:6744–51.
[172] Groot RD, Warren PB. Dissipative particle dynamics: bridging the gap between atomistic and mesoscopic simulation. J Chem Phys 1997;107:4423–35.
[173] Groot RD. Applications of dissipative particle dynamics. Lect Notes Phys 2004;640:5–38.